Study of Nanocomposite Laminates and Failure Analysis of Pin Joints

Thesis

Submitted in partial fulfillment for the award of degree

of

DOCTOR OF PHILOSOPHY

By

MANJEET SINGH

(Registration No.: 901208005)

Under the guidance of

Dr. Haripada Bhunia
Professor
Chemical Engg. Department
Thapar Institute of Engineering & Technology, Patiala

Dr. Jaswinder Singh Saini
Associate Professor
Mechanical Engg. Department
Thapar Institute of Engineering & Technology, Patiala

MECHANICAL ENGINEERING DEPARTMENT
THAPAR INSTITUTE OF ENGINEERING & TECHNOLOGY
(Deemed to be University)
Patiala-147004, Punjab, India
www.thapar.edu

May 2018

Dedicated

To

My Brother

Mr. Harpreet Singh Sekhon

And

My Wife

Mrs. Shubhpreet Kaur

Certificate

This is to certify that the thesis entitled **"Study of Nanocomposite Laminates and Failure Analysis of Pin Joints"** being submitted by Mr. Manjeet Singh to Mechanical Engineering Department, Thapar Institute of Engineering & Technology, Patiala for the award of degree of **Doctor of Philosophy,** is a record of bonafide research work carried out by him under our guidance and supervision and has fulfilled the requirements for the submission of the thesis, which to our knowledge has reached the requisite standard.

The results embodied in the thesis have not been submitted in part or full to any other University or Institute for the award of any degree or diploma.

11/5/2018

Dr. Haripada Bhunia
Professor,
Chemical Engg. Department,
Thapar Institute of Engineering & Technology,
Patiala

11/5/18

Dr. Jaswinder Singh Saini
Associate Professor,
Mechanical Engg. Department,
Thapar Institute of Engineering & Technology,
Patiala

Acknowledgements

Undertaking this PhD has been a truly life-changing experience for me and it would not have been possible to do without the support and guidance that I received from many people.

First of all, I am extremely grateful to my research guides, **Dr. Jaswinder Singh Saini**, Associate Professor, Mechanical Engineering Department and **Dr. Haripada Bhunia**, Professor, Chemical Engineering Department for their valuable guidance, scholarly inputs and consistent encouragement I received throughout the research work. It's been a great honor to work under their guidance.

My profound gratitude to **Prof. Prakash Gopalan**, Director, Thapar Institute of Engineering & Technology, **Dr. O.P. Pandey**, Dean of Research & Sponsored Projects, Thapar Institute of Engineering & Technology and **Dr. S.K. Mohapatra**, Head, Mechanical Engineering Department, Thapar Institute of Engineering & Technology for their motivation provided to me throughout the period of research.

I am also thankful to my doctoral committee members, **Dr. Kulvir Singh**, Professor, School of Physics and Material Sciences, Thapar Institute of Engineering & Technology, **Dr. Deepak Jain**, Assistant Professor, Mechanical Engineering Department, Thapar Institute of Engineering & Technology, **Dr. Dheeraj Gupta**, Associate Professor, Mechanical Engineering Department, Thapar Institute of Engineering & Technology and **Dr. V.P. Agarwal**, Visiting Professor, Mechanical Engineering Department, Thapar Institute of Engineering & Technology for advising and guiding me towards the right directions. I am greatly indebted to all the staff members of Mechanical Engineering Department, Thapar Institute of Engineering & Technology, Patiala.

My deep appreciation goes out to my colleagues, **Mr. Kulwinder Singh**, **Mr. Mandeep Singh**, **Mr. Gaurav Singla** and **Mr. Paramdeep Singh** for their constant help and encouragement. I express my deepest gratitude to all my family members and friends. I could not have reached today's point without their help and best wishes.

Above all, I am thankful to the Almighty God for planning everything for my life and choosing me to perform this research work.

Manjeet Singh

Manjeet Singh

Abstract

Fiber reinforced composites have high demand as a structural material, often in load bearing applications. This is because of their light weight with high strength, environment resistance and high durability. Fiber reinforced composites are required to be joined in the different applications for the efficient design and assembly of the structures. These joints exhibit poor performance and unexpected failure due to the stress concentration around or vicinity of the holes. The main objective of the present work is to increase the performance of the joints prepared from glass fiber reinforced composites with the addition of the nanofiller, with different fiber orientations and with different geometric parameters.

The effect of the different ply orientations and nanofiller on the bearing strength and failure mode of the pin joints were investigated both experimentally and numerically. Glass-epoxy composite laminates were prepared with [0°/45°/90°], [0°/45°/0°] and [0°/90°/0°] ply orientations. Nanoclay filler with 1, 2, 3, 4 and 5 wt.% were added in epoxy for the said orientations to prepare the single hole pin joints. Results show that the strength of the pin joints is significantly dependent on both the ply orientations and nanofiller wt.%. The joint geometry *i.e.*, distance from the free edge of specimen to the diameter of the hole (E/D) ratio and width of the specimen to the diameter of the hole (W/D) ratio were also investigated in single hole configuration. The E/D and W/D ratios were varied from 2 to 5. Results show that the bearing strength and failure mode were significantly affected by the geometric parameters.

Taguchi method was used to optimize the geometric parameters for double holes pin joint configurations. The orthogonal array, the signal-to-noise ratio, and analysis of variance were employed to study the effect of geometric parameters on the bearing strength of the joints. Geometric parameters, *i.e.*, distance from the free edge of the specimen to the diameter of the first hole (E/D) ratio, width of the specimen to the diameter of the hole (W/D) ratio, distance between the two holes to the diameter of the hole (P/D) ratio and side width to the diameter of the hole (K/D) ratio, were investigated for the serial and parallel hole configurations. The results demonstrate that the E/D ratio is the most significant parameter to increase the bearing strength in both serial and parallel double pin joint configurations. Its percentage contribution is about 84.5% and 64.23% in serial and parallel pin joint configurations, respectively.

For multi holes pin joint configurations, the geometric parameters *i.e.*, distance from the free edge of the specimen to the diameter of the first two holes (E/D) ratio, distance between two holes along the length of the specimen to the diameter of the hole (F/D) ratio, distance between the two holes along the width of the specimen to the diameter of the hole (P/D) ratio and side width to diameter (S/D) ratio, were studied for their effect on strength and failure modes of the joint. Design of experiments along with Taguchi method was used for the optimization of different geometric parameters. ANOVA was applied to determine the influence of individual geometric parameter on the strength of joint. The results demonstrate that E/D and F/D ratios are the most significant parameters to increase the strength of multi holes pin joint configurations. Their percentage contributions were about 62% to 65% and 23% to 26%, respectively.

The characteristic curve method along with Tsai-Wu failure criteria was used to compare the numerical and the experimental results. A good agreement was obtained between the numerical and experimental predictions.

Publications

Publications from the present work in peer-reviewed (SCI) journals

(i) **Singh M**, Saini JS and Bhunia H. To study the contribution of different geometric parameters on the failure load for multi holes pin Joints prepared from glass/epoxy nanoclay laminates. *Journal of Composite Materials* 2018; 52 (5): 629–644. (impact factor: 1.494)

(ii) **Sekhon M**, Saini JS, Singla G and Bhunia H. Influence of nanoparticle fillers content on the bearing strength behavior of glass fiber reinforced epoxy composites pin joints. *Journal of Materials: Design and Applications* 2017; 231 (8): 641-656. (impact factor: 1.625)

(iii) **Singh M**, Saini JS, Bhunia H and Singh P. Application of Taguchi method in the optimization of geometric parameters for double pin joint configurations made from glass–epoxy nanoclay laminates. *Journal of Composite Materials* 2017; 51 (19): 2689-2706. (impact factor: 1.494)

(iv) **Singh M**, Saini JS and Bhunia H. Investigation on failure modes for pin joints made from unidirectional glass-epoxy nanoclay laminates. *Fatigue & Fracture of Engineering Materials & Structures* 2016; 39 (3): 320-334. (impact factor: 2.335)

(v) **Singh M**, Bhunia H and Saini JS. Effect of ply orientation on strength and failure mode of pin jointed unidirectional glass-epoxy nanoclay laminates. *Defence Science Journal* 2015; 65 (6): 489-499. (impact factor: 0.5)

Table of Contents

List of Figures

List of Tables

List of Symbols and Abbreviations

ANOVA	Analysis of variance
B	Bearing mode of failure
D	Diameter of the hole
DGEBA	Di Glycidyl Ether of Bisphenol-A
DOE	Design of Experiment
DF	Degree of freedom
E	Distance from the free edge of specimen
E_1	Longitudinal tensile modulus
E_2	Transverse tensile modulus
F	Distance between two holes along the length of the specimen
F_{opt}	Optimum value of force
FEM	Finite element method
FI	Failure Index
FRP	Fiber reinforced polymers
G_{12}	Shear modulus
GFRP	Glass fiber reinforced polymers
Gsm	Gram per mm^2
N	Net tension
OA	Orthogonal array
P_{max}	Maximum load
P	Distance between the two holes along the width of the specimen
R_{oc}	Characteristic length in compression
R_{ot}	Characteristic length in tension
S	Shear failure strength
S	Shearing
SEM	Scanning electron microscopy
S/N ratio	Signal to noise ratio
SS_d	Sum of the squared deviations
SS_e	Sum of the squared error

SS_T	Total Sum of the squared deviation
T	Thickness of the specimen
UTM	Universal testing machine
W	Width of the specimen
wt.%	Weight percentage
X_t	Longitudinal tensile strength
X_c	Longitudinal compressive strength
XRD	X-Ray Diffraction
Y_t	Transverse tensile strength
Y_c	Transverse compressive failure strength
ν_{12}	Poisson ratio
Θ	Failure angle
σ_1	Maximum principal stress
σ_2	Minimum principal stress
σ_6	Maximum shear stress

Chapter 1 - Introduction

The present era is in high demand of materials with their requirements in different fields to increase the strength without much increase in the weight. Exhaustive research is being carried out worldwide for developing such new materials. Till now conventional metals and their alloys were the principal materials used in the industry for this purpose due to their high strength, low cost, ease of moulding and other treatment processes to play with their strength. But these materials have certain drawbacks, such as lesser resistance to corrosion and lesser strength to weight ratio. To overcome these drawbacks of conventional metals and alloys, composite materials are developed as they have unusual combinations of properties like, high strength and stiffness with low weight along with high mechanical performance (Jones, 1999).

Composite material is a multiphase material that is artificially made, as opposed to one that occurs or forms naturally. One phase is a matrix and other phase is a reinforcement. The matrix material surrounds and supports the reinforcement materials by maintaining their relative positions. The reinforcements impart their special mechanical and physical properties to enhance the matrix properties. These two categories of constituent materials are also called two phases of composites (Callister, 2007). Modern composite materials are usually optimized to achieve a particular balance of properties for a given range of applications. The properties of the composites are the function of the properties of constituent phases, their relative amounts and the geometry of the dispersed face. Dispersed phase geometry in this context mean the shape of the particle and the particle size, distribution and the orientation (Callister, 2007).

1.1 Classification of Composites

Mainly the composites are classified in two broad categories based on their constituent. These are (Callister, 2007):

(i) Matrix constituent: Matrix is a continuous material into which the reinforcement is embedded. It comprises of Organic Matrix Composites (OMCs), Metal Matrix Composites (MMCs) and Ceramic Matrix Composites (CMCs). Further OMC is classified into Polymer Matrix Composite and Carbon Matrix Composites.

(ii) Reinforced constituent: Reinforcement constituent is stronger than the matrix constituent and is embedded into matrix material. Reinforcement material enhances the various mechanical and physical properties of the composites. The second level of classifications is described with respect to reinforcement form which comprises of laminar composites, fiber reinforced composites, and particulate composites as shown in the Fig. 1.1. Fiber reinforced composites are of two type *i.e.*, discontinuous and continuous fibers.

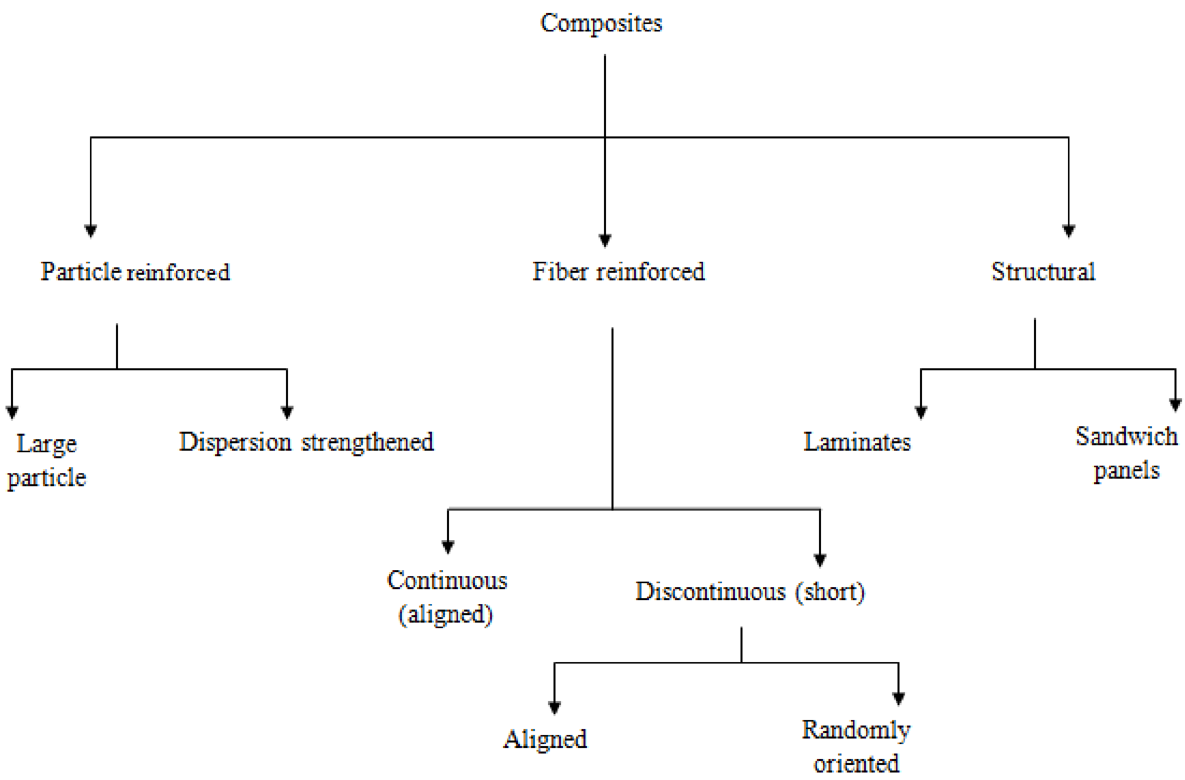

Fig. 1.1 Classification of composites with respect to reinforcement constituent (Callister, 2007)

1.2 Polymer Matrix Composites

The composite materials having a polymer (resin) as a matrix constituent which are reinforced by the fibers or particulate materials are known as Polymer matrix composites (Jones, 1999). There are two phases in polymer matrix composites - Continuous (Matrix) and Discontinuous (Reinforcement). The reinforcement constituent bears the maximum load as matrix transfers the load to the reinforcement. The matrix phase holds the reinforcements together, protects the composite from environmental degradation and gives a finish, colour, texture and durability to composite material. There are two main kinds of polymers i.e., thermosets and thermoplastics (Chawla, 1998).

(i) Thermosets: Thermosets comprises of cross-linked/network structures with all molecules having covalent bonds. On heating, thermosets do not soften, rather they disintegrate. They cannot be reshaped once they are solidified by process of cross-linking.

The main examples of thermosets are phenolics, silicone, polyesters, epoxies, melamine and polyimides (Chawla, 1998).

(ii) Thermoplastics: They consist of branched/linear chain molecules having weak intermolecular bonds and strong intramolecular bonds. Heat and pressure can alter their shape and they can be changed into any shape at high temperature (Chawla, 1998). Examples of thermoplastics include polyacetals, nylons, polyether imide, polycarbonate, polyethylene, polystyrene, polypropylene, polyether ether ketone, polyphenylene sulfide etc.

Recent studies have shown that addition of very small percentage of nanoparticles to the polymer composites as reinforcements significantly improves their strength. Nanoparticles are those materials which have their dimensions of the order of $10^{-9}\ m$ (Fakirov *et al.*, 2016). But it must be ensured that these nanoparticles do not agglomerate while their disbursement to the polymer composites. Such composites which have nanoparticles as the second phase of reinforcement to polymer are called polymer nanocomposites. Fibers are used as reinforcement in the polymer matrix as they are much stronger and stiffer than the polymer and bear maximum load which is transferred by the polymer matrix to the reinforcing fiber. Due to this fiber reinforced polymer composites have high strength and stiffness with low weight. Glass, boron, carbon and Kevlar fibers are commonly used as reinforcement in the polymer matrix (Hammed, 2009). Glass fiber reinforced composites offer the most reliable engineering materials compared with other composites by virtue of a large technology base, low cost of the fiber, stability, transparency, chemical resistance and hardness (Asi, 2009; Karakuzu *et al.*, 2008 b).

1.3 Glass Fiber Reinforced Polymer

Glass fibers reinforced polymer composites have continuous polymer as the matrix and embedded glass fiber as the reinforcing constituents. Glass fibers reinforced polymer composites have wide application in industry as it is produced from easily available raw materials. A variety of manufactured chemicals and natural minerals are used as basic raw materials for manufacturing glass fiber. Silica sand, limestone, and soda ash are the major constituents along with other ingredients that can include alumina, kaolin clay, nepheline syenite, borax and magnesite.

Glass fiber reinforced polymer composites exhibits different properties in all geometrical directions showing its anisotropic nature (Jones, 1999). These properties include poisson's ratio, modulus of elasticity, ultimate strength etc.

The applications of glass fiber reinforced polymer composites covers a wide area of applications ranging from aerospace, marine, automobile, civil, energy, transport, medical and defence, to name a few (Karakuzu *et al.*, 2008 a). The design of lighter and stronger materials is the key to success in this field. These materials are to be designed for high temperature usage and offer better corrosion resistance than metals. In order to achieve specific geometries and features, structural elements made up of composite materials generally need to be joined (Nerillia *et al.*, 2015; Davim *et al.*, 2004).

1.4 Joints in Composites

The applications of composites in different fields need these composites to be joined with each other or with other metal/alloy components. Otherwise also, to get ease in transportation of material, and to get flexibility in application, it is always convenient to manufacture various parts and then join them together as per requirement (Icten *et al.*, 2006). But these joints form a weak part in the components and hence invite the failure at early stages.

A new direction of concern is opened in the world of composites by the joining of fiber reinforced composites with other materials. The assembly of composites can be processed by joining parts which becomes an imperative and necessary domain (Qin *et al.*, 2013). The joining seems to be simple but it is much more than that because it is a critical issue. Stress concentration and improper design in a joint can cause structural failure in a joint (Irisarri *et al.*, 2012). It also adds manufacturing cost and labor cost to the product. There are two joining methods which depend upon the application area and complexity of the structure. They are Adhesive joints (permanent Joint) and Mechanical joints (semi-permanent or temporary joint) (Atas, 2009). The adhesive joints are not easy to disassemble. If disassembled, it will result in damage of one main component. So, the mechanical joints are used as it is easy to disassemble without damaging the main components.

1.4.1 Adhesive Joints

In adhesive joints, components are joined with the help of filler material called adhesive. These joints are made with two substrates called adherents using adhesives like epoxy, methyl acrylate, cyanoacrylates, anaerobic, silicones, or phenolic. Adhesive are selected on the basis of cost, service environment, type of composites and applications. The type of failure in adhesive joints is of two types which comprises of adhesive failure and cohesive failure. The failure between the adherent and adhesive which occurs at interface is called adhesive failure. When the bond between adhesive and the substrate material has high strength whereas the inherent strength of adhesive or substrate is low then cohesive failure occurs (Mehrabadi, 2012). The factors like type of adhesive, wettability of adhesive, mechanical properties of adhesive and adherent bonding between adhesive and adherent, influence the failure of adhesively bonded joints.

1.4.2 Mechanical Joints

In the mechanical joints, fasteners are inserted into the holes, drilled in the joining components. It includes bolting, riveting, screw and pin joints. The structural failure of mechanical joints are caused by number of factors that include loading direction, mechanical properties of fasteners, stress concentration, delamination, fiber pull out, matrix burning during drilling and cutting of fiber reinforced composites and location of hole in composite plate (Khashaba *et al.*, 2013).

Mechanical joints are temporary joints which can be used to assemble and disassemble of the parent components (Sen *et al.*, 2008). The repair and maintenance of the parent components without destroying them are the main reason of favouring mechanical joints over adhesive joints.

1.5 Design of Mechanically Fastened Joints

The mechanical joints may fail either due to the failure of the composite plate having the joint or due to the failure of the fastener. If the fasteners are stronger than the composite plate, the focus is on the behaviour of composite plate and types of failure in the composite plate. To study the failure behaviour of composite plates, the pin joints are used as they are simple to analyze.

1.5.1 Pin Joints

In fiber reinforced polymer composites, the pin joints can be used to study the failure behavior of the composite plates as these are easy to assemble and disassemble with no clamping force on the composite plates (Karakuzu *et al.*, 2008 a). A hole is drilled in the plate and a pin is inserted in the hole which is far stronger than the polymer composite plate. The load which is exerted will cause the failure in the composite plate as the pin will not be affected by the applied load. Hence, the joint's strength wholly depends on the plate's strength. Local damage and stress concentration are created by pin joints that further lead to decrease in the strength of joint (Icten *et al.*, 2006, Li *et al.*, 2014). The failure analysis around the hole in the pin joint is highly critical for the design of joints. So much attention is needed to determine the modes of failure and the strength of pin joint.

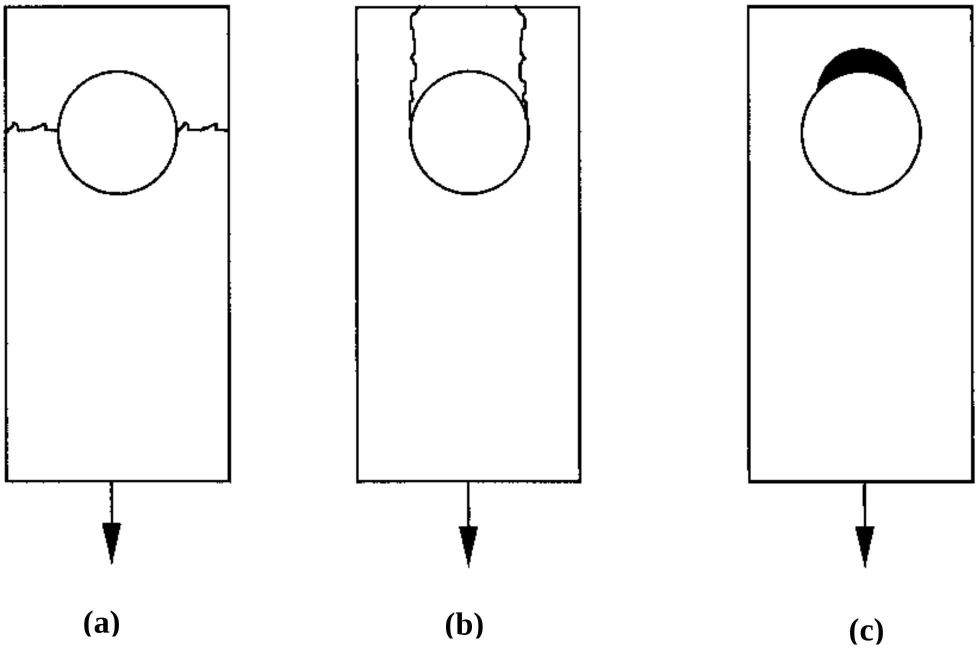

Fig. 1.2 Basic failure modes (Pisano *et al.*, 2012) (a) Net tension (b) Shear out (c) Bearing

Figure 1.2 shows the three basic modes of failure in pin joints *i.e.* Net tension, Shear out and Bearing mode (Sen and Sayman, 2011). The catastrophic nature of failure modes are in net tension and shear out modes which occurs without any warning whereas the bearing mode of failure holds the maximum load carrying capacity (Asi, 2009, Okutan *et al.*, 2001).

(i) Net tension failure: In the net tension mode of failure, the split occurs along the line perpendicular to the longitudinal edges. It generally occurs, when the ratio of width of the specimen to the diameter of hole is very small (Ondurucu *et al.*, 2012). If W is the width of the composite plate, D is the diameter of the hole, t is the thickness of the plate, P_t is the failure load of the member, then the net tension strength (σ_t) of the plate will be given by equation (1.1) (Kweon *et al.*, 2004).

$$P_t = (W - D) \times t \times \sigma_t \tag{1.1}$$

(ii) Shear out failure: In shear out failure, the split occurs along the line from the hole towards the transverse edge. In such cases the material ahead of the hole moves out with the increase of the load. The shearing strength of the plate (τ_s) can be mathematically defined by the equation (1.2) (Okutan *et al.*, 2001).

$$P_s = 2 \times E \times t \times \tau_s \quad (1.2)$$

Where, E is the edge distance *i.e.* the distance from edge to the center of the hole and P_s is the failure load of the plate.

(iii) Bearing failure: Bearing failure occurs when the plate fails to resist the crushing force exerted by the pin. In such failures the hole widens in the direction of the force applied. Bearing strength (σ_c) of the plate is given by equation (1.3) (Icten *et al.*, 2006).

$$P_c = D \times t \times \sigma_c \quad (1.3)$$

Where, P_c is the crushing failure load of the plate.

1.5.2 Strength Parameters

To decrease failure in pin joints, it is needed to increase the strength of the joint. The following are the properties that affect the joint strength (Scalea *et al.*, 1998; Chen *et al.*, 1994; Aktas and Dirikolu, 2004).

(i) Material properties: It includes type of fiber material and its orientation, type of matrix material, and stacking sequence of laminate.

(ii) Geometric properties: It includes geometry of composite plate (Length, Width and Thickness), size and location of the hole in the composite plate.

(iii) Fastener properties: It includes type, size and preloading of fastener, size of hole and tolerance.

(iv) Design properties: It includes the application of the joints depending upon the loading direction, loading type, joint type (single lap, double lap), geometry of joint (pitch, edge distance, hole pattern etc.), environment and failure criteria.

1.6 Thesis Overview

As discussed in the previous sections, glass fiber reinforced composites have wide applications in different areas. These areas require the components to be joined with each other. The mechanical joints are preferred when the components need to be assembled and disassembled as per their requirements. A hole is to be drilled to insert a fastener to prepare a mechanical joint. These joints are the potentially weakness in the structure and exhibits the unexpected failure. Thus, for the efficient design of the structure, analysis of the mechanical joints in composites is important and complicated due to the anisotropic nature composites and stress concentration around the hole. So, the present work deals with the failure analysis of the pin joints in the glass fiber reinforced polymer composites and to improve the performance of the pin joints under the influence of geometric and material properties. Glass fiber reinforced laminates with addition of nanofillers were prepared using the hand layup method and cured using compression moulding machine. Tsai-Wu failure theory along with the characteristic curve method in finite element method was used to analyze the failure of the pin joints numerically, which was further validated with experimental testing of the same.

This thesis is divided into seven chapters.

Chapter 1 gives the basic introduction of the polymer composites and the joints. It covers the various parameters and types of the failure in the joints of the fiber reinforced polymer composites.

Chapter 2 gives the literature review of the failure analysis of pin joints in glass fiber reinforced composite laminates. It also gives the literature on the performance of composites with the addition of the filler materials.

Chapter 3 deals with the discussion of different type of materials, methods along with the testing procedure which are used for the preparation of the polymer composite laminates. The effect of nanoclay on the mechanical properties is determined using the different ASTM standard for their testing. The effect of nanoclay was studied for three ply orientation *i.e.*, [0°/45°/90°], [0°/45°/0°] and [0°/90°/0°].

Chapter 4 is the study of the effect of the nanoclay on the bearing strength and failure mode of the single hole pin joints which were investigated both experimentally and numerically. The strength of [0°/45°/0°] and [0°/90°/0°] ply orientation were compared with and without the addition of the nanoclay content. Geometric parameters, *i.e*. E/D ratio and W/D ratio were investigated. The E/D and W/D ratios were varied from 2 to 5.

Chapter 5 presents the failure analysis of the double holes pin joint *i.e.*, serial and parallel holes using Taguchi method to reduce the experimental cost and time. Geometric parameters that are varied in case of double serial holes configuration are E/D, W/D and P/D ratio, P is the distance between the two holes and D is the diameter of the holes. In case of double parallel holes configuration the geometric parameters varied are E/D, P/D and K/D ratio where K is the distance between the side edge and the hole nearer to it. The geometric parameters *i.e.,* E/D, W/D and P/D ratio in case of serial hole configuration were varied from 2 to 5, whereas geometric parameters in case of parallel hole configuration were varied as: E/D from 2 to 5, K/D from 1 to 4 and P/D from 2 to 5.

Chapter 6 deals with the failure analysis of the multi holes pin joint to study the contribution of different geometric parameters on the resistive force. Multi holes pin joints were prepared from the [0°/90°/0°] ply orientation, with 3 wt.% of the nanoclay. Three holes and four holes pin joint configurations were studied with four independent geometric parameters. Taguchi method was used to analyze the contributions of these geometric parameters on the strength of the multi holes pin joint.

Chapter 7 presents the conclusions and future scope of the work.

Chapter 2 - Literature Review

A comprehensive literature has been studied and presented in this chapter which will lead to identification of the gap in literature and objectives of the present research work. Now a days fiber reinforced polymer composites are widely used in load bearing applications. For the design of structures different components are required to be joined. These joint are the weak parts due to the stress concentration around the hole drilled to make joint. These high stress concentration areas result in structural failure of the components. The problem further complicates due to anisotropic nature of the material. The strength of the joints in fiber reinforced polymer composites depends on the various parameters *i.e.*, material, geometric parameters, number and type of the fasteners used in the joints. The strength of the joint is increased if the laminates strength is increased. So, the literature has been studied in two broad areas which are given below.

(i) The effect of the different parameters on the failure load and failure modes of the pin joints.

(ii) The effect of the nanofillers in the polymer composite laminates which can be used to prepare the pin joints.

2.1 Study the Effect of Different Parameters on the Strength of Pin Joints

The strength of pin joints depends upon material properties, the stacking sequence of the fibers, geometrical properties, number of holes in the composite plate and the direction of the applied load. A number of researchers have studied the behavior of the joints under the influence of such parameters, both experimentally and numerically. The following sections show the literature study of pin joints under different parameters.

2.1.1 Effect of the Stacking Sequence on the Strength of the Pin Joints

Large number of the researchers found that the fiber orientation or laminates lay-up affect the strength of the joints. Baba (2006) examined the effect of two ply orientations *i.e.*, $[0/90/0]_s$ and $[90/0/90]_s$ in the single hole pinned joint which were prepared from E/glass-epoxy composite laminates. Pin joints were analyzed experimentally as well as numerically to determine the strength of the joints. It was observed that $[0/90/0]_s$ ply orientation had the higher strength as compared to $[90/0/90]_s$ ply orientation for higher value of E/D and W/D ratio. Okutan and Karakuzu (2003) considered $[0/\pm45]_s$ and $[90/\pm45]_s$ ply orientation to analyze the bearing, net tension, and shear out strength of the single hole pinned joints. Pin joints, having the orientation $[0/\pm45]_s$ took higher load which was corresponding to the higher bearing strength. Geometric parameters E/D and W/D had the remarkable effect on the failure modes of the pin joint. Six ply orientation *i.e.,* $[0/\pm45]_s$, $[\pm45]_{2s}$, $[0/90/0]_s$, $[90/0/90]_s$, $[90/0]_{2s}$ and $[90/\pm45]_s$ were studied for the single hole pin joints by Baba (2006). The effect of joint geometry was analyzed by varying E/D and W/D ratio from 1 to 5 and 2 to 5 respectively. The strength was increased by increasing the width and edge distance up to certain value beyond which the increase in strength is insignificant. Higher effect in the strength was observed in the $[90/0]_{2s}$ and $[0/90/0]_s$ ply orientation with the variation in E/D and W/D ratio. It was also shown that for the shear out failure there was the crack occurrence in the matrix material and brittle fracture occurred in fiber for the bearing failure (Ondurucu *et al.*, 2012).

Mechanical joints were also studied under the influence of preload conditions along with the geometric parameters. Three ply orientations *i.e.*, $[0/0/45/45]_s$, $[0/0/45/-45]_s$, and $[0/0/30/30]_s$ were used to prepare the mechanical joint with single hole. These laminates were prepared from the glass fiber epoxy composites. It was observed that preload considerably affected the strength and failure modes. It was also observed that the material and geometric parameters fully influenced the strength and failure behavior of the joints (Sen *et al.*, 2008). Finite Element Method along with Tsai- Wu failure criteria (Tsai and Wu, 1971) was also used to find the stress distribution around the hole and to analyze the effect of the stacking sequence in the single hole pin joint (Petrovic *et al.*, 2012).

2.1.2 Effect of Geometric Parameters on the Strength of the Single Hole Pin Joints

In single hole pin joints, as shown in the Fig. 2.1, diameter of the hole, edge distance and width of the specimens are the main dimensions which are required to locate the hole symmetrically in the composite plates. Edge distance to diameter of hole (E/D) ratio and width to diameter of hole (W/D) ratio gives the systematic approach to analyze these dimension which includes the effect of the diameter of the hole. E/D and W/D are the two geometric properties or parameters which were studied by the number of researchers to analyze the strength and failure modes in single hole pin joints.

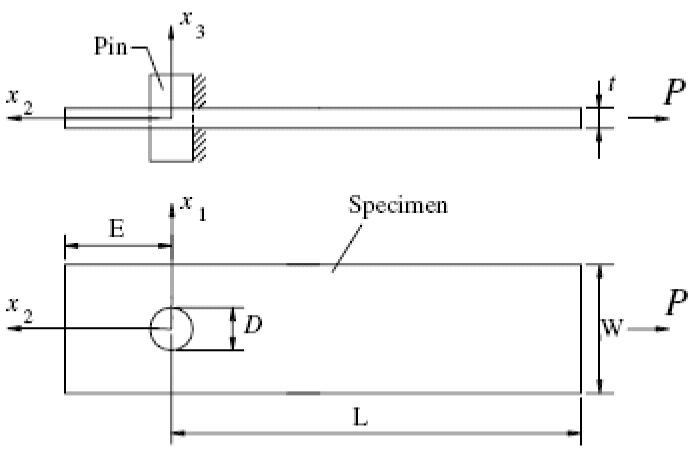

Fig. 2.1 Geometry of the composite plate with circular hole and inserted pin (Icten *et al.*, 2006)

Okutan *et al.* (2001) examined the effects of E/D and W/D ratio on the bearing strength of single hole pin joints prepared from woven laminated composites. Laminates were prepared from glass/epoxy composites using compression moulding method. It was observed that the when E/D and W/D ratio, increased the loading capacity of the pin joints increased. The tests were carried out in Universal Testing Machine. Load-displacement curves also depicted that for lower value of W/D ratio, displacement was 0.2 mm which was further increased to 0.8 mm with increasing the W/D ratio. Beyond some critical values of E/D and W/D ratios the increase in the loading capacity was insignificant. McCarthy *et al.* (2005) developed the three dimensional FEM analysis to study the behavior of single lap, single bolt joint. The non-linear FEM code was generated in MSC.Marc. which was validated with the experimental findings. Material modeling was done for the graphite/epoxy composites. The validated model was also used to analyze the effect clearance on joint stress state, stiffness and failure initiation. Icten *et al.* (2006) used two dimensional FEM analysis to determine the failure load and failure mode in the single hole pin joints. Three failure theories were used in the finite element analysis *i.e.,* Maximum Stress, Hashin and Hoffman criteria. The numerical results were verified from the experimental testing of the pin joint prepared from woven kevlar epoxy composite laminate.

Failure load and failure modes of single and double hole pined joint was investigated with the variation of E/D and W/D ratios, numerically and experimentally. Characteristic curve method was used along with the Yamada-Sun failure theory. Finite element analysis was done to find the stress distribution around the hole. It was observed that joints fail with the progressive mode of failure when E/D and W/D ratio were greater than four (Aktas *et al.*, 2009). Atas (2009) investigated the effect of non-orthogonal fiber with small weaving angle and E/D and W/D ratios, on the loading capacity of pined joint. The identical orientation showed the lesser load carrying capacity and undesirable damage in the single hole pin joint. Irisari *et al.* (2012) and Atas and Soutis (2014) used cohesive elements in the viscoelastic models along with the progressive damage approach to analyze the mechanical fasteners in the composite laminates. The numerical model was also used to analyze the propagation and delamination damage in the laminates. Numerical results were verified with the experimental testing of the joints. Protruding head or countersink fasteners effect on the strength, failure mode and stiffness of the mechanical joint in composite was analyzed with finite element analysis which was further verified with the experimental findings (Qin *et al.*, 2013). Limit analysis approach was also used to analyze the strength of pin joints analytically. This approach was further used to analyze the effect of interface and joint geometry in the pin joint (Limam *et al.*, 2011). Aktas (2011) studied the effect of E/D and W/D ratio on the failure load and failure mode of the single hole and double serial holes pin joints. The distance between two holes was kept constant to analyze the failure load and failure mode of the serial hole pin joints. Numerical analysis was done using the ANSYS software program and Yamada Sun failure theory. Olmedo *et al.* (2014) proposed an analytical model which combined characteristic curve model and mass spring model to analyze the bearing strength and stiffness of the pin joints. Spring elements were used to find out the stiffness in all plies which was used to calculate the bearing load. Spring model was helpful to find out the displacement which was necessary to calculate the stresses on the characteristic curve.

Asi (2010) observed that the bearing strength of the single hole pin joint was increased with the addition of Al_2O_3 particles. Al_2O_3 particles were added in the glass epoxy composites, which were used to prepare the pin joints. Al_2O_3 particles were loaded with three different wt. % *i.e.,* 7.5, 10 and 15 wt. %. Highest bearing strength of the pin joint was achieved with 10 wt.% loading of the Al_2O_3 particles. Beyond the 10 wt. % loading of the Al_2O_3 particles the bearing strength of the pin joints was decreased. Arun *et al.* (2014) analyzed the mechanical joints of glass fiber reinforced polymer with addition of TiO_2 and ZnS loading in the matrix materials. The strength of mechanical joints was increased with addition TiO_2 and ZnS fillers and was higher up to 2 vol.% of these fillers. The strength of mechanical joint was higher with the addition of ZnS filler as compared to the addition of TiO_2 filler in the matrix.

2.1.3 Effect of Geometric Parameters on the Strength of Multi Hole Pin Joints

Loading capacity of the joint can be increased by increasing the number of fasteners. To insert the numbers of fasteners in the composite plate multiples holes are drilled. The numbers of the geometric dimensions to locate the holes in composite plate are increased. Numbers of researchers have studied these different geometric parameters both experimentally and numerically. These parameters were required to specify the location of holes in the multi holes joints.

Karakuzu *et al.* (2008 a, 2008 b) investigated the effect of three geometric parameters on the failure mode and failure load in the double holes pin joints. Pin joints were prepared from woven glass-vinylester laminates with serial and parallel holes configuration. Three geometric parameters *i.e.*, edge distance to diameter of hole (E/D) ratio, distance between the upper or lower edge and centre of the hole to hole diameter (K/D) ratio and the distance between the holes to diameter (M/D) ratio were studied in the parallel holes configuration. E/D, W/D and M/D ratios were investigated in the serial holes configuration. It was seen that E/D ratio was the most effective parameter to increase the strength of the double holes pin joint. K/D and M/D ratio were not as effective as E/D ratio. Whereas, in serial hole pin joint, W/D showed the influence on the failure load and failure mode of the pin joint. It was suggested that W/D and E/D should be greater than three for the bearing mode of failure. Progressive damage analysis with Hashin failure theory was used to analyze the pin joints numerically and results were compared with the experimental outcomes.

Three hole pin joints were investigated with three geometric parameters *i.e.*, E/D ratio, distance between two holes in longitudinal direction to hole diameter (F/D) ratio and distance between holes in transverse direction to hole diameter (G/D) ratio. The E/D, F/D and G/D ratios were varied from 1 to 5, 2 to 6 and 3 to 5 respectively. At low value of E/D ratio, joints fail with shear out failure mode and mode of failure changed when E/D ratio increased. Loading capacity of the joint increased with increase in the value of E/D, F/D and G/D ratio. G/D ratio showed the least effect on the load bearing capacity of the pin joint (Karakuzu *et al.*, 2010). Kishore *et al.* (2009) also studied three and four holes pin joint configurations by considering the three geometric parameters. These joints were tested experimental and numerically. Tsai-Wu failure theory associated with degradation in mechanical properties was used in finite element analysis to evaluate the failure modes and failure load of pin joints. Pisano *et al.* (2012, 2013) proposed limit analysis approach to analyze the failure mode and failure load of the multi pin joints. This method was used at lamina level of the laminate associated with Tsai-Wu failure criteria. Numerical results were verified with existing experimental results.

2.2 Effect of Different Nanofillers in the Polymer Composite Laminates

The various mechanical properties of the polymer composites were enhanced with the addition of nanofillers in the matrix materials. This enhanced materials can be used for the preparation of the pin joints to obtain the higher strength of the joints. A comprehensive literature has been reviewed and presented for different nanoparticles which were used in the polymer composites.

2.2.1 Effect of the SiO_2 and TiO_2 in Polymer Matrix

Chang *et al*. (2005, 2006) investigated the performances of epoxy-based composites, filled with short carbon fibre, graphite, PTFE and nano-TiO_2 in different proportions and combinations. The patterns of frictional coefficient, wear resistance and contact temperature were examined by a pin-on-disc apparatus in a dry sliding condition under different contact pressures and sliding velocities. The experimental results indicated that the addition of nano-TiO_2 could apparently reduce the frictional coefficient, and consequently reduce the contact temperature of fibre-reinforced epoxy composites. As a result, the wear resistance of the composites was significantly enhanced, especially at extreme wear conditions. Compared to traditional fillers, epoxy nanocomposites attained improved wear resistance and load-carrying capacity.

Li *et al.* (2007) modified epoxy resin with nano-SiO_2 (30-40 nm) and 3 μm, respectively, and γ-glycidoxypropyltrimethoxy silane. The bonded stationary phase was formed with γ-glycidoxypropyltrimethoxy silane between nano-SiO_2 and epoxy resin which is indicated by IR spectra. Thermogravimetric analysis, impact strength and bulk resistivity tests showed that initial decomposition temperature, impact strength and bulk resistivity of epoxy resin-based composite increased and then decreased after nano-SiO_2 content reached upto 4 wt.%. The optimal values were 323^{o}C, 89.2 kJ m^{-2} and 3.56×1014 Ωcm, respectively. The similar behavior was observed on standard SiO_2/epoxy resin-based composites with optimal values as 308°C, 17.13 kJm^{-2} and 2.80×1014 Ωcm, respectively.

It was also shown that the toughness of nano-SiO_2/Epoxy resin-based composite and standard SiO_2/epoxy resin-based composite increased and then decreased after nano-SiO_2 and standard SiO_2 content reached upto 4 wt.%.

Uddin and Sun (2008) developed a technique to improve the strength of unidirectional composites by enhancing the matrix properties through nanoparticles infusion. To make fiber composites a commercially available standard DGEBA epoxy with silica nanoparticles were used. After the experimentation the TEM images showed very uniform dispersion of silica nanoparticles with a size distribution of about 20 nm. Compression test revealed a substantial improvement of 40% in elastic modulus of the modified epoxy. To fabricate unidirectional E-glass fiber reinforced silica/epoxy nanocomposites, a modified vacuum assisted resin transfer molding process was used and inclusion of silica nanoparticles dramatically increased the longitudinal compressive strength and moderately increased the longitudinal and transverse tensile strengths. In the end the compression testing results were verified by microbuckling model.

Zhu *et al*. (2007) prepared Silica/polyurethane (SiO_2/PU) nanocomposites. The properties of SiO_2/PU-modified electrophoretically prepared membrane had a significant improvement as compared to those of unmodified and PU-modified membranes. It was noteworthy that both strength and toughness of the electrophoretically prepared membrane increased considerably due to incorporation of rigid silica encapsulated by tough PU.

Yao *et al*. (2008) studied Macro/microscopic fracture characterizations of the SiO_2/epoxy nanocomposite experimentally. Both the load–displacement curve and the static fracture toughness were obtained using a three point bending test. Full field deformation information around the crack tip in nanocomposites was investigated using digital speckle correlation method. The microscopic fracture characterizations and crack propagation behavior were analyzed by means of SEM and FE-SEM. The influences of nanoparticle SiO_2 content on fracture behaviors of nanocomposites were analyzed. The results showed that the nanocomposite with 3 wt.% nanoparticle had higher fracture toughness and larger deformation resisting capability than other nanocomposites.

Bittmann *et al*. (2011) studied about the ultrasonic dispersion of nanoparticles in epoxy resin. The affect of sonicating with and without mechanical stirring on the particle size was investigated. The effect of TiO_2-nanoparticles into the epoxy resin on the mechanical performance was examined using three point bending, Charpy, impact and fracture toughness tests and demonstrated that the TiO_2-nanoparticles lead to a simultaneous improvement of all the given properties. The best mechanical properties were gained for the nanocomposite with 10 vol.% of particle content, except for the Charpy toughness, which was maximum at a filler content of 2 vol.%.

Jumahat *et al.* (2012) studied the effect of nanosilica on the tensile stress-strain response of Epikote 828 epoxy polymer and a 40 wt.% nanosilica/epoxy masterbatch was used to prepare a series of nanocomposites with 5–25 wt.% of nanosilica content. The static uniaxial tensile tests were conducted and the tensile stress-strain response and tensile properties of unmodified and nanomodified epoxy polymers were investigated. Transmission electron microscopy was used and the degree of dispersion of the silica nanosphere particle in the epoxy matrix was investigated. It was found that the incorporation of a well-disperse nanosilica improved the tensile properties of the polymer. The addition of 25 wt.% nanosilica enhanced the tensile modulus and strength to about 38% and 24%, respectively, compared to the neat polymer without sacrificing the failure strain.

Hua *et al.* (2013) investigated the mechanical behavior of TiO_2 nanoparticle-reinforced resin-based dental composites through the validated nanoscale RVE. The effective Young's modulus and yield strength of the composite increased almost linearly with the increase of nanoparticle from 1 vol.% to 5 vol.% considering perfect nanoparticle dispersion. The effective Young's modulus and yield strength of the composite was dependent on the interphase stiffness, while its sensitivity with respect to nanoparticle stiffness was minimal. Nanoparticles with larger aspect ratio improved the bulk response of the composites. For nanoparticle aspect ratio larger than 30, the reinforcing effect reached saturation. These results were used to enhance the fundamental understanding of mechanical behavior of nanoparticle-reinforced resin-based dental composites, and provided guidance for optimizing the compositions of dental composites.

2.2.2 Effect of Nanoclay in the Polymer Matrix

Myskove *et al.* (2003) investigated the influence of montmorillonite concentration and the temperature regime on the cure rate and mechanical properties of the composite material. The addition of the modified clay to the epoxy-amine hardener system influenced the rate of curing reaction. The presence of clay increased the modulus both in the glassy state and in the rubbery region. The addition of clay considerably improved the tensile mechanical properties of epoxy systems.

Lam *et al.* (2005) experimentally studied the hardness and interlaminar shear properties of nanoclay/epoxy composites with different amount of nanoclay content, which formed different sizes of nanoclay/epoxy clusters after mixing in an extruder. The micro-hardness of the composites could be enhanced when a small amount of nanoclay was added into the epoxy. However, there was an optimal limit after which the hardness was dropped as nanoclay content was increased. This might be due to the size of the clusters reaching a crucial limit and therefore the reinforcing function of the nanoclays decreased. Interlaminar shear test showed the short beam shear strength of the epoxy decreased after adding few percents of nanoclay particles. A shiny surface of the clusters, captured from the fractured samples also revealed that a weak interfacial bond existed between the cluster and matrix, which led to poor short beam strength of the composites.

Brunner *et al.* (2006) investigated the effect of nano-modified epoxy matrix on the delamination resistance in a fiber-reinforced laminate as compared to a laminate with neat epoxy as matrix material. An increase between 40-50% in fracture toughness and around 10-20% in energy release was observed in nano-modified epoxy relative to the neat epoxy. With the addition of 10 wt.% of functionalized organosilicate clay, increase in tensile and compressive modulus by more than 50% was observed.

Chowdhury *et al.* (2007) prepared woven carbon/epoxy laminates with the epoxy modified using Nanomer I-28E nanoclay at different weight percentages. Thermomechanical and flexural properties of the nanophased composites were determined and compared with those of neat samples. The microstructural characterization was carried out through Scanning Electron Microscopy. The improvement of about 31% and 21% was observed in strength and modulus, respectively. The properties were maximum at 2 wt.% of nanoclay in carbon/SC-15 epoxy composites.

Jawahar *et al.* (2006) investigated the clay-thermoset polyester nanocomposites and conventional clay filled composites. Composites were prepared with clay contents of 1 wt.%, 3 wt.% and 5 wt.%. Tribological property of the nanocomposite system was studied to assess the influence of nanoclay which was compared with conventional clay filled composites. The nanocomposites exhibited a maximum of 85% improvement in wear resistance and 35% decrease in coefficient of friction. The highest wear resistant and least coefficient of friction was observed in the nanocomposite with a clay content of 3 wt.%.

Kim *et al.* (2008) mixed nano-particle additives such as carbon black and nanoclay with epoxy resin in order to improve the fracture toughness of epoxy resin. The fracture toughness was measured using the single edge notched bend specimen at the room (25^oC) and cryogenic temperature (-150^oC). The results showed that reinforcement with nano-particles improved the fracture toughness at the room temperature, but decreased the fracture toughness at the cryogenic temperature in spite of their toughening effect. If the nano-particle reinforced matrix is used for a composite laminate, the interlaminar fracture toughness and the impact characteristic can be improved at the room temperature where as at the cryogenic temperature, un-reinforced epoxy may be able to provide better structural characteristics. Studies revealed that nanoclay improved adhesion of fiber and matrix, resulting in increase of the mechanical properties of composites.

Sundaram *et al.* (2008) prepared FRP with nanocomposites in the combination of polyester resin, E-glass fiber, and nano-montmorillonite (nanoclay) and studied their mechanical properties. The nano-FRP had high ultimate tensile strength and there was 50% improvement in ultimate tensile strength at 5 wt.% of nanoclay.

Mohan *et al.* (2009) studied the effect of curing temperature on nanocomposite structure and its properties. It was observed that properties and structure of nanocomposites was governed by curing temperature and clay content in the matrix. Higher curing temperature showed the increased mechanical properties over low curing temperature. Maximum increase in tensile properties was observed for 2 wt.% of nanoclay concentration irrespective of curing conditions.

Li *et al*. (2011) completely exfoliated epoxy/clay nanocomposites with comprehensive high performance using Nano-disassembling method. In this method, nano-SiO_2 was added into the montmorillonite and epoxy mixture system as disassembler to interact with montmorillonite (MMT). Due to the strong interaction between nanoscale particles, the MMT layers were completely disassembled into elemental nanometric mono-platelets. These mono-platelets took interlacing arrangement with the disassembler particles in the resultant nanocomposites. At the optimal MMT content of 5 phr, tensile modulus and tensile strength increased by 64.2 and 52.3%, respectively. Flexural modulus enhanced by 7.1%, flexural strength by 14.6% and notch impact strength by 37.7%. Glass transition temperature and thermal decomposition temperature moved to higher temperatures by 10.1 and 5.7 ^oC, respectively.

Azeez *et al.* (2012) reviewed the work carried out on epoxy clay nanocomposites. It was stated that the final morphology, physical, chemical and barrier properties of the nanocomposites were influenced by processing method, clay modifier and curing agents. Epoxy clay nanocomposites showed remarkable improvement in tensile, flexural and fracture toughness properties. Thermal stability and barrier properties were significantly improved by the incorporation of clay particles to epoxy systems. Coefficient of Thermal Expansion and water permeation of the nanocomposite were reduced considerably.

Jumahat *et al.* (2012) studied the effect of montmorillonite clay on the compressive properties of Epikote 828 epoxy and prepared a series of epoxy-based nanocomposites with 1-5 wt.% nanoclay content. Using transmission electron microscopy the degree of dispersion and exfoliation was investigated. The static uniaxial compression tests were conducted in order to study the effect of nanoclay on the compressive stress-strain behaviour and compressive properties of the Epikote 828 polymer. It was found that the compressive properties depend on the degree of exfoliation of the clay nanoplatelets in the epoxy and recorded reduction in compressive strength for 1 wt.% and 3 wt.% of nanoclay. It was seen that the intercalated structure of nanoclay in the polymer created high localized stresses in the matrix during compression which led to premature failure.

Zhou *et al.* (2012) performed Dynamic Mechanical Analysis (DMA), Thermogravimetric Analysis (TGA), and flexural tests on unfilled, 1, 2, 3, and 4 wt.% clay filled SC-15 epoxy to identify the effect of clay weight fraction on thermal and mechanical properties of the epoxy matrix. The flexural results indicate that 2 wt.% clay filled epoxy showed the highest improvement in flexural strength. The DMA studies also revealed that 2 wt.% system exhibit the highest storage modulus and Tg as compared to neat and other weight fractions. Based on these results, the nanophased epoxy with 2 wt.% clay was then utilized in a vacuum assisted resin transfer molding set up with carbon fabric to prepare the laminated composites. The effectiveness of clay addition on thermal and mechanical properties of composites was evaluated by TGA, DMA, tensile, flexural, and fatigue test. 5^oC increase in glass transition temperature was observed in nanocomposite, and the tensile and flexural strengths improved by 5.7 and 13.5 %, respectively as compared to the neat composite. Based on the experimental results, a linear damage model combined with the Weibull distribution function was established to describe static failure of neat and nanophased carbon/epoxy.

2.3 The Scope and Objectives of Thesis

It has been observed that a large part of the research is focused on the performance of mechanical joints in fiber reinforced composites, both experimentally and numerically. The research is mainly carried out for the influence of two main parameters on the failure response of pin joints. First is the geometric parameters, the other is the material parameters related to arrangement of composite laminates. Very limited amount of work is reported on failure analysis of mechanical joints with the addition of different filler materials. The static tensile strength of the joints can be increased with the addition of different filler nanoparticles. The effect of different filler materials can be studied for single and multi pin joints. It was also seen that the strength of laminates also depends upon the orientation of fiber. On the basis of literature review discussed above, following gaps has been identified:

(i) Very limited amount of work is reported on the failure analysis of mechanical joints with the addition of different filler materials. The static tensile strength of the joints can be increased with the addition of different filler nanoparticles. The effect of different filler materials can be studied for single hole and multi holes pin joints.

(ii) The strength of the laminates changes with the orientation of the fiber. So the different orientation of the fiber can be studied to analysis the failure of the laminates. Change in orientation of the fiber can be studied to analysis their effect on the strength of the laminates.

(iii) For the multi hole joints, limited number of geometric parameters were studied and their individual contributions to increase the load carrying capacity of the mechanical joint were not analyzed.

The following objectives were planned for the research as per the gap identified in the literature

(i) Preparation of epoxy based unidirectional glass fabric nanocomposite laminates with different orientations of fabric.

(ii) Characterization of nanocomposite laminates using UTM, SEM and XRD.

(iii) Preparation of pin joint samples based upon optimized nanocomposite laminates.

(iv) Failure analysis and validation of pin joints for unfilled and filled glass epoxy nanocomposites.

Chapter 3 deals with the discussion of the materials and the basic process to prepare the laminates.

Chapter 3 - Materials, Methods and Testing

The present chapter deals with the discussion of different type of materials, methods along with the testing procedures which are used for the polymer composite laminates.

3.1 Materials

Materials used for the preparation of the laminates were epoxy, hardener, accelerator and glass fabric.

3.1.1 Resin

Epoxy as matrix material was used in the present work because of its higher adhesive bonding with glass fiber, higher strength and stiffness as compared to the other thermo set materials. The epoxy used 'L-12' also known as Lapox is DGEBA (Di Glycidyl Ether of Bisphenol-A). K-12 hardener and K-13 accelerator were used. Resin *i.e.*, (epoxy, hardener and accelerator) were supplied by Atul Ltd., Gujarat, India (www.atul.co.in). The properties of epoxy, hardener and accelerator are shown in Table 3.1 to 3.3.

Table 3.1 Physical properties of resin

Description	Density (g/cm^3)	Viscosity (mPa.s)
Epoxy(L-12)	1.1-1.2	9000-12000
Hardener(K-12)	1.15-1.25	150-230
Accelerator(K-13)	0.88-0.92	<10

Table 3.2 Mechanical properties of resin

Description	Specific Gravity	Tensile Strength (MPa)	Elastic Modulus in Tension (MPa)	Flexural Strength (MPa)	Compressive Strength (MPa)	Impact Strength (kJ/m^2)
L-12(100) + K12(100) + K-13	1.80-1.85	70-90	15000-16000	100-120	190-210	4-7

Table 3.3 Processing properties of resin

Property	Resin:Hardener:Accelerator Ratio (w/w)	Initial Mix Viscosity @40^0C (cPs)	Minimum Curing Schedule (Hours)
value	100:100:0.1-2	450	120^0C/2h 160^0C/(1/2)h

3.1.2 Unidirectional Glass Fiber

Unidirectional glass fiber was used as a reinforcing material to prepare the composite laminates because of its high strength to weight ratio and high stiffness to weight ratio. Unidirectional glass fiber was supplied by the Owens Corning India Pvt. Ltd, Mumbai, India (www.owenscorningindia.com). It was Advantex Unidirectional 1200 gsm glass fiber as shown in Fig. 3.1.

Fig. 3.1 Unidirectional glass fiber

Mechanical and physical properties of unidirectional glass fiber are shown in Table 3.4 and 3.5.

Table 3.4 Mechanical properties of unidirectional glass fiber

Description	Tensile strength (N/mm^2)	Tensile modulus in tension (GPa)	Elongation at breaking load (%)
Glass fabric	3100-3800	80-81	4.6

Table 3.5 Physical properties of unidirectional glass fiber

Description	Fiber type	Density(g/cm^3)	Area density (gsm)	Refractive index
Glass fabric	Advantex	2.62	1200	1.560-1.562

3.1.3 Nanoclay

Nanoclay, Cloisite 30B, was used because it has platelet shaped particle which can be dispersed in the epoxy resin. Cloisite 30B is a natural montmorillonite modified with a quaternary ammonium salt. Cloisite 30B is an additive for plastics to improve various physical and mechanical properties. It was supplied by the Connell Bros. Company Pvt. Ltd., Mumbai, India (www.connellbrothers.com). Physical properties of Cloisite 30B are given in the Table 3.6.

Table 3.6 Physical properties of Cloisite 30B

Composition	Moisture	Typical dry particle size (µm)	Packed bulk density (g/l)	Density (g/cm^3)	X ray results (nm)
Alkyl quaternary ammonium salt bentonite	<3%	<10	365	1.98	d_{001} = 1.85

3.2 Material Processing and Sample Preparation

Laminates were prepared using DGEBA based epoxy resin as matrix and glass fiber as reinforcement. There are several methods for the preparation of laminates. Hand layup technique along with compression moulding was used in the present work. The procedure used for the preparation of the laminates is given below.

3.2.1 Addition of Nanoclay in Epoxy Resin

The nanoparticles *i.e.*, nanoclay were mixed in the ratio of 1, 2, 3, 4 and 5 wt. %. in the epoxy resin. After this, hardener was mixed in the epoxy resin and then accelerator was added to the solution to accelerate the process. Mass ratio in terms of parts per hundred of fiber is given in Table 3.7.

Table 3.7 Nanoclay-resin formulation as per hundred parts of resin

Sr. No.	Nanoclay (wt.%)	Parts per hundred of resin		
		Resin	Fiber	nanoclay
1	1	100	152.04	1.01
2	2	100	152.04	2.04
3	3	100	152.04	3.09
4	4	100	152.04	4.17
5	5	100	152.04	5.26

3.2.2 Stirring of Epoxy-Clay Mixture in Homogenizer

The mixture of resin and nanoclay were homogenized using a homogenizer at 14000 rpm for 15 minutes and brought to a state where the constituents were equally distributed throughout the mixture. The IKA T25 homogenizer was used in the present work.

Homogenizer initiates the crystallization process and breaks down the molecules of resin to such a smaller size so that they remain evenly dispersed instead of rising to the top. It is based on the principle of turbulence. The energy dissipating in the liquid generates intense turbulent eddies. These eddies are of the same size as of average diameter of constituents. The intense energy of turbulence and localized pressure differences are responsible for tearing of molecules into reduced average size. The molecules of resin disperse thoroughly with the molecules of nanoclay.

3.2.3 Sonication of Epoxy-Nanoclay Mixture

After the process of homogenization, the mixture was sonicated for 10 minutes using a sonicator. Q Sonica 700 with probe diameter 0.5” was used in the present work. The ultrasonic waves were passed through the mixture so that the constituent particles get agitated. Sonication was done with the amplitude of 60 Hz and pulse on - off time as 25 and 20 seconds, respectively.

3.2.4 Addition of Hardener and Accelerator in Epoxy-Nanoclay Mixture

After sonication process, keeping hardener to resin ratio as 1:1, hardener and accelerator were added to the epoxy-nanoclay mixture. The mixture was kept under homogenization for 15 minutes for ensuring proper mixing of all the solution. Thereafter, the resin was ready for preparation of laminated composites.

3.2.5 Hand Layup Technique

It is the simplest and oldest open moulding method to fabricate polymer composite materials. Glass fiber was cut into the required sizes with a cutter. Placing the first layer of the glass fiber on the Teflon sheet, resin was applied on it with a brush and then second layer was placed on it. The resin was applied on the second layer and the third layer was placed for the preparing the laminates with three layers of glass fiber. The hand roller was used to remove any entrapped air particles between the layers and facilitate the laminate to stick together. The laminates were prepared with different ply orientation and left for curing for 24 hours.

3.2.6 Compression Moulding

It is a closed-mould composite manufacturing process that uses force to mould a material. In the compression moulding process, a laminate was placed between metal plates. The heating of laminate was done up to 150^0C and a constant compressive force of 120 kN was applied for 30 minutes. The combination of heat and pressure produces a laminate with low void content and high fiber volume fraction. The laminate was cooled and was taken out of the hydraulic press. The compression moulding used in the present work has the capacity of 500 kN.

3.3 Mechanical Properties and ASTM Standards used for the Laminates

As per the above discussed method, laminates were prepared for the different orientation of the fiber with and without the addition of the nanoclay. Laminates were prepared with the different orientations *i.e.*, [0°/45°/90°], [0°/45°/0°] and [0°/90°/0°] of the fiber, with and without the addition of the nanoclay to analyze the mechanical properties of the laminates. The addition of the nanoclay were in the 1, 2, 3, 4 and 5 wt.% .

3.3.1 ASTM Standards used for the Laminate Testing

Composite laminates are non-homogeneous and anisotropic in nature. So their orthotropic mechanical properties were calculated along different material direction *i.e.* longitudinal and transverse directional.

Tensile and shear test were performed to calculate the different mechanical properties *i.e.*, Longitudinal Modulus (E_1), Transverse Modulus (E_2), Laminate Shear Strength (S), Longitudinal Strength in Tension (X_t), Transverse Strength in Tension (Y_t), Poisson Ratio (ν_{12}), Longitudinal Strength in Compression (X_c) and Transverse Strength in Compression (Y_c).

The shear tests were performed at 25 ± 2 ^{0}C on a Zwick-Roell Universal Testing Machine – Model Z010, Zwick-Roell, Germany, according to ASTM D5379 standard. A crosshead speed of 2 mm/min was maintained. At least three specimens of each blend were tested and the average values were reported. The Iosipescu test specimen, shown in Fig. 3.2, was tested using Iosipescu test fixture.

The specimens were placed in Iosipescu test fixture, in which the specimen was centered using the alignment pin and lightly clamped with the adjustable wedges. Then the load was applied to the specimen.

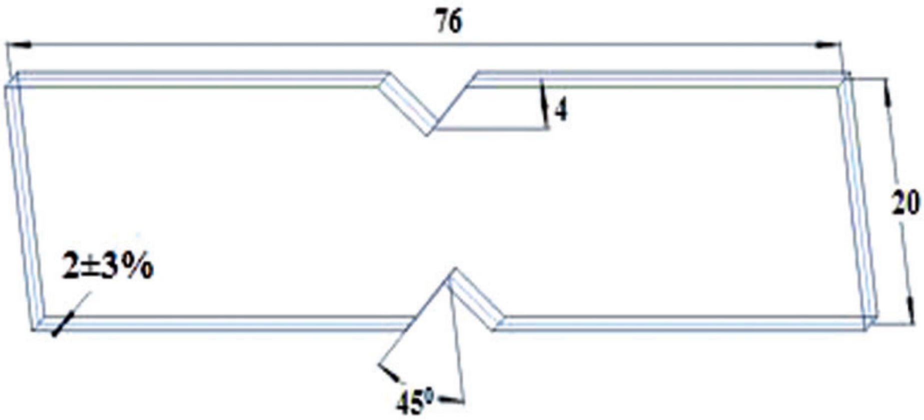

Fig. 3.2 Geometry of the Iosipescu shear test specimen

The tensile tests were performed at 25 ± 2 ^{0}C on a Zwick-Roell Universal Testing Machine – Model Z010, Zwick-Roell, Germany, according to ASTM D3039 standard. The grip to grip separation of the samples having 138 mm gauge length was 238 mm at the start position. A crosshead speed of 2 mm/min was maintained. At least three specimens of each blend were tested and the average values were reported.

Table 3.8 shows the different ASTM standards used for the testing of the various mechanical properties.

Table 3.8 Properties and ASTM standards

Tests/ Properties	**Symbols**	**Geometry**	**ASTM standard**
Longitudinal Tensile Test	E_1, X_t	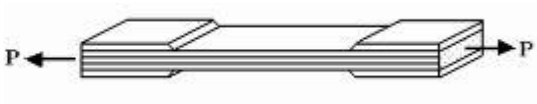	D3039
Transverse tensile test	E_2, Y_t	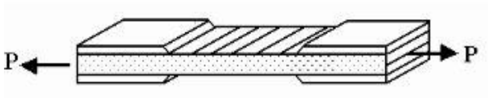	D3039
Shear Strength	S	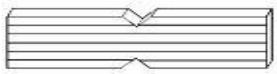	D 5379
Longitudinal Compressive Test	X_c		D3410-75
Transverse compressive Test	Y_c	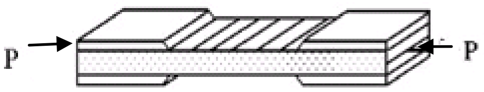	D3410-75

3.4 Mechanical Properties of Laminates

The results obtained for different ply orientations for various compositions of nanoclay are shown in Fig. 3.3.

It can be seen from Fig. 3.3 that the tensile modulus and tensile strength of the glass fiber reinforced epoxy composite for all the ply orientations increased up to 3 wt.% of nanoclay. Dispersed filler particles act as mechanical interlocking between the fiber and epoxy matrix which creates a high friction coefficient. The decrease in tensile modulus and tensile strength beyond 3 wt.% is due to the presence of a large agglomerate phase in the matrix which deteriorates their mechanical properties. Agglomeration may easily happen for smaller particles at higher filler contents due to the reduced interparticle distance (Friedrich *et al.*, 2005).

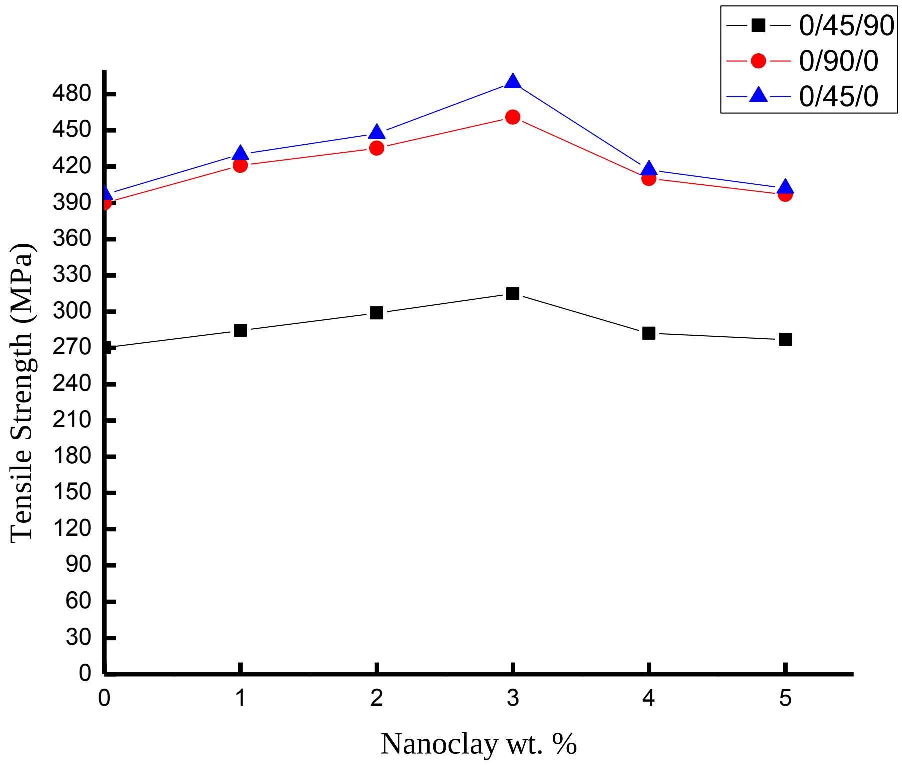

(a)

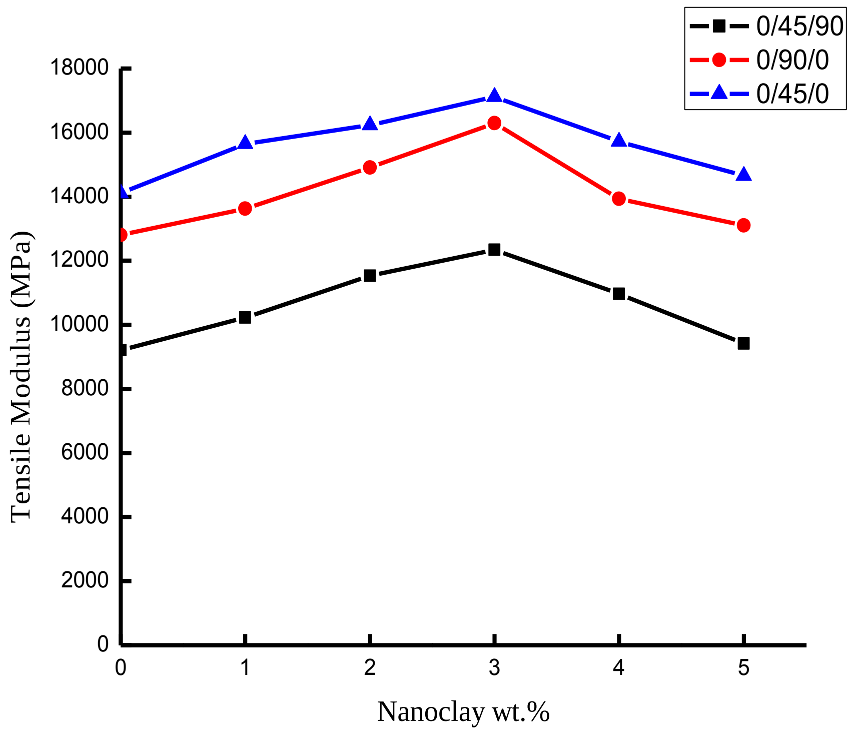

(b)

Fig. 3.3 (a) Tensile strength vs. weight percentage of nanoclay (b) Tensile Modulus vs. weight percentage of nanoclay

Table 3.9 shows the different mechanical properties of glass/epoxy nanocomposite laminates with different orientation of fiber and with different wt.% of nanoclay. Mechanical properties shown in Table 3.9 clearly show that the tensile and shear strength of the [0°/45°/90°] ply orientation with addition of 3 wt.% of nanoclay were very less as compared to the [0°/45°/0°] and [0°/90°/0°] ply orientations. It can be seen that [0°/45°/0°] ply orientation has higher longitudinal properties than the [0°/90°/0°] orientations whereas [0°/90°/0°] ply orientations have higher transverse properties than the [0°/45°/0°] ply orientation.

Table 3.9 Mechanical properties of glass fiber/epoxy composite laminate

Mechanical Property	**Symbol (Units)**	**Without nanoclay**			**3 wt.% of nanoclay**		
		[0°/45°/0°]	**[0°/90°/0°]**	**[0°/45°/90°]**	**[0°/45°/0°]**	**[0°/90°/0°]**	**[0°/45°/90°]**
Longitudinal Modulus	E_1 (MPa)	14112.45	12809.23	9213.23	17113.6	16297.3	12345.7
Transverse Modulus	E_2 (MPa)	6214.67	7802.23	5589.98	7145.67	8824.45	7324.56
Laminate Shear Strength	S (MPa)	123.45	155.68	132.14	139.44	178.45	151.12
Longitudinal Strength in Tension	X_t (MPa)	397.18	390.76	270.12	489.57	461.67	321.23
Transverse Strength in Tension	Y_t (MPa)	190.34	255.98	211.54	212.65	293.4	248.12
Poisson Ratio	ν_{12}	0.33	0.32	0.32	0.325	0.31	0.3378
Longitudinal Strength in Compression	X_c (MPa)	330.89	324.11	240.72	422.24	407.11	296.51
Transverse Strength in Compression	Y_c (MPa)	182.33	224.45	165.12	197.18	272.14	207.12

So both [0°/45°/0°] and [0°/90°/0°] ply orientations with the addition of 3 wt.% of nanoclay were selected for making the pin joints to compare their bearing strength and failure modes.

3.5 SEM and X-Ray Diffraction (XRD) Analysis

SEM and XRD analysis were done for the prepared resin and laminates to study the the dispersion of nanoclay in the epoxy. Figure 3.4 shows the SEM images of the resin and the laminates.

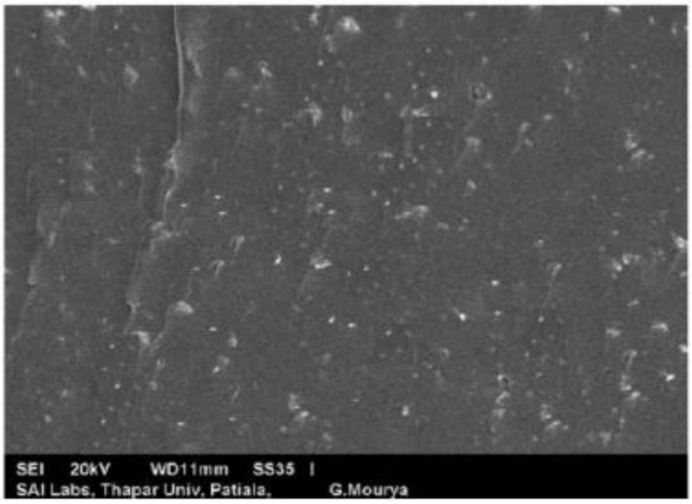

(a)

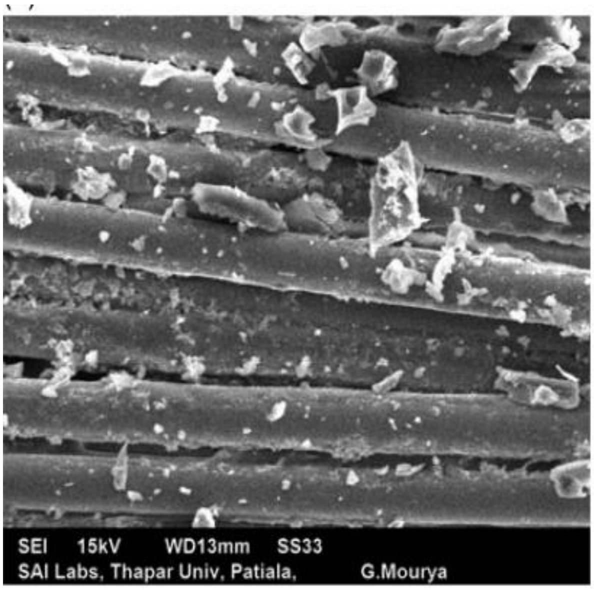

(b)

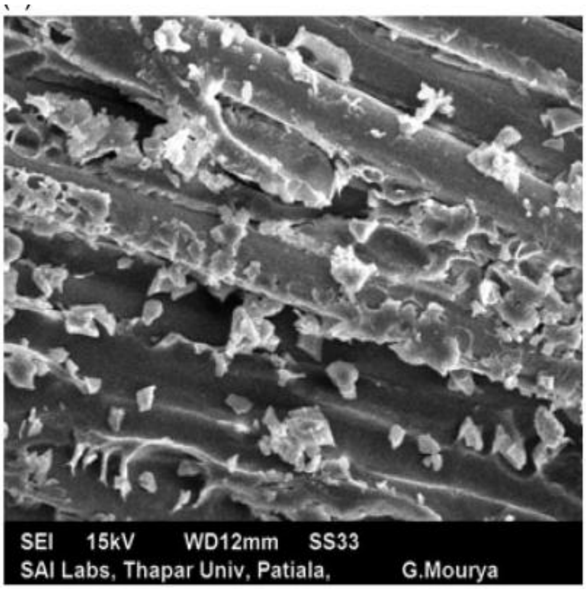

(c)

Fig. 3.4 SEM images (a) Epoxy with 3 wt.% of nanoclay (b) Laminates prepared from neat epoxy (c) Laminates prepared from epoxy with 3 wt.% of nanoclay

It can be seen from Fig. 3.4 (a) that there is uniform dispersion of the nanoclay particles in the epoxy. Proper dispersion of nanoclay particles in the resin generates large surface area interaction of polymer-filler with fiber. This interaction promotes the stronger interfacial bond between the fiber and the polymer. It can also be seen in Fig. 3.4 that the resin prepared with nanoclay had higher bonding with fiber than the neat epoxy shown in Fig. 3.4 (b). This indicates the formation of good interfacial bond between fiber and epoxy when mixed with nanoclay.

The X-Ray Diffraction (XRD) experiments were conducted on the samples of neat epoxy resin and epoxy resin with 3 wt.% of nanoclay. Figure 3.5 shows the angle 2θ and d-spacing value for epoxy resin with and without the nanoclay content.

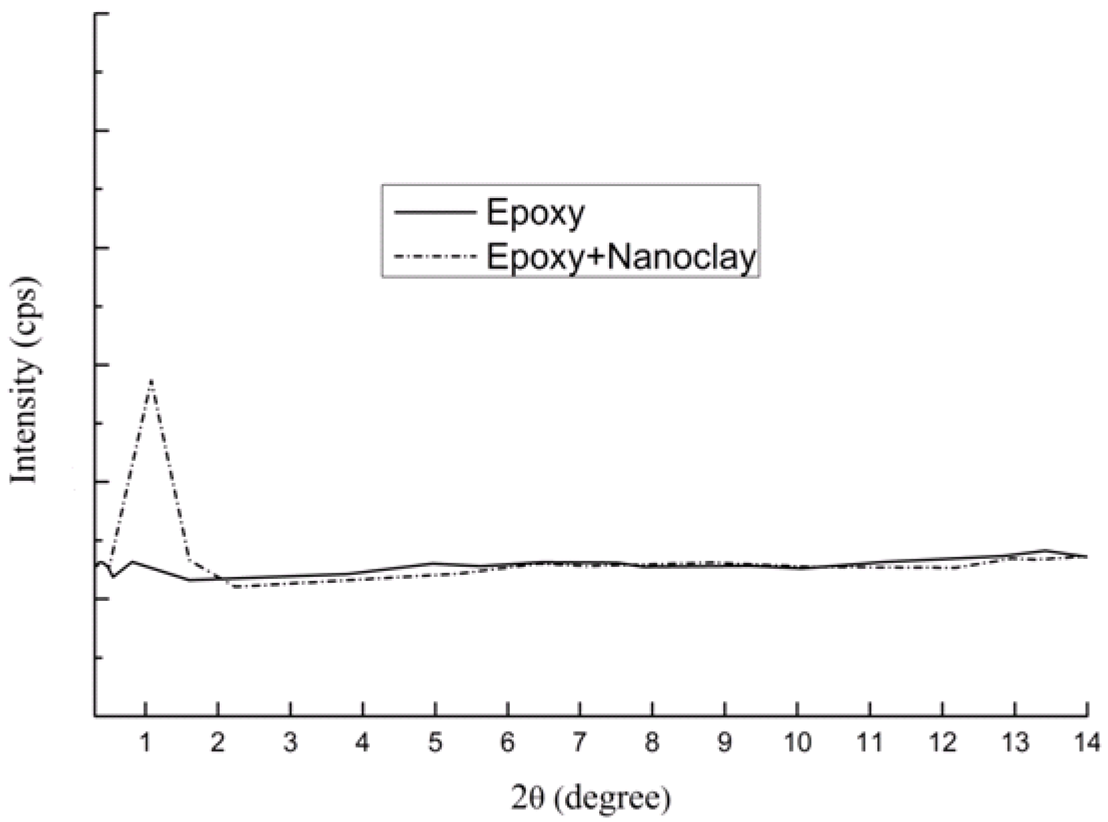

Fig. 3.5 XRD pattern for the neat epoxy and with 3 wt.% of nanoclay

It can be seen from Fig. 3.5, that there is no peak observed for neat epoxy resin due to the amorphous structure of the epoxy. Epoxy resin with 3 wt.% of nanoclay content exhibits a strong peak at 2θ = 1.07º, which corresponds to a d-spacing or basal spacing of 82.46 Å, determined using Bragg's Law (Callister, 2007). This result indicates the intercalated structure of the nanocomposite.

After the characterization of the prepared laminates, the pin joints were prepared using both [0°/45°/0°] and [0°/90°/0°] ply orientations with 3 wt.% of nanoclay. The failure modes for pin joints prepared from both these orientations were studied and comparison was done with pin joints prepared from laminates without the nanoclay particles.

3.6 Closure

The present chapter gave the description of the materials and the basic procedure used for the preparation of the laminates. The laminates were prepared with the addition of 1 to 5 wt.% of nanoclay particles with three different ply orientations *i.e.*, [0°/45°/90°], [0°/90°/0°] and [0°/45°/0°]. It was seen that the tensile modulus and tensile strength of the glass fiber reinforced epoxy composites for all the ply orientations, increased up to 3 wt.% of nanoclay particles. It was also seen that the [0°/45°/0°] ply orientation had higher longitudinal properties than the [0°/90°/0°] ply orientation whereas [0°/90°/0°] ply orientation had higher transverse properties than the [0°/45°/0°] ply orientations.

The next chapter deals with the failure analysis of single hole pin joints prepared using both [0°/45°/0°] and [0°/90°/0°] ply orientations with the addition of 3 wt.% of nanoclay particles.

Chapter 4 - Failure Analysis of Single Hole Pin Joint

In the present chapter, the effect of the ply orientations *i.e.*, [0°/45°/0°] and [0°/90°/0°] on the bearing strength and failure modes of the single hole pin joints configuration was investigated, both experimentally and numerically. Geometric parameters, *i.e.*, the distance from the free edge of the specimen to the diameter of the hole (E/D) ratio and width of the specimen to the diameter of the hole (W/D) ratio were investigated for the bearing strength and failure modes of the single hole pin joints.

4.1 Pin Joint Configurations

As discussed in the previous chapter, the strength of glass epoxy laminates increased with the addition of nanoclay content and was higher for 3 wt.% of nanoclay content for the three ply orientations. Beyond the 3 wt.% of nanoclay, strength decreased due to the presence of agglomeration in the laminates. The tensile and shear strength of the [0°/45°/90°] ply orientation with addition of 3 wt.% of nanoclay were very less as compared to the [0°/45°/0°] and [0°/90°/0°] ply orientations. It was also seen that [0°/45°/0°] ply orientation had higher longitudinal properties than the [0°/90°/0°] orientations whereas [0°/90°/0°] ply orientations had higher transverse properties than the [0°/45°/0°] ply orientation.

Single hole pin joints were prepared, from the glass epoxy with 3 wt.% of nanoclay laminates for the two ply orientation *i.e.*, [0°/45°/0°] and [0°/90°/0°]. The comparison was done with pin joint prepared from the glass epoxy laminates without nanoclay content. The joint was prepared with a composite plate of length (L), width (W), thickness (t) and a single pin hole of diameter (D). The diameter of the hole was fixed to 4 mm for inserting a rigid pin. The hole was located along the centerline of the plate at a distance, E from one end of the plate. The single hole pin joint is shown in Fig. 4.1. A tensile load was applied on the plate which was resisted by the rigid pin. Load was parallel to the plate and was symmetric with respect to the centerline. Hence the load could not create bending moments about the x, y, or z-axis.

Edge distance to hole diameter (E/D) and width to diameter (W/D) ratios in the specimen were varied from 2 to 5. The samples were prepared with different E/D and W/D ratios, given in Table 4.1, for the two different ply orientations *i.e.*, [0°/45°/0°] and [0°/90°/0°].

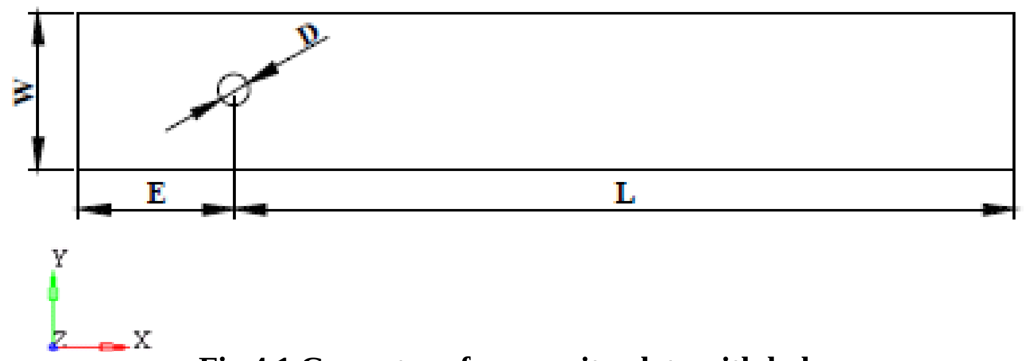

Fig.4.1 Geometry of composite plate with hole

Table 4.1 Geometries of pin-joints samples tested for different ply orientations

E/D ratio	W/D ratio	Diameter of Hole(mm)	E (mm)	W (mm)	Thickness(mm)	Length from hole to edge(mm)
2	2	4	8	8	2	100
	3	4	8	12	2	100
	4	4	8	16	2	100
	5	4	8	20	2	100
3	2	4	12	8	2	100
	3	4	12	12	2	100
	4	4	12	16	2	100
	5	4	12	20	2	100
4	2	4	16	8	2	100
	3	4	16	12	2	100
	4	4	16	16	2	100
	5	4	16	20	2	100
5	2	4	20	8	2	100
	3	4	20	12	2	100
	4	4	20	16	2	100
	5	4	20	20	2	100

The analysis of the pin joints was done both numerically and experimentally, for comparison of the strength and failure modes of different ply orientations along with the different geometric parameters. Table 4.1 shows the different geometries of the pin joints which were investigated.

4.2 Experimental Testing of Pin Joint

Samples of the pin joints were prepared, as per the geometry shown in Fig. 4.1, with different geometric parameters which are given in Table 4.1. These samples were tested on a Zwick-Roell Universal Testing Machine – Model Z010, Zwick-Roell, Germany, with the help of the fixture. Fixture used for the testing of pin join is shown in Fig. 4.2.

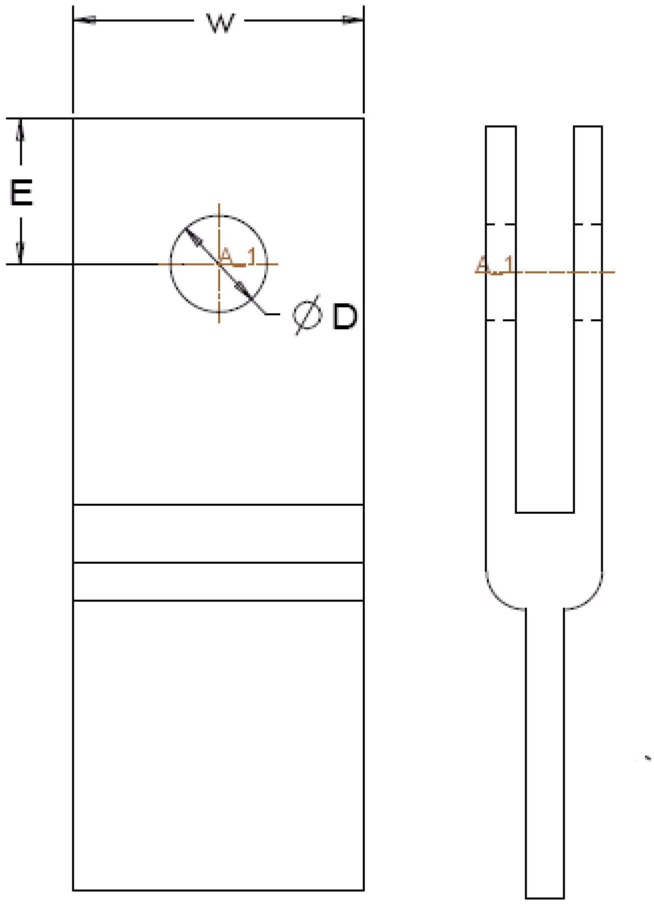

Fig. 4.2 Basic shape of the fixture

4.2.1 Results of Neat Glass Epoxy Composite Laminates

Pin joints samples for ply orientations [$0^o/45^o/0^o$] and [$0^o/90^o/0^o$] without nanoclay were tested to determine the bearing strength and failure modes. Figure 4.3 shows the stress vs. strain plots for the [$0^o/90^o/0^o$] ply orientation without the nanoclay for different geometric parameters. Similarly, stress vs. strain plots for the [$0^o/45^o/0^o$] ply orientation are shown in the Fig. 4.4. It can be seen from the Figs. 4.3 and 4.4 that the strength of the pin joints is higher for the [$0^o/90^o/0^o$] ply orientations as compared to [$0^o/45^o/0^o$] ply orientations.

Pin joint may fail with three basic modes of failure *i.e.*, net tension, shear out and bearing. Joint failure with the net-tension and shear out failure modes is immediate without any warning. These failures result from excessive tensile and shear stresses. However, bearing failure is progressive and occurs in the material immediately adjacent to the contact area between the pin and the laminate. It is primarily caused by the compressive stresses acting on the hole surface. Bearing failure is often considered as the desirable mode because it usually gives a higher strength. Other modes of failure should be avoided through proper design of the joint geometry and composite material itself. So, the optimal W/D and E/D ratios should be chosen to avoid such immediate failure in the joints. The basic modes of failure can be easily judged from the stress vs. strain graphs of the specimens.

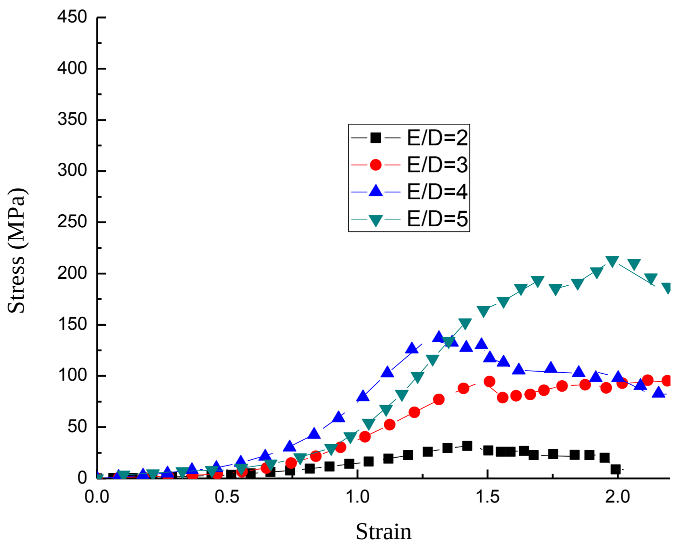

(a)

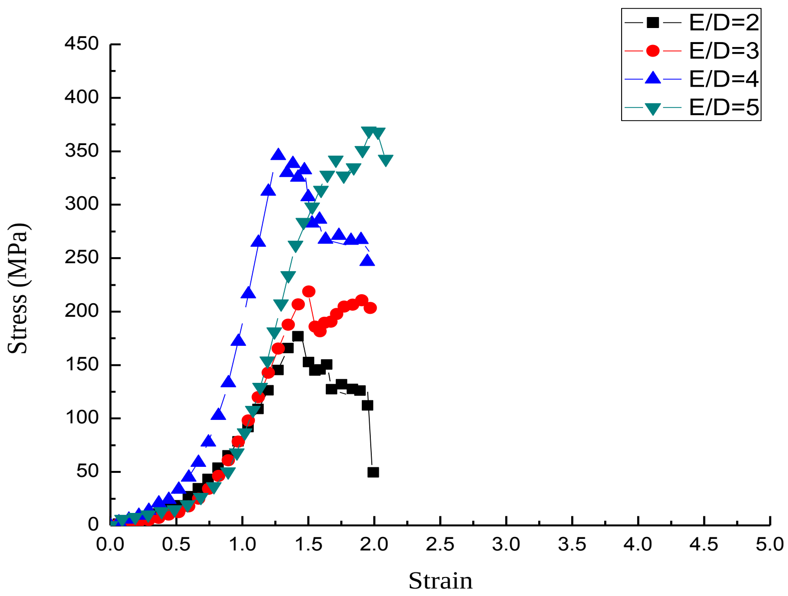

(b)

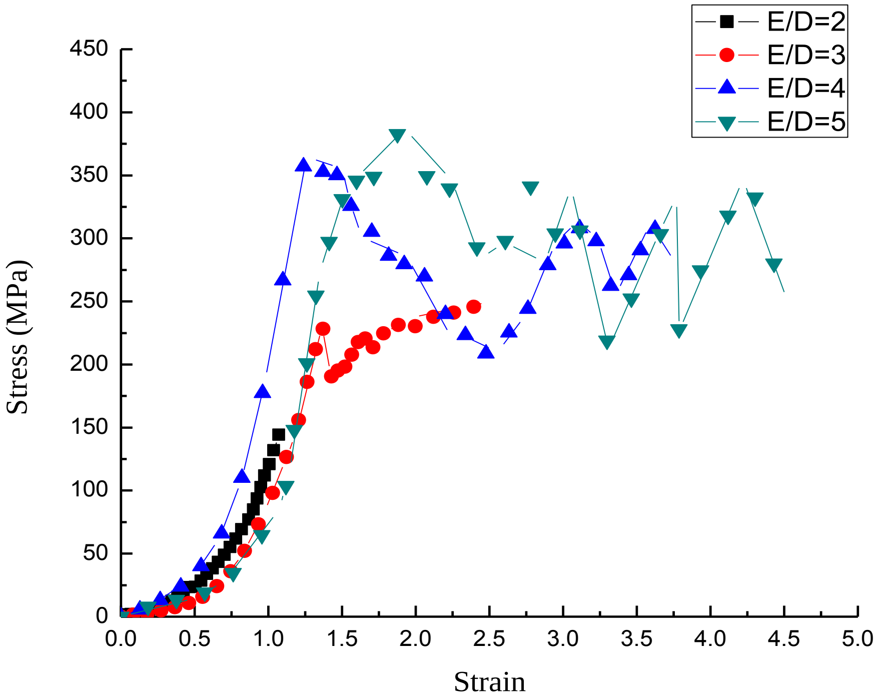

(c)

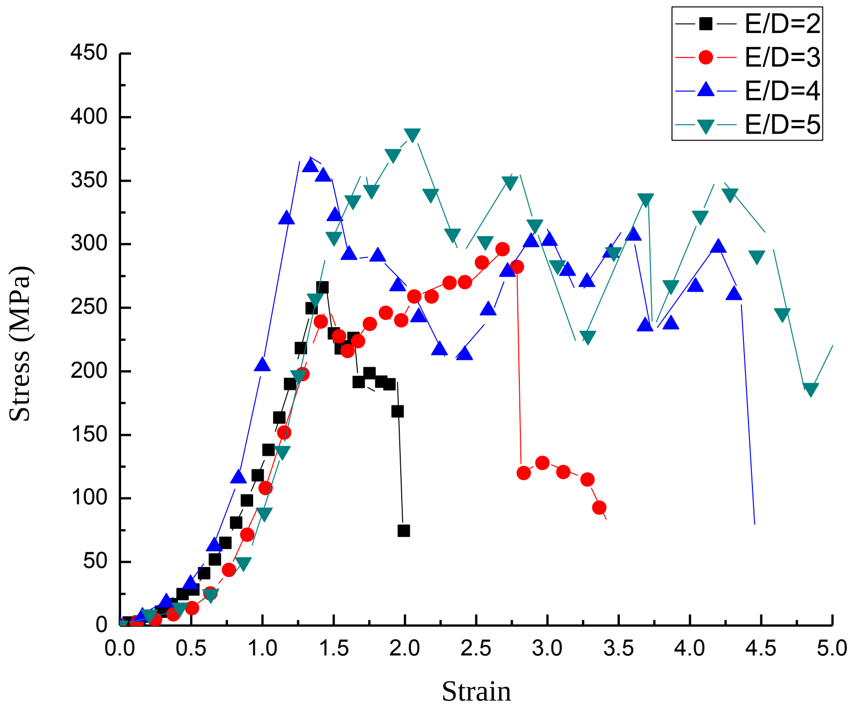

(d)

Fig. 4.3 Stress vs. Strain curves of pin joints for ply orientation [0^o/90^o/0^o] without nanoclay (a)W/D=2 (b) W/D=3 (c) W/D=4 (d) W/D=5

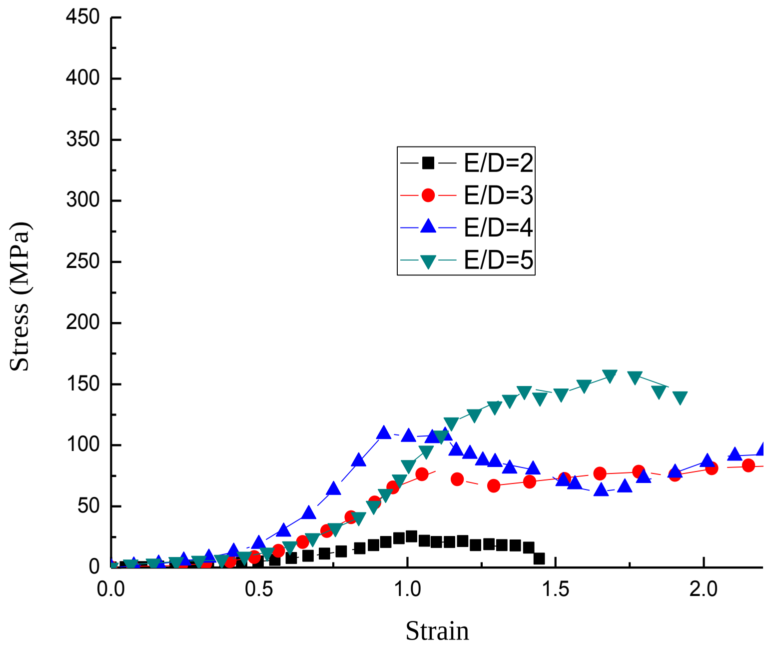

Stress (MPa)
Strain
E/D=2
E/D=3
E/D=4
E/D=5

(a)

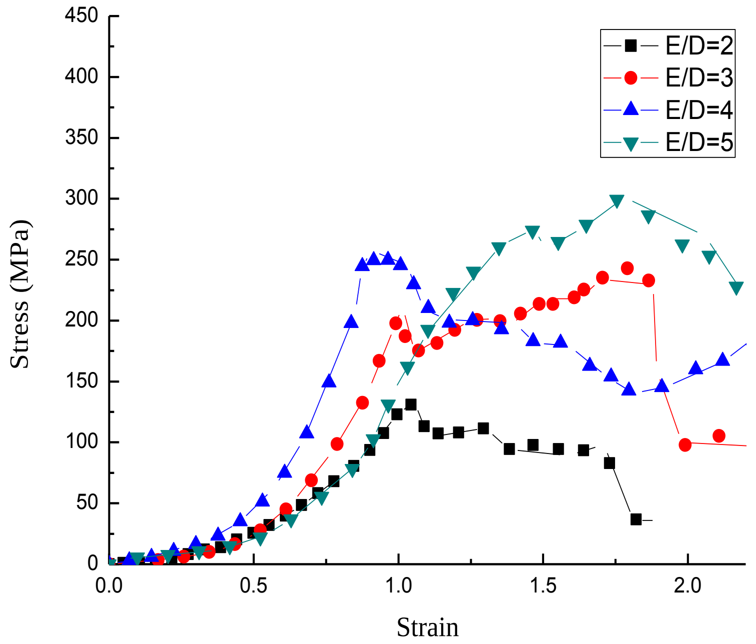

Stress (MPa)
Strain
E/D=2
E/D=3
E/D=4
E/D=5

(b)

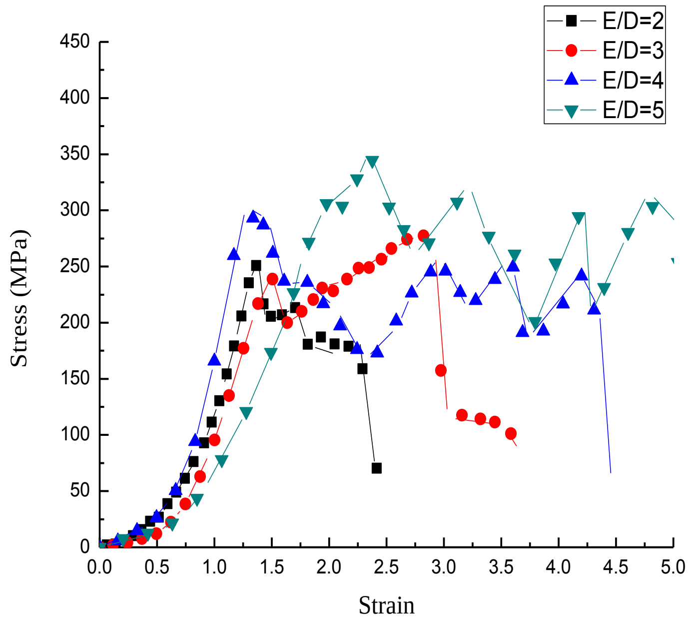

(c)

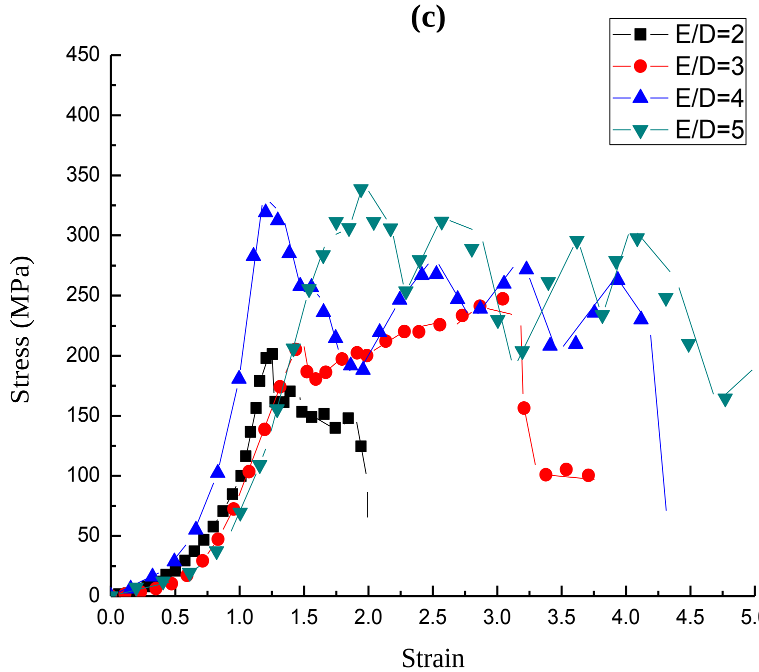

(d)

Fig. 4.4 Stress vs. Strain curves of [illegible]ts for ply orientation [0°/45°/0°] without nanoclay (a)W/D=2 (b) W/D=3 (c) W/D=4 (d) W/D=5

Figures 4.3 and 4.4 shows that for low W/D ratio *i.e.*, 2 and 3, there is a sudden or decrease after some peak points, which means it has failed either with net tension or shearing. If the curve decrease after a peak point suddenly then failure mode is net tension. On the other hand, if the curve decreases suddenly after some peak points then failure mode is shear out. The net tension failure mode is directly related to the width of the specimen. For W/D ratio to be 4 and 5, it can be seen that after the peak point, the values decreases to some extend and thereafter moves forward with zig-zag formation. This is due to the bearing failure mode. The matrix fracture, delamination between laminates, fiber breakages, fiber matrix interface deformation etc., may be the reasons for the zig-zag formation of the curve. The bearing mode of failure occurs for W/D ≥ 4 and E/D ≥ 4 which is independent of the ply orientations. Net-tension and shear out failure modes occur with small W/D and E/D values, respectively. So, the optimal W/D and E/D ratios should be chosen to avoid such immediate failure in the joints. It can be seen from Figs. 4.3 and 4.4 that the bearing mode of failure occurs for W/D ≥ 4 and E/D ≥ 4.

4.2.2 Results of Pin Joint With 3 Wt.% of Nanoclay

It was shown in Chapter 3 that the addition of nanoclay enhances the mechanical properties of the glass epoxy composites. The properties increased with increase in wt.% of nanoclay. The mechanical properties were maximum at 3 wt.% of nanoclay. Hence the pin joints were prepared by adding 3 wt.% of nanoclay to glass epoxy laminates. The joints were prepared for both [0^o/45^o/0^o] and [0^o/90^o/0^o] the ply orientations by varying the geometric parameters E/D and W/D ratios, from 2 to 5. The graphical plots of these results are shown in Figs. 4.5 and 4.6.

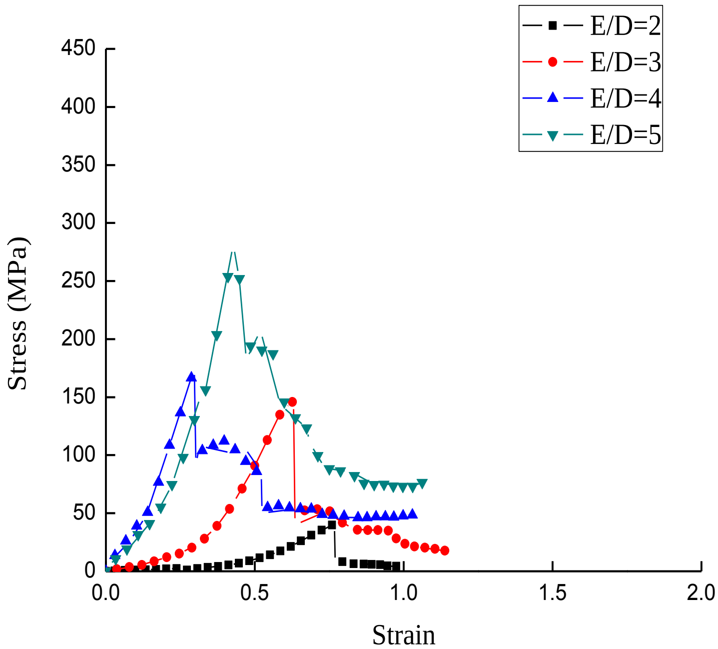

(a)

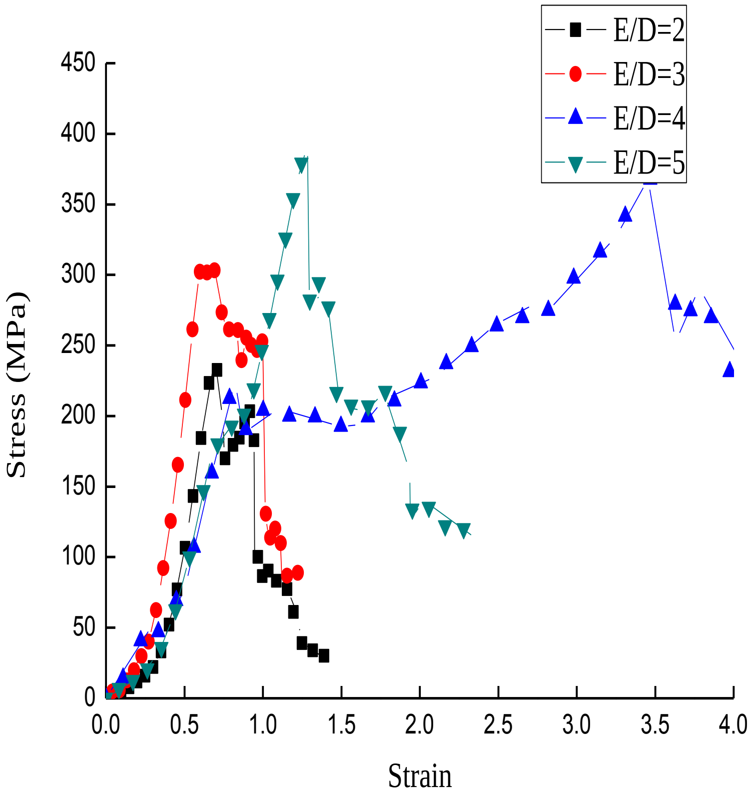
E/D=2
E/D=3
E/D=4
E/D=5
Stress (MPa)
Strain
0
50
100
150
200
250
300
350
400
450
0.0
0.5
1.0
1.5
2.0
2.5
3.0
3.5
4.0

(b)

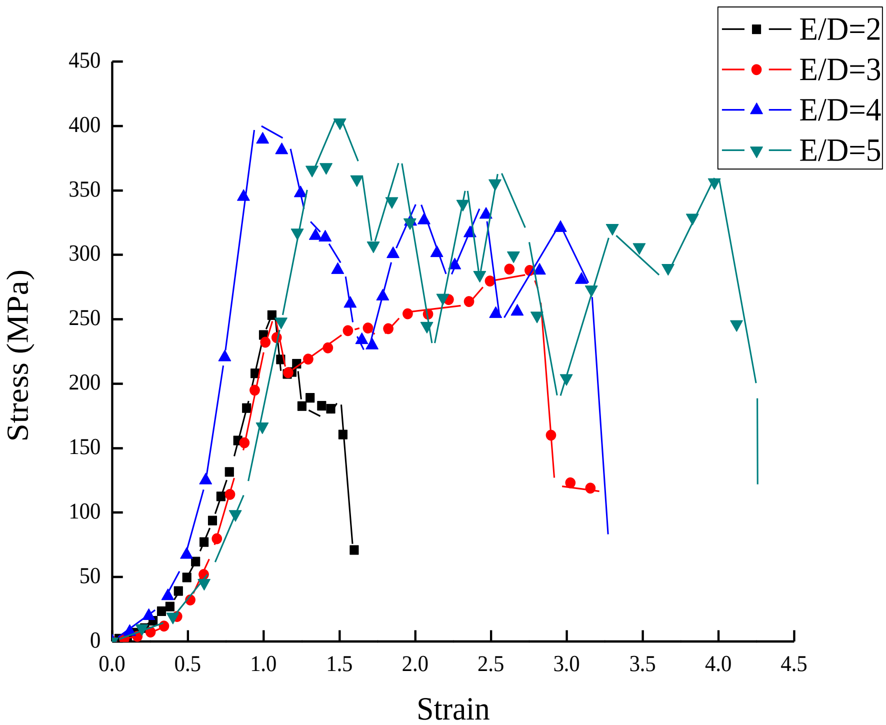
E/D=2
E/D=3
E/D=4
E/D=5
Stress (MPa)
Strain
0
50
100
150
200
250
300
350
400
450
0.0
0.5
1.0
1.5
2.0
2.5
3.0
3.5
4.0
4.5

(c)

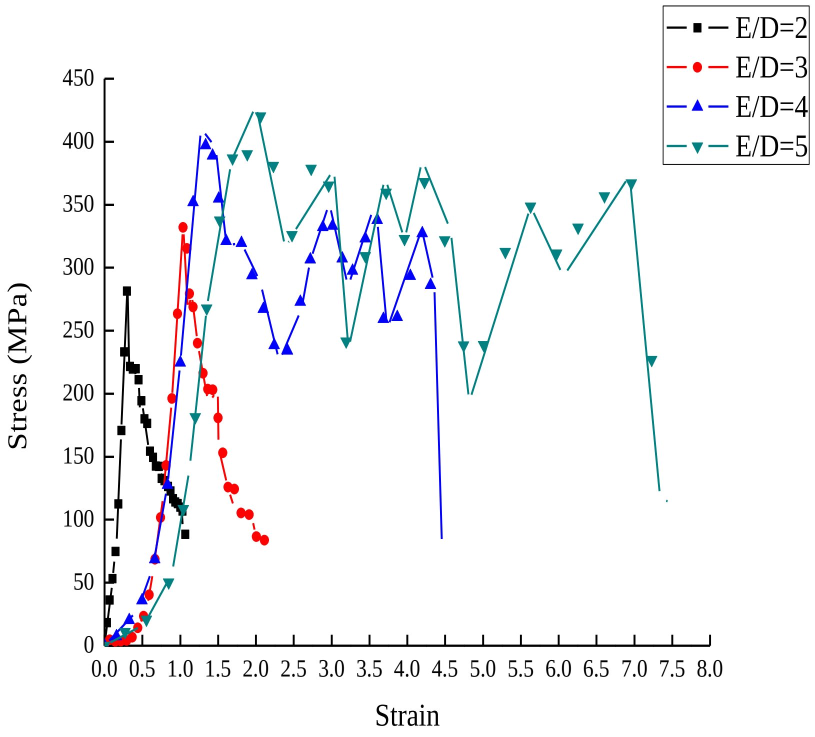

(d)

Fig. 4.5 Stress vs. Strain curves of pin joints for ply orientation [0°/90°/0°] with 3 wt.% of nanoclay (a)W/D=2 (b) W/D=3 (c) W/D=4 (d) W/D=5

It can be seen from Figs. 4.5 and 4.6 that for low W/D ratio *i.e.*, 2 and 3 joint has failed either with net tension or shearing. The bearing mode of failure is occurring for W/D ≥ 4 and E/D ≥ 4.

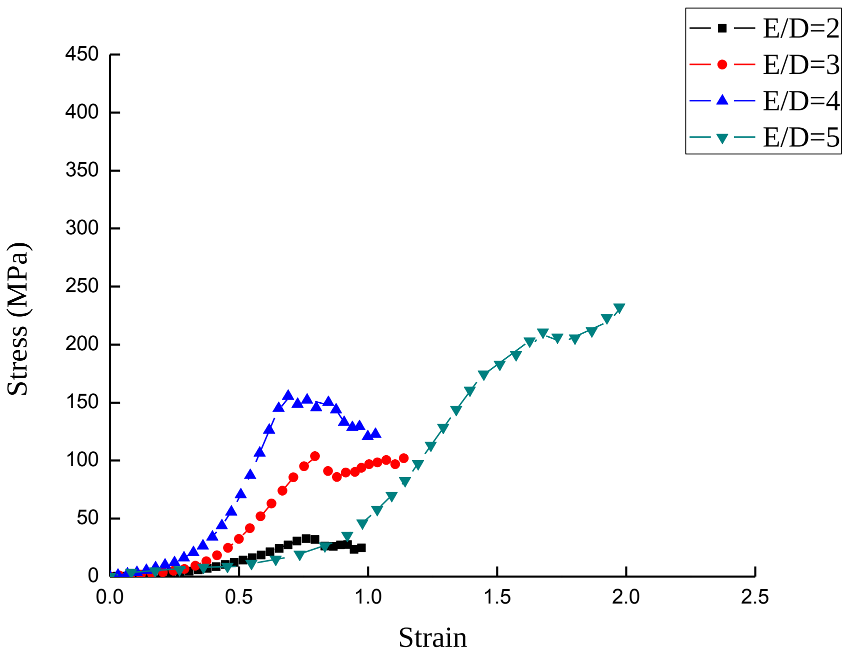

(a)

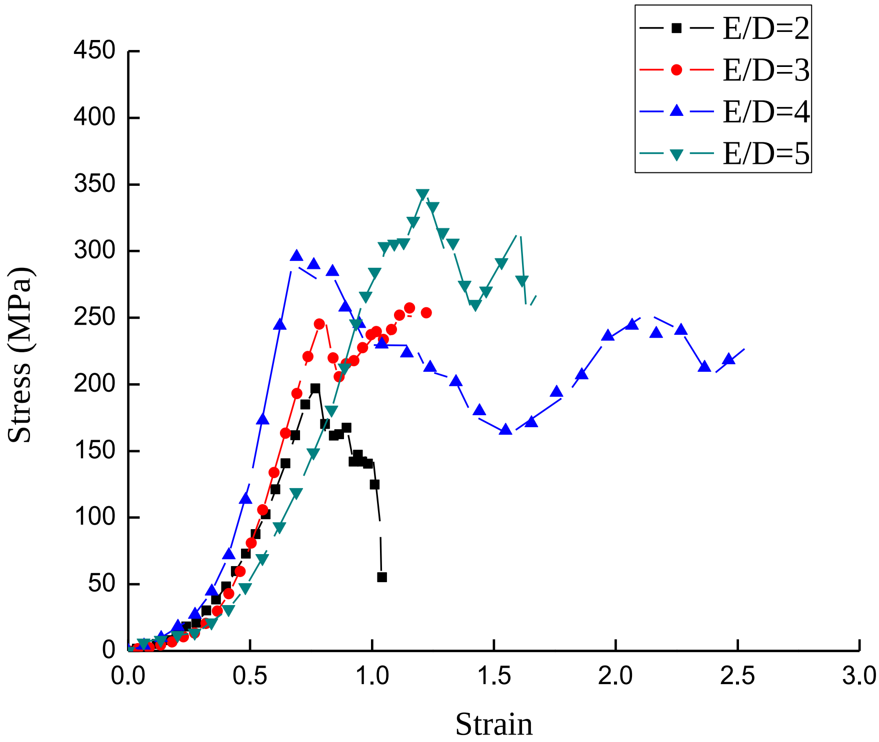

E/D=2
E/D=3
E/D=4
E/D=5
Stress (MPa)
Strain
0
50
100
150
200
250
300
350
400
450
0.0
0.5
1.0
1.5
2.0
2.5
3.0

(b)

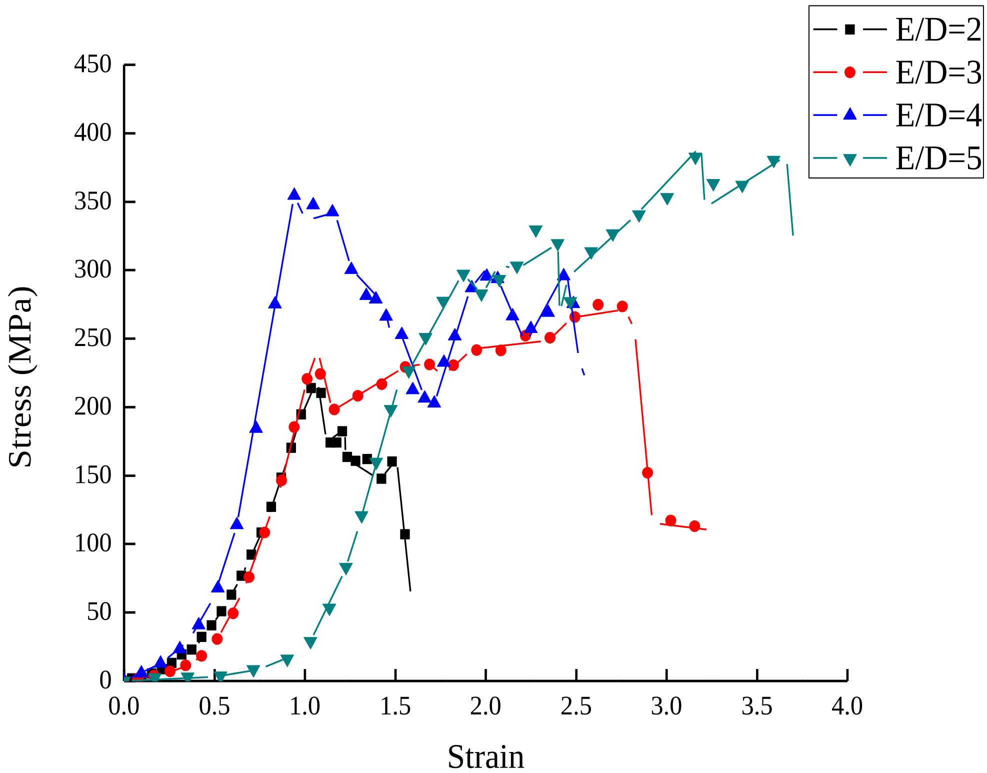

E/D=2
E/D=3
E/D=4
E/D=5
Stress (MPa)
Strain
0
50
100
150
200
250
300
350
400
450
0.0
0.5
1.0
1.5
2.0
2.5
3.0
3.5
4.0

(c)

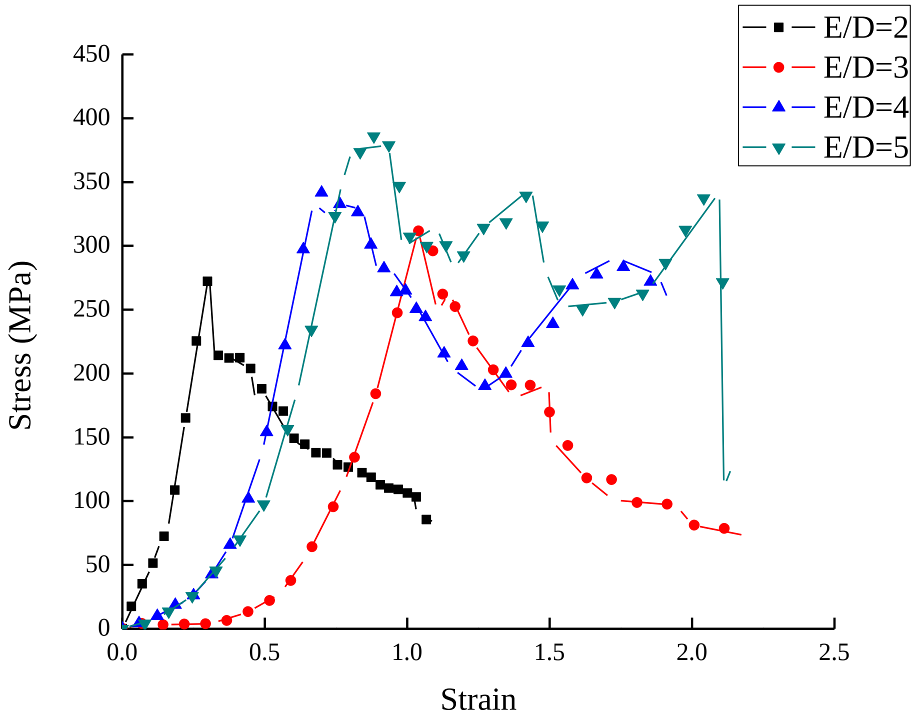

(d)

Fig. 4.6 Stress vs. Strain curves of pin joints for ply orientation [0°/45°/0°] with 3 wt.% of nanoclay (a) W/D=2 (b) W/D=3 (c) W/D=4 (d) W/D=5

Table 4.2 Net Tension (N), Shear Out (S) and Bearing (B) types of failure modes

Ratios	W/D=2 E/D=3	W/D=2 E/D=3	W/D=4 E/D=2	W/D=5 E/D=2	W/D=5 E/D=5	W/D=5 E/D=4
Specimens						
Failure Modes	N	N	S	S	B	B
Ply Orientations	[0°/45°/0°]	[0°/90°/0°]	[0°/45°/0°]	[0°/90°/0°]	[0°/45°/0°]	[0°/90°/0°]

It can be seen from Figs. 4.3 to 4.6 that the modes of failure for the two ply orientations are nearly same but the [0°/90°/0°] ply orientation bears more tensile stress than [0°/45°/0°] ply orientation. Specimens showing each type of the failure in different E/D and W/D ratio are given in the Table 4.2.

Figures 4.7 and 4.8 show the comparison of bearing strength for the [$0^o/45^o/0^o$] and [$0^o/90^o/0^o$] ply orientation with and without the addition of nanoclay content.

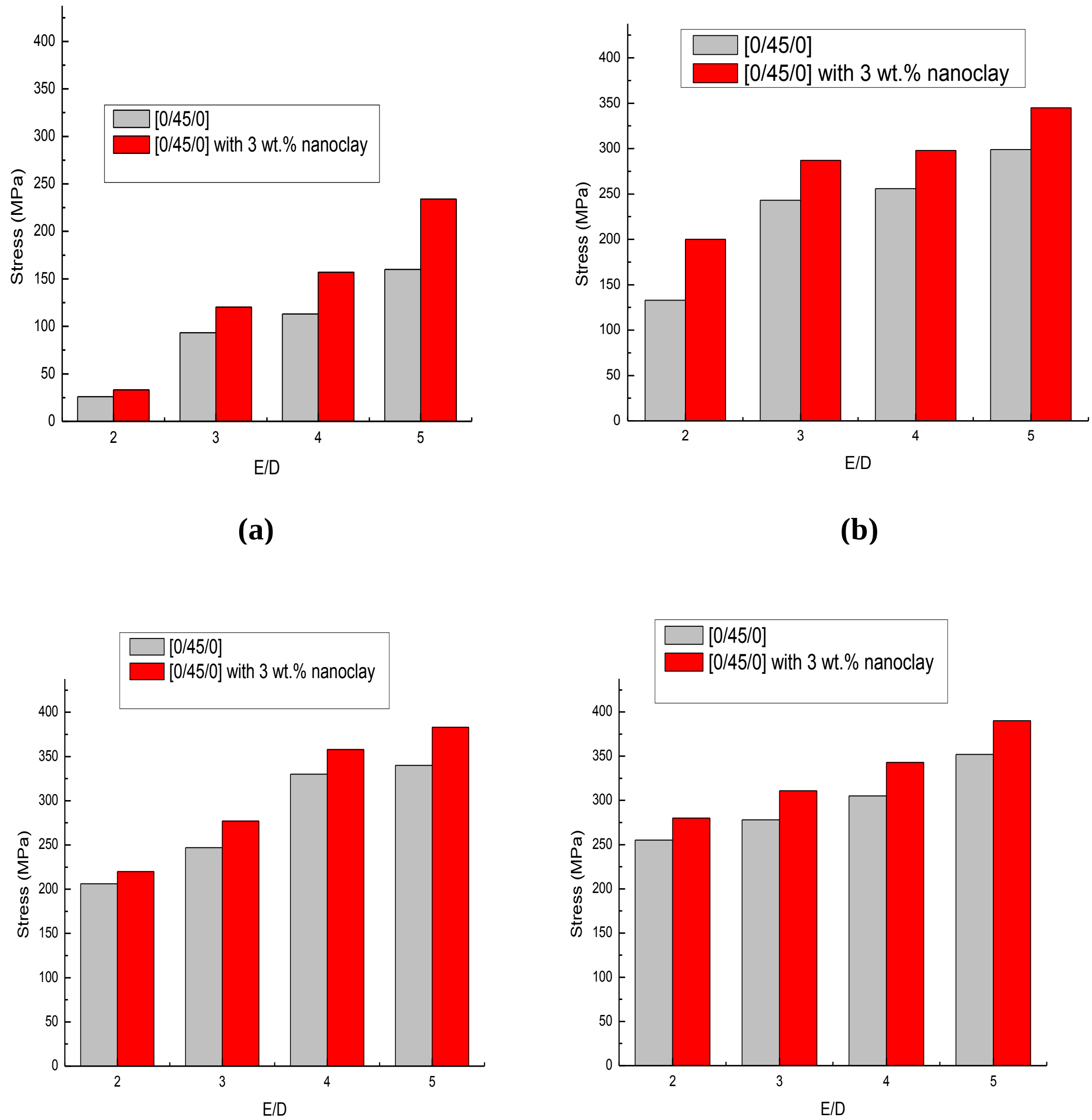

(a) (b)

(c) (d)

Fig. 4.7 Comparison of bearing strength of [$0^o/45^o/0^o$] ply orientation pin joints for neat and 3 wt.% of nanoclay samples (a) W/D=2 (b) W/D=3 (c) W/D=4 (d) W/D=5

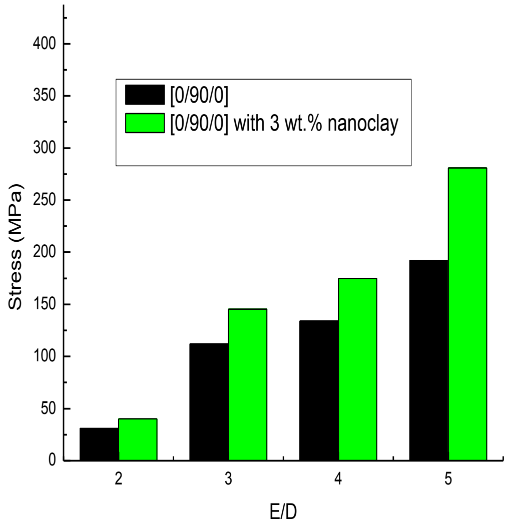

(a)

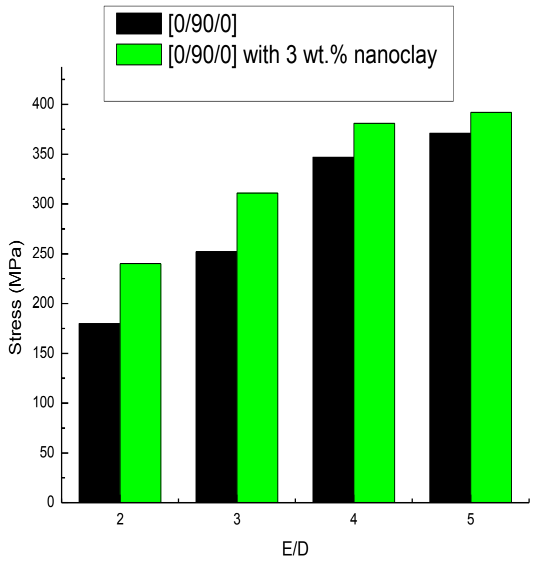

(b)

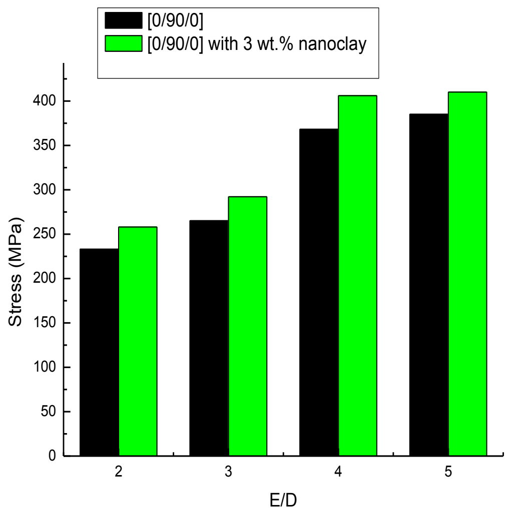

(c)

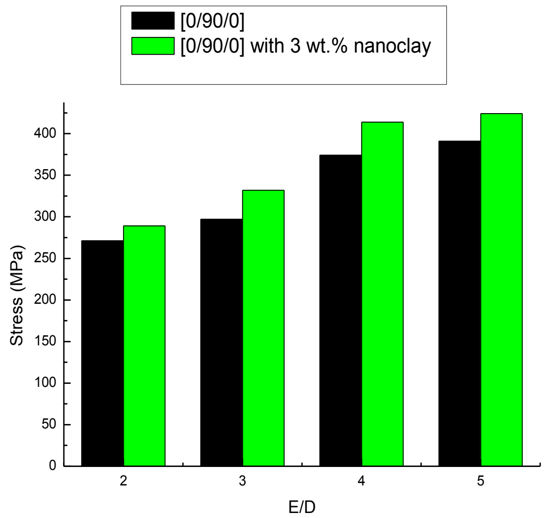

(d)

Fig. 4.8 Comparison of bearing strength of [$0^o/90^o/0^o$] ply orientation pin joints for neat and 3 wt.% of nanoclay samples (a) W/D=2 (b) W/D=3 (c) W/D=4 (d) W/D=5

It can be seen from Figs. 4.7 and 4.8 that the bearing strength is higher for 3 wt.% of nanoclay pin joints than neat epoxy pin joints for respective ply orientations. The strength of the pin joint with addition of 3 wt.% nanoclay is 10 to 15 % higher for different orientations as compared to the joints without the nanoclay contents. This is because of the strong interfacial bond promoted by the nanoclay between the fiber and the polymer.

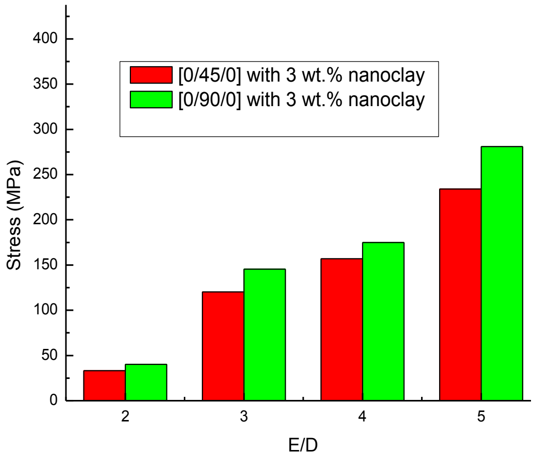

(a)

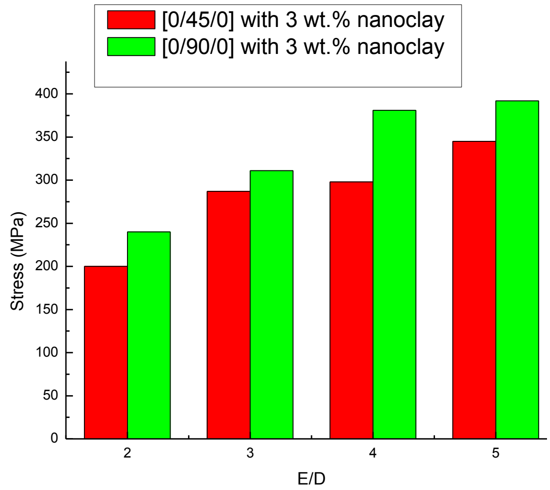

(b)

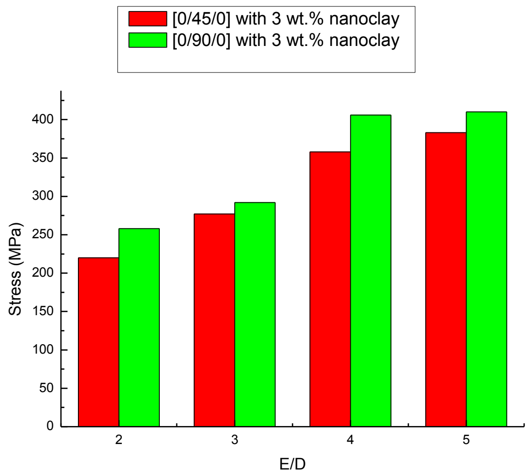

(c)

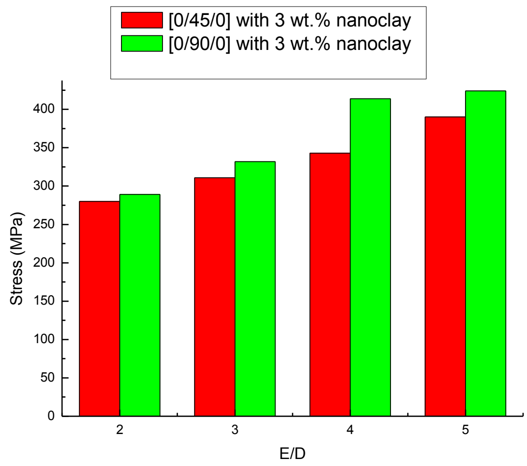

(d)

Fig. 4.9 Comparison of bearing strength of [0°/45°/0°] and [0°/90°/0°] ply orientations pin joints with 3 wt.% of nanoclay samples (a) W/D=2 (b) W/D=3 (c) W/D=4 (d) W/D=5

Figure 4.9 shows the comparison of the [0°/45°/0°] and [0°/90°/0°] ply orientations pin joints with 3 wt.% of nanoclay. Ply orientation [0°/90°/0°] gives the higher bearing strength than [0°/45°/0°] ply orientation. This is due to the fact that the [0°/90°/0°] ply orientation had higher transverse mechanical properties than the [0°/45°/0°] ply orientations. It can also be seen from Fig. 4.9 that the [0°/90°/0°] ply orientation has approximate 10-12% higher bearing strength as compared to [0°/45°/0°] orientation with 3 wt.% of nanoclay.

4.3 Numerical Analysis

Numerical analysis of the pin joints was done using finite element methods. Finite element method is a very versatile tool which can be used for analysis of nanocomposite laminates (Singh *et al.*, 2016; Agnihotri *et al.*; 2012). Several strength prediction methods for composite joints have been proposed by different researchers (Olmedo *et al.*, 2014; Li *et al.*, 2014; Whitney e*t al.* 1974; Chang *et al.*, 1982) which are based upon stress concentration, failure index, etc. However, one of the most efficient methods for predicting the strength is the characteristic curve method (Whitney *et al.* 1974; Chang *et al.*, 1982).

4.3.1 Characteristic Curve Method

The laminates which are used for the mechanical joints, *i.e.*, rivets, bolts and pins are under the influence of stress concentration around the fastener holes. Due to the stress concentration, high tensile stresses are produced on the both side of the hole, along the transverse direction of loading, whereas high compressive stresses are produced in the front area of the hole. It is observed that the failure considered in the stress concentration region generally give the underestimation of the strength and structural failure of the joint. Characteristic curve method is used to predict the strength of the joint by considering the failure beyond the stress concentration region, but on an artificial curve known as characteristic curve.

Characteristic curve is an artificial curve that is made with the help of characteristic lengths determined by the joint tests namely bearing test and tensile test. The curve is drawn according to the equation (4.1) using the determined values of characteristic lengths.

$$\mathrm{R_c} = \mathrm{D}/2 + \mathrm{R_{ot}} + (\mathrm{R_{ot}} - \mathrm{R_{oc}}) \cos \phi \qquad (4.1)$$

Where, $\mathrm{R_{oc}}$ is the characteristic length in compression, $\mathrm{R_{ot}}$ is the characteristic length in tension, D is the diameter of the hole and ϕ is the angle, which is measured clockwise or anti-clockwise from the direction of applied load. It can be measured clockwise as well as anticlockwise due to the symmetry of the curve around the base line. The characteristic curve along with nomenclature is shown in the Fig. 4.10. After drawing the curve, an appropriate failure theory is applied on the curve. Failure theory gives the failure index on the curve, the failure modes are detected on the basis of maximum value of failure index and its location on the characteristic curve. The failure modes can be judged using the failure angle (θ) as per equation (4.2).

$$\begin{aligned} 0^{o} \le \theta \le 15^{o} &: \text{Bearing failure} \\ 30^{o} \le \theta \le 60^{o} &: \text{Shear-out failure} \\ 75^{o} \le \theta \le 90^{o} &: \text{Net-tension failure} \end{aligned} \tag{4.2}$$

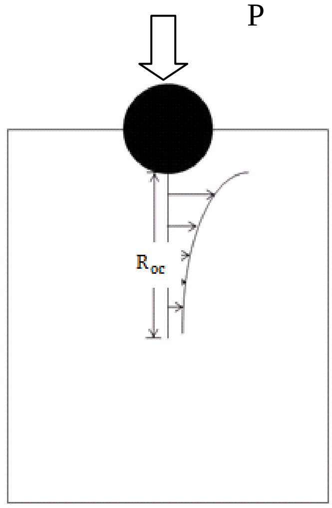

(a)

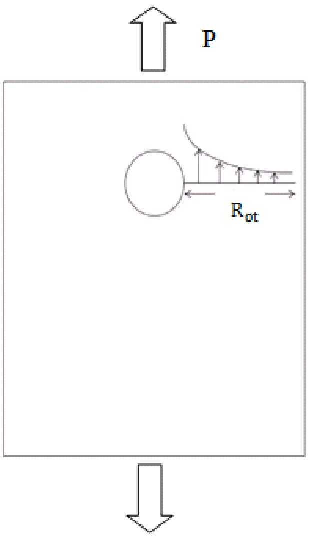

(b)

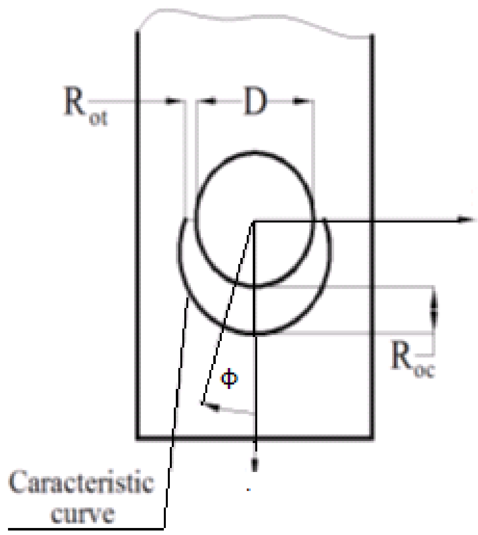

(c)

Fig. 4.10 Schematic representation of (Kweon *et al.*, 2004) (a) Bearing test (b) Tensile test (c) Characteristic curve

The conventional method of determining the characteristic lengths in tension and compression involved the conducting of bearing test for characteristic length in compression and tensile test for characteristic length in tension. But these characteristic lengths can also be determined using finite element method. The curve was drawn using finite element method as per the procedure given in the following section.

4.3.2 Methodology used to draw a Characteristic Curve

In order to draw the characteristic curve, the characteristic lengths were required which were found using finite element method.

- **Characteristic length in compression**

The laminate with the different configuration had been modeled in the Hypermesh analysis package. A compressive force (P) was applied to the hole. The bearing strength of the specimen was calculated by the equation (4.3).

$$\text{Mean bearing strength} = \mathrm{P}/(D \times t) \quad (4.3)$$

Where, D is the diameter of the hole and t is the thickness of the laminate. Then the point ahead of the hole along the x-axis was located such that the equivalent stress was equal to the mean bearing strength. The distance from the edge of the hole to this point where the equivalent stress becomes equal to the mean bearing stress is called the characteristic length in compression ($\mathrm{R_{oc}}$)

- **Characteristic length in tension**

The laminate with the same configuration was subjected to the tensile load (P) applied symmetrically along the x-axis. The mean tensile strength was calculated by equation (4.4).

$$\text{Mean tensile strength} = \frac{\mathrm{P}}{(\mathrm{W}-\mathrm{D})\times \mathrm{t}} \quad (4.4)$$

Where, W is the width of the plate, D is the diameter of the hole and t is the thickness of the laminate. The point from the edge of the hole in the transverse direction was located such that the equivalent stress is equal to the mean tensile strength. The distance from the hole edge to the point where the equivalent stress is equal to the mean tensile strength is called the characteristic length in tension ($\mathrm{R_{ot}}$).

After finding the values of the characteristic lengths, the characteristic curve equation was used to draw the characteristic curve by varying the angle, ϕ, from 0° to 90°. The complete curve was drawn using the 'mirror' option available in the modeling package.

4.3.3 Calculation of Failure Index

Tsai-Wu failure theory (Tsai and Wu, 1971) is a quadratic theory in which the stresses produced in the laminate have the interactions with the orthotropic properties of the laminates and give the value of Failure Index (*FI*). FI defines the failure of the laminate and is calculated as per the equation (4.5).

If $FI < 1$; there is no failure in the composite laminate

If $FI \geq 1$; there is failure in the composite laminate

The following methodology had been adopted in order to obtain the values of failure index for all the nodes lying on the characteristic curve. The calculations for failure index for all the nodes located on the characteristic curve, were done using the Tsai- Wu failure theory. The methodology involved determination of maximum principal stress (σ_1), minimum principal stress (σ_2) and maximum shear stress (σ_6). The Tsai-Wu failure theory (Tsai and Wu, 1971) is given by the equation (4.5).

$$F_1\sigma_1 + F_2\sigma_2 + F_{11}\sigma_1^2 + F_{22}\sigma_2^2 + F_{66}\sigma_6^2 + 2F_{12}\sigma_1\sigma_2 = FI \quad (4.5)$$

The values of F_1, F_2, F_{11}, F_{22}, F_{66} and F_{12} depend on the orthotropic mechanical properties of the composite which were given in Table 3.9 of chapter 3. The six parameters F_1, F_2, F_{11}, F_{22}, F_{66} and F_{12} depend upon longitudinal tensile strength (X_t), transverse tensile strength (Y_t), longitudinal compressive strength (X_c), transverse compressive strength (Y_c) and shear failure strength (S), and are calculated using equations (4.6) to (4.11).

$$F_{11} = \frac{1}{X_t X_c} \quad (4.6)$$

$$F_1 = \frac{1}{X_t} - \frac{1}{X_c} \quad (4.7)$$

$$F_{22} = \frac{1}{Y_t Y_c} \quad (4.8)$$

$$F_2 = \frac{1}{Y_t} - \frac{1}{Y_c} \tag{4.9}$$

$$F_{66} = \frac{1}{S^2} \tag{4.10}$$

$$F_{12} = -0.5\sqrt{F_{11}F_{22}} \tag{4.11}$$

4.3.4 Finite Element Analysis using Characteristic Curve Method

Geometric model of pin joint was made in Hypermesh analysis package for 3 wt.% of nanoclay by varying W/D and E/D ratios. The laminates were modeled using the two ply orientations of [$0^o/45^o/0^o$] and [$0^o/90^o/0^o$]. The different ply orientations were specified as per the 'Hyper Laminate' module available in Hypermesh package. The fiber orientation, thickness of each ply and Tsai-Wu failure theory were specified in this module for the finite element analysis of the joint. Figure 4.11 show the modeling of the laminates along with the Tsai-Wu failure theory used for the finite element analysis in Hypermesh package.

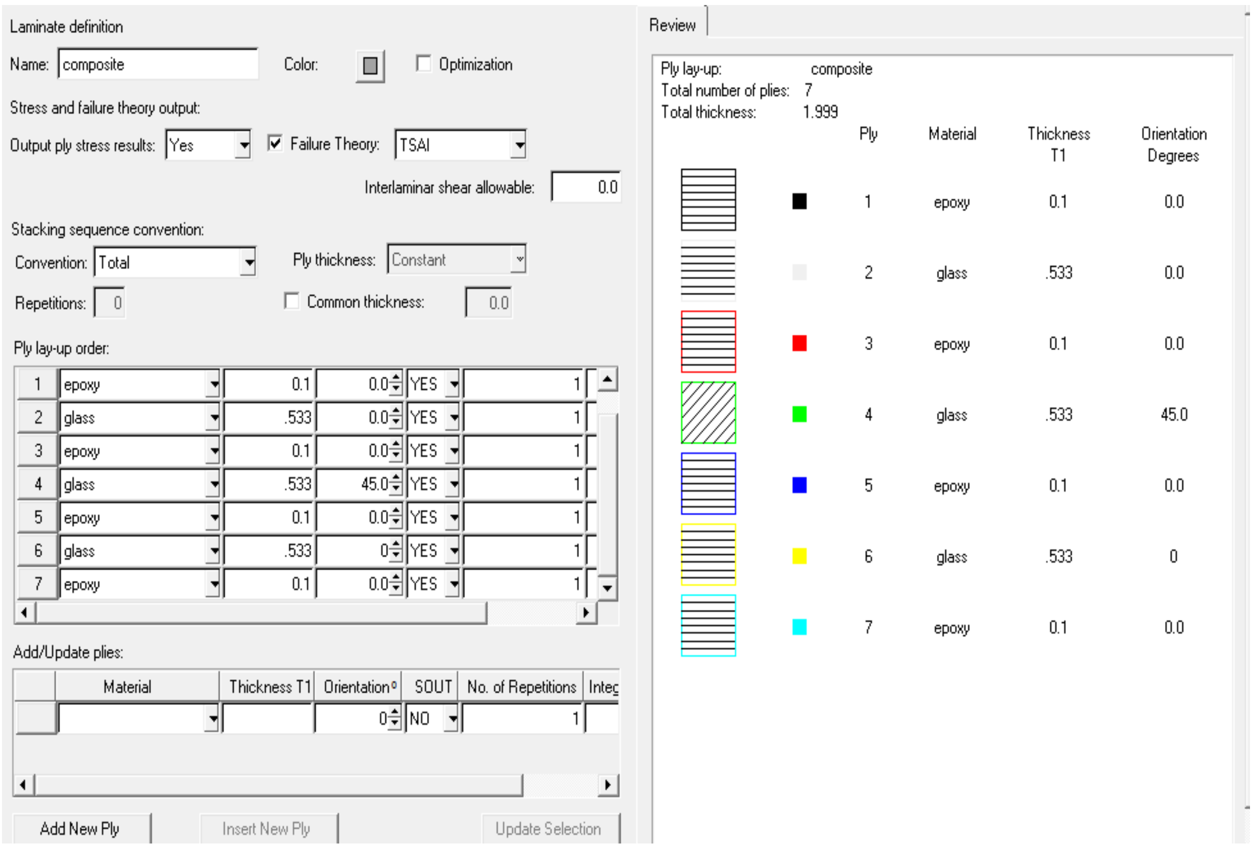

Fig. 4.11 Ply Orientation as specified for analysis

The ply orientation was symmetric with respect to the z = 0 plane. Perfect bonding between each ply was assumed. The composite plate was loaded with an in-plane load, P for the pinned joint.

Model was meshed using quadrilateral elements. One end of the composite laminates was fixed and the force was exerted through the pin of the hole, as shown in Fig. 4.12.

The characteristics curve, as shown in Fig. 4.12, was made using the R_{ot} and R_{oc} values as calculated by the procedure discussed in the previous section. Failure angle was measured using the FI value on the characteristic curve for all the geometric parameters for both the ply orientations.

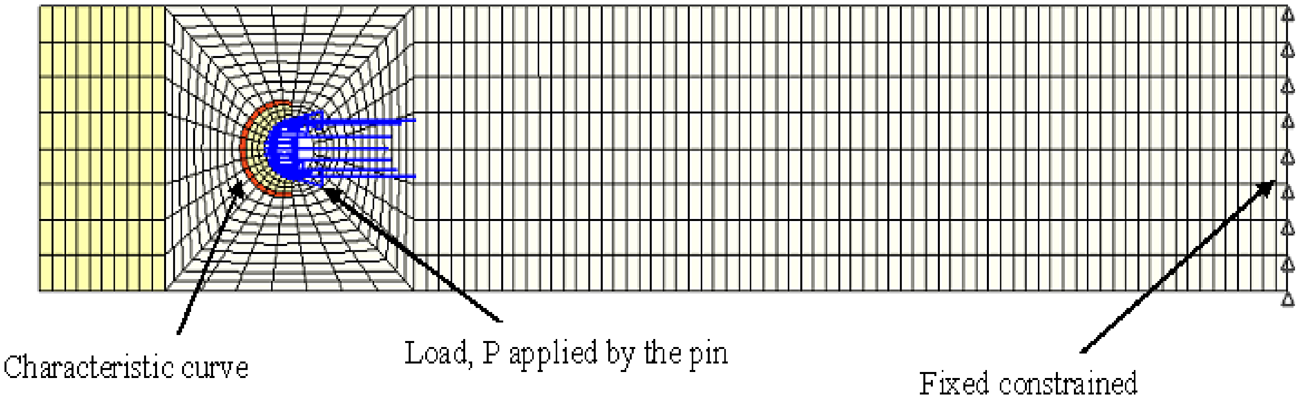

Fig. 4.12 Boundary conditions and characteristic curve

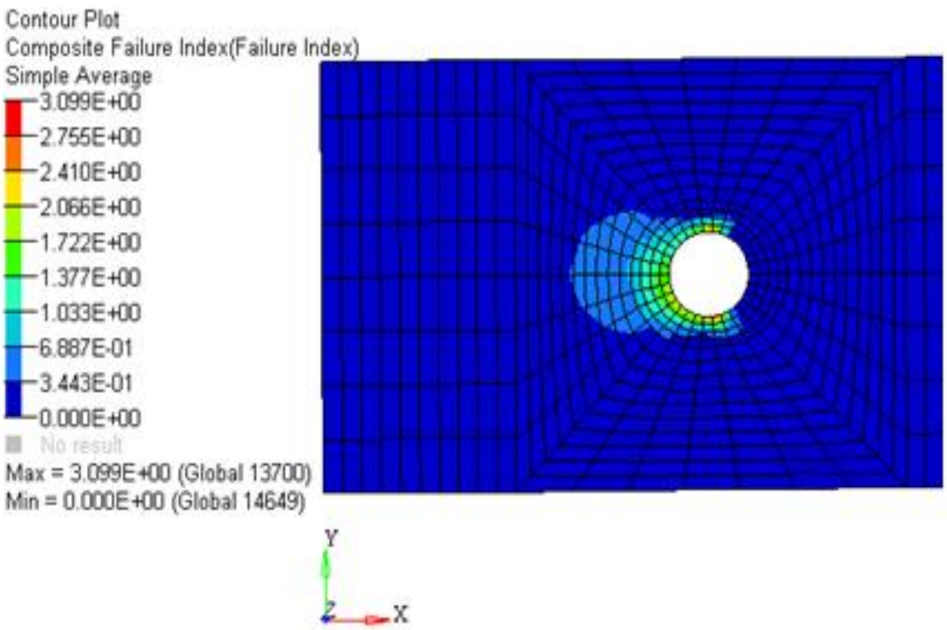

Fig. 4.13 *FI* value for W/D=4 and E/D=4 around the hole

Figure 4.13 shows the *FI* values around the hole for one of the geometric parameters *i.e.*, W/D = 4 and E/D = 4. *FI* values and failure angle were determined on the characteristic curve. Figure 4.14 shows the three basic failures by calculating the *FI* and failure angle on the characteristic curve. *FI* was calculated on the nodes which were locating on the characteristic curve. Failure angle (θ) was calculated at the point where *FI* value was maximum. The *FI* values and failure angles were calculated for all the value of W/D and E/D ratios.

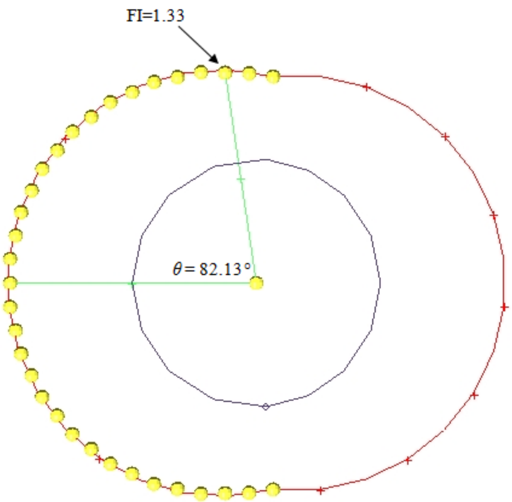

(a)

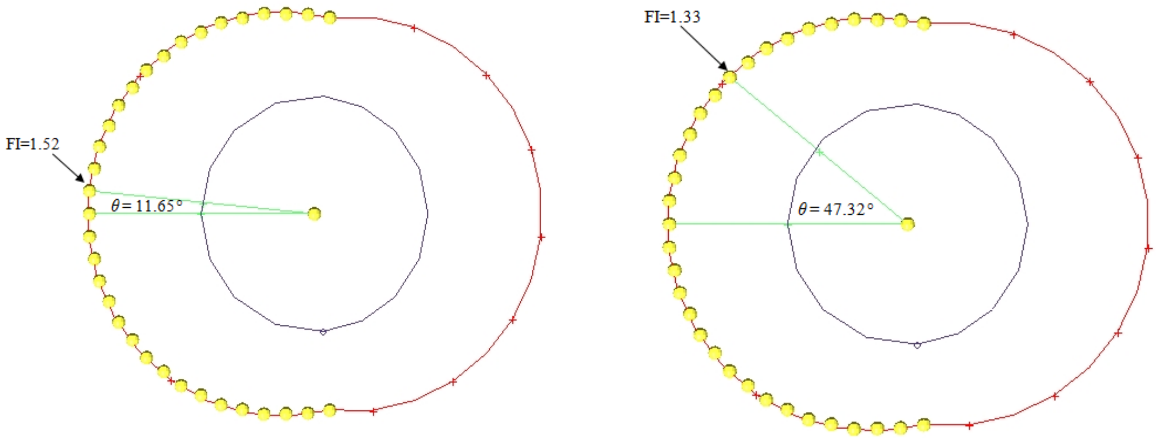

(b) **(c)**

Fig. 4.14 *FI* and failure angle on characteristic curve for (a) Net-Tension (b) Bearing (c) Shear-out

The failure modes based upon failure angle for all the different W/D and E/D ratios are given in Table 4.3.

Table 4.3 Comparison of failure modes for the specimens experimentally and numerically

Specimen	Experimentally		Numerically by calculating the failure index and failure angle	
	[0°/45°/0°]	[0°/90°/0°]	[0°/45°/0°]	[0°/90°/0°]
W/D=2, E/D=2	N	N	N+S	N+S
W/D=2,E/D=3	N	N	N	N
W/D=2,E/D=4	N	N	B+N	B+N
W/D=2, E/D=5	N	B+N	B+N	B+N
W/D=3, E/D=2	N	N	N+S	N+S
W/D=3,E/D=3	B+N	N	S	N+S
W/D=3,E/D=4	B+N	B+N	B+S	B+S
W/D=3, E/D=5	B+N	B+N	B	B
W/D=4, E/D=2	S	S	S	S
W/D=4,E/D=3	B+S	B+S	B+S	B+S
W/D=4,E/D=4	B+S	B	B	B
W/D=4, E/D=5	B	B	B	B
W/D=5, E/D=2	S	S	S	S
W/D=5,E/D=3	B+S	S+B	S	S+B
W/D=5,E/D=4	B+S	B	B	B
W/D=5, E/D=5	B	B	B	B

The comparison of the numerical and experimental results for the different W/D and E/D ratios for the 3 wt.% of nanoclay composite laminate specimen is also given in Table 4.3. Experimentally, failure modes for the pin joints can be determined from the stress vs.

strain plots as mentioned in the sections 4.2.1 and 4.2.2 which were shown in Fig. 4.5 and 4.6.

From Table 4.2, it can be seen that for W/D as 2, the failure modes were net tensions for all value of E/D ratios.

When W/D is 3, the failure modes are net tension or mixed mode of failure *i.e.*, bearing followed by net tension which was depend upon the E/D ratio. At low value of E/D ratio, the failure mode was net tension which changed to mixed mode of failure when E/D ratio was increased.

Shear out mode of failure occurred when W/D≥4 and E/D ≤ 3. When E/D ratio increased the mode of failure changed from shear out to bearing failure mode. For W/D≥4 and E/D≥4 there was bearing failure mode in all the specimens. The bearing failure mode was the most desirable failure mode due to its high load carrying capacity. The minor differences between experimental and FEM results are due to the manual preparation of large number of specimen.

4.4 Closure

In the present chapter, the effect of the [0°/45°/0°] and [0°/90°/0°] ply orientations and nanoclay content on the bearing strength and failure mode of the single hole pin joints was investigated, both experimentally and numerically. As discussed in the previous chapter, the strength of [0°/45°/0°] and [0°/90°/0°] ply orientations was higher as compared to [0°/45°/90°] ply orientation. So, the bearing strength and modes of failure of the single hole pin joints was compared [0°/45°/0°] and [0°/90°/0°] ply orientations with and without the the addition of 3 wt. % of nanoclay. The strength of the single hole pin joints was drastically dependent on both ply orientations and nanoclay wt.%. The ply orientation of [0°/45°/0°] had higher mechanical properties in longitudinal direction whereas ply orientations [0°/90°/0°] had high mechanical properties in transverse direction. It was observed that the bearing strength of the pin joints depend on both longitudinal and transverse mechanical properties. Results show that the bearing strength of [0°/90°/0°] ply orientation is about 10-12% higher than the bearing strength of [0°/45°/0°] ply orientation.

It was also observed that the type of failure was totally dependent on the geometric parameter *i.e.*, W/D and E/D ratios. Net tension and shear out failure modes occurred with small W/D and E/D values, respectively. These failures were immediate and without warning. So, the bearing failure is desirable, as it is progressive failure and joint with bearing mode of failure give the higher strength. The bearing mode of failure occurs for W/D and E/D ratios to be greater than 4. Finite element method was used to analyze the mode of failure using Tsai-Wu failure criterion along with the characteristic curve method. The results were in good correlation with the experimental ones.

The work in the present chapter was extended for double holes pin joints. The failure analysis of double holes pin joints is given in the next chapter.

Chapter 5 - Failure Analysis of Double Hole Pin Joint

As discussed in the previous chapter, for a single hole pin joint configuration the effect of two geometric parameter were studied along with two ply orientations *i.e.*,[0°/45°/0°] and [0°/90°/0°]. [0°/90°/0°] ply orientation had the higher strength as compared to the [0°/45°/0°] ply orientation which was further increased with addition of the 3 wt. % of nanoclay. The two geometric parameters *i.e.*, E/D and W/D ratios affected the bearing strength and the failure modes of the single hole pin joints.

The strength or load carrying capacity of the joint can be increased with the increase in number of fasteners in the joint. As the number of fasteners are increased, the number of geometric parameter to position the holes are also increased. The present chapter deals with the failure analysis of the joint with two holes. The double holes pin joints are prepared from [0°/90°/0°] ply orientation, with and without the addition of nanoclay. In the double pin joints, there are two possible configurations, *i.e.*, serial and parallel. In both these configurations, there are maximum of three independent geometric parameters that can be investigated. The geometric parameters were varied in both the cases *i.e.,* serial holes and parallel holes resulting into need of preparation of large number of specimens for the testing. Geometric parameters that were varied in case of double serial hole configuration were E/D, W/D and P/D ratio, where E is the distance between the free edge of the specimen and the first hole, W is the width of the specimen, P is the distance between the two holes and D is the diameter of the holes. In case of double parallel hole configuration the geometric parameters E/D, P/D and K/D ratio were varied. E is the distance between the free edge and the holes, P is the distance between the holes and K is the distance between the side edge and the hole nearer to it. The geometric parameters in case of serial hole configuration were varied as, E/D ratio from 2 to 5, W/D ratio from 2 to 5 and P/D ratio from 2 to 5, whereas geometric parameters in case of parallel hole configuration were varied as, E/D from 2 to 5, K/D from 1 to 4 and P/D from 2 to 5. These parameters are shown in the Fig. 5.1 along with the geometry of the laminates with serial and parallel double holes in the laminates.

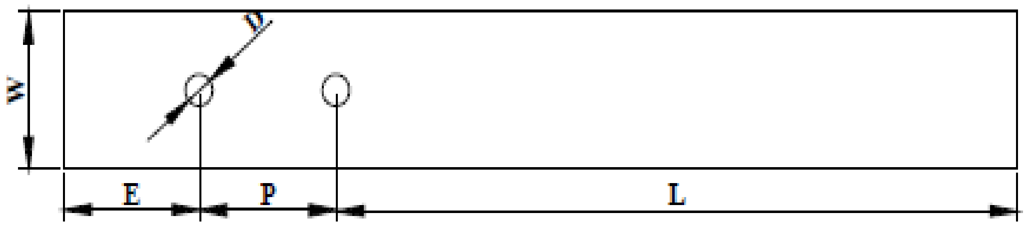

(a)

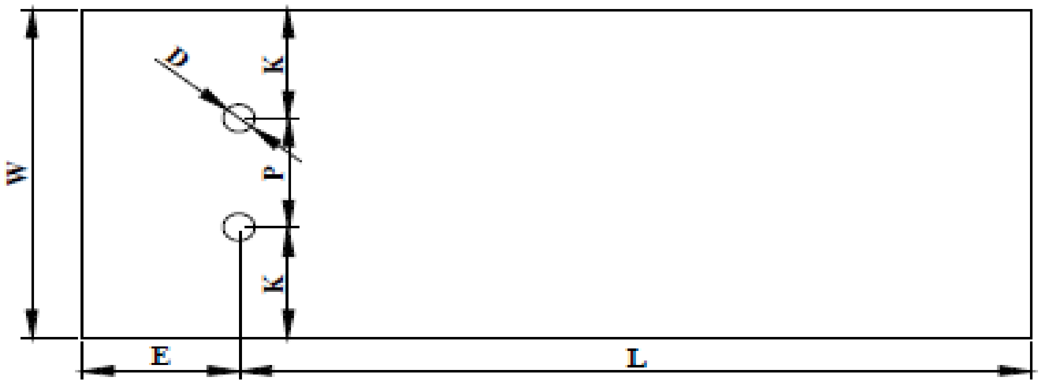

(b)

Fig. 5.1 Laminates with two holes in (a) Serial configuration (b) Parallel configuration

The total number of geometric parameters in each case is three with four levels of each parameter. Hence the total number of specimens required to be prepared as per the full factorial design for each case would be 4^3 *i.e.*, 64. So it would require a total of 128 samples for both the configurations. Making large number of specimens would utilize large amount of material which involve high cost and large amount of time. Design of Experiment can be used to reduce the number of specimens. Design of experiments is used for analyzing the influence of some specific variables on the experimental results (Nian *et al.*, 1999). Taguchi method is one of a standardized version of design of experiments which is used in the present work.

5.1 Taguchi Method

Taguchi method is one of the powerful statistical tool, which is used to study the effect of number of parameters on quality characteristic by giving the limited set of experiments. Taguchi method has been used by number of researchers from different areas (Anawa *et al.*, 2008; Nian *et al.*, 1999; Bhutta *et al.*, 2011; Ghani *et al.*; 2004) to analyze the influence of specific variables on the experimental results. In the present work, Taguchi method was used to analyze the effect of different geometric parameters on the strength of double holes pin joints. The basic steps that were used in Taguchi approach are shown in the Fig. 5.2.

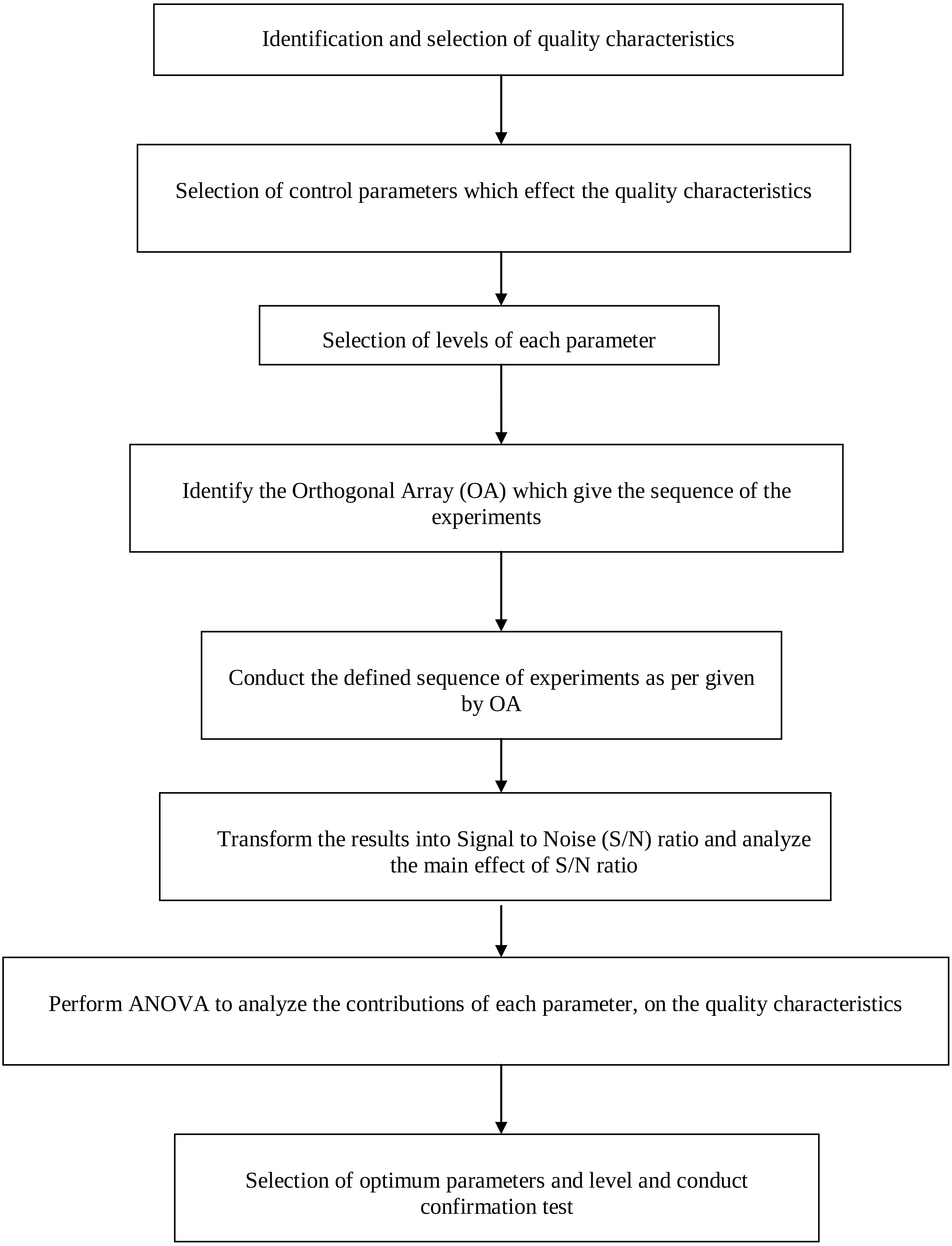

Fig. 5.2 Basic steps used in Taguchi approach

Table 5.1 shows the variation of the input geometric parameters for serial and parallel holes configurations.

Table 5.1 Input parameters for the serial and parallel hole configurations

Levels	Parameters for serial hole configurations			Parameters for parallel hole configurations		
	E/D	**W/D**	**P/D**	**E/D**	**K/D**	**P/D**
L1	2	2	2	2	1	2
L2	3	3	3	3	2	3
L3	4	4	4	4	3	4
L4	5	5	5	5	4	5

5.1.1 Orthogonal Array

Taguchi method has a set of specially designed tables which reduce the total number of experiments to be conducted to a very small number, by selecting only a few combinations of parameters and level for conducting the experiments. Orthogonal arrays are selected on the basis of the total number of parameters and levels of each parameter in the available problem. The degrees of freedom are the main criteria of selection of the orthogonal array. According to the rule, the degrees of freedom of the problem must be less than or equal to the degree of freedom of the selected orthogonal array. The availability of the orthogonal array with the required parameter-level combination must be available. In the present study, L16 orthogonal array was selected, because the degree of freedom of the orthogonal array which is 15 for L16, was greater than the degree of freedom of the present problem. The degree of freedom of the present problem is 9. L16 denotes that a total of 16 trials have to be run with 16 different combinations of parameters and level (Roy, 2010).

The orthogonal array was generated in the MINITAB software, which automatically gave the 16 parameter-level combinations to be considered for experimentation. Pin joints were prepared as per the generated orthogonal array, with and without the addition of the nanoclay. The generated orthogonal array for both serial and parallel holes configurations is shown in Table 5.2.

Table 5.2 Orthogonal array generated in MINITAB

Experimental run	For serial hole configuration			For parallel hole configuration		
	E/D	W/D	P/D	E/D	K/D	P/D
1	2	2	2	2	1	2
2	2	3	3	2	2	3
3	2	4	4	2	3	4
4	2	5	5	2	4	5
5	3	2	3	3	1	3
6	3	3	2	3	2	2
7	3	4	5	3	3	5
8	3	5	4	3	4	4
9	4	2	4	4	1	4
10	4	3	5	4	2	5
11	4	4	2	4	3	2
12	4	5	3	4	4	3
13	5	2	5	5	1	5
14	5	3	4	5	2	4
15	5	4	3	5	3	3
16	5	5	2	5	4	2

5.1.2 Analysis of the Signal-to-Noise (S/N) Ratio

As discussed in the previous chapter, there are three basic failure modes in pin joints *i.e.*, net tension, shear out and bearing. Bearing failure is often considered as the desirable mode because it usually gives a higher strength. Other modes of failure should be avoided through proper design of the joint geometry and composite material.

There are three quality characteristics for a product that indicate the direction of desirability of the results, *i.e.* the higher-the-better, the lower-the-better, or the nominal-the-better (Roy, 2010). The selection of a particular quality characteristic depends upon the desired variable which can be maximized, minimized, or can be kept within a particular range.

In the present work, the resistive force, which was the measure of bearing strength, was the response variable or quality characteristic which is to be maximized, so the higher-the-better quality characteristic was applied.

Signal is the effect of change in factor on the response of the quality characteristic, whereas noise is the effect of uncontrollable factors on the response of quality characteristic in the experiment (Roy, 2010). The Signal to Noise (S/N) ratio is a measure of the variation within an experiment when noise is present. S/N ratio consolidates several repetitions into one value that reflects the amount of variations present (Roy, 2010). The S/N ratio is calculated on the basis of the selected quality characteristic. For higher-the-better characteristic, the S/N ratio is calculated using equation (5.1).

$$S/N_H = -10\log\left(\frac{1}{n}\sum_{i=1}^{n}\frac{1}{y_i^2}\right) \tag{5.1}$$

Where, n is the number of repetitions and y is the observed data. In the present work, the observed data was the experimental value of the resistive force during three repetitions under the same set of conditions. The tests were performed on Zwick-Roell Universal Testing Machine with the help of a fixture. The basic shape of the fixture used for testing of the double hole pin joints is shown in Fig. 5.3. The fixture was designed such that all the combinations of different geometric parameters for both serial and parallel configurations can be tested on it. Tables 5.3 and 5.4 show the experimental results for the resistive force, corresponding S/N ratio, and the type of failure mode for serial and parallel hole configurations, respectively. The resistive forces given in Tables 5.3 and 5.4 are the average values after testing, at least three specimens for each run for both the neat and

3 wt.% of nanoclay specimens. In Tables 5.3 and 5.4, the symbols N, S and B are for net tension, shear out and bearing type of failure mode.

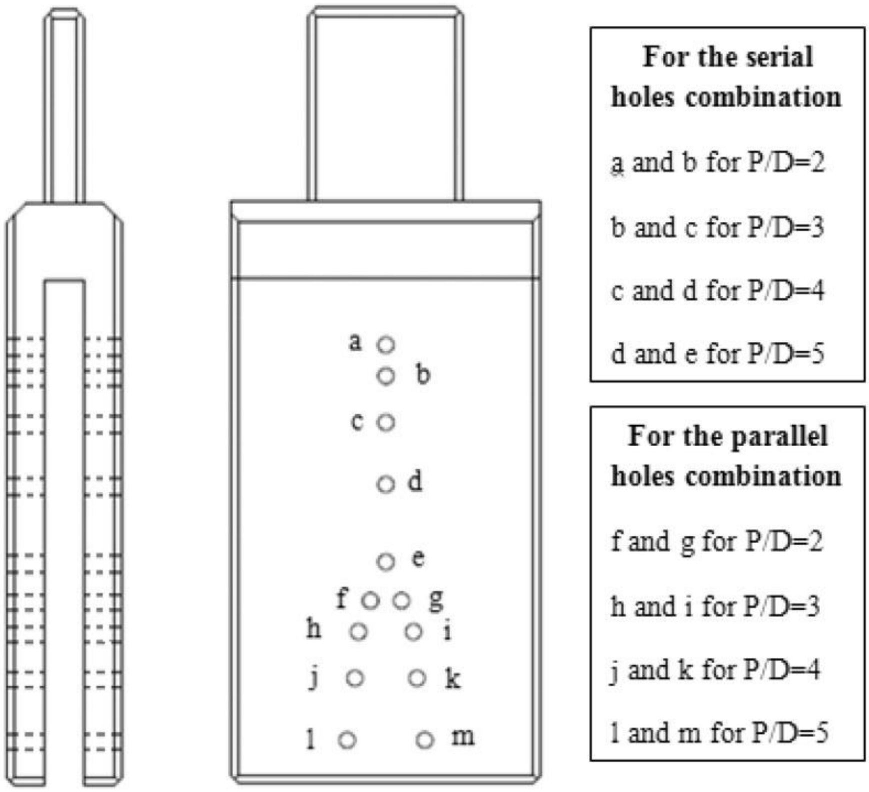

Fig. 5.3 Basic shape of the fixture used for tested serial and parallel hole configurations

It can be seen from Table 5.3 and 5.4 that the resistive force increases with the addition of nanoclay for both the serial and parallel joint configurations. The improvement of bearing strength by addition of nanoclay into the matrix may be attributed to the strong interfacial bonding between the fiber and matrix which contributes for higher bearing strength (Friedrich *et al.*, 2005).

The failure modes were seen from the resistive force vs. displacement testing of all the experiments run on the UTM machine. The resistive force vs. displacement plots for each type of the failure is given in the Figs. 5.4 and 5.5 for serial and parallel hole configurations, respectively. Figure 5.4 shows the plots for the resistive force and displacement variations depicting the type of failure mode in serial hole configurations with the addition of nanoclay. The plots were given only for three different combinations of E/D, W/D, and P/D pertaining to each of the type of failure modes.

Table 5.3 Experimental results of the resistive force and corresponding S/N response for the serial holes configuration

Experimental run	E/D	W/D	P/D	Without nanoclay		With 3 wt. % of nanoclay		Failure modes
				Average resistive force (N)	S/N ratio (dB)	Average resistive force (N)	S/N ratio (dB)	
1	2	2	2	940	59.4626	2910	69.2779	N
2	2	3	3	1830	65.2490	3630	71.1981	S
3	2	4	4	2930	69.3374	4210	72.4856	S
4	2	5	5	3040	69.6575	4280	72.6289	BS
5	3	2	3	3590	71.1019	4740	73.5156	N
6	3	3	2	3950	71.9319	5260	74.4197	BN
7	3	4	5	4560	73.1793	5910	75.4317	B
8	3	5	4	4620	73.2928	6080	75.6781	B
9	4	2	4	4690	73.4235	6120	75.7350	N
10	4	3	5	4930	73.8569	6430	76.1642	BN
11	4	4	2	4750	73.5339	6380	76.0964	B
12	4	5	3	5110	74.1684	6640	76.4434	B
13	5	2	5	4590	73.2363	6250	75.9176	N
14	5	3	4	4730	73.4972	6410	76.1372	BN
15	5	4	3	5080	74.1173	6620	76.4172	B
16	5	5	2	4440	72.9477	6090	75.6923	B

Table 5.4 Experimental results of the resistive force and corresponding S/N response for the parallel holes configuration

Experimental run	E/D	K/D	P/D	Without nanoclay		With 3 wt.% of nanoclay		Failure modes
				Average Resistive Force (N)	S/N ratio (dB)	Average Resistive Force (N)	S/N ratio (dB)	
1	2	1	2	470	53.4420	820	58.2763	BN
2	2	2	3	1390	62.8603	1520	63.6369	S
3	2	3	4	2380	67.5315	2940	69.3669	S
4	2	4	5	2590	68.2660	2990	69.5134	S
5	3	1	3	2090	66.4029	2570	68.1987	BN
6	3	2	2	2910	69.2779	3110	69.8552	S
7	3	3	5	3700	71.3640	4010	72.0629	BS
8	3	4	4	3380	70.5783	4000	72.0412	B
9	4	1	4	3510	70.9061	4030	72.1061	BN
10	4	2	5	3890	71.7990	4780	73.5886	B
11	4	3	2	4300	72.6694	5170	74.2698	B
12	4	4	3	4380	72.8295	5200	74.3201	B
13	5	1	5	3260	70.2644	4040	72.1276	BN
14	5	2	4	3640	71.2220	4540	73.1411	B
15	5	3	3	4410	72.8888	5400	74.6479	B
16	5	4	2	4310	72.6895	5200	74.3201	B

It can be seen from Fig. 5.4 (a) that there was a sudden decrease after a peak point, which means it was failed with net tension type of failure mode. Figure 5.4 (b) shows that there was a decrease after couple of peak points confirming that the shear out failure modes occurred in the joint. In Fig. 5.4 (c), it can be seen that after the peak point, the values decreases to some extent and thereafter remain constant with zig–zag formation. This was due to the bearing failure mode.

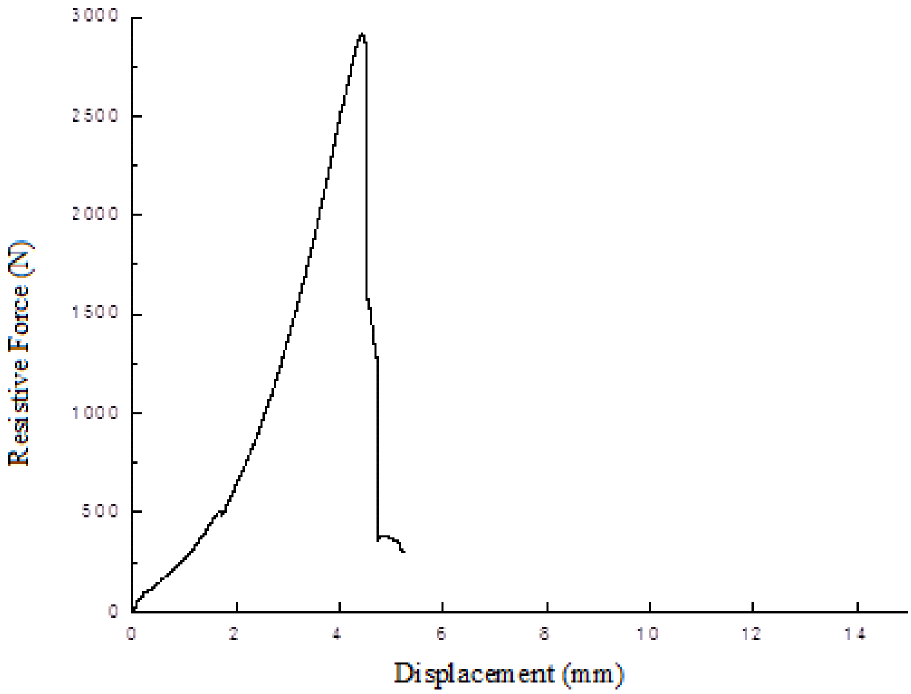

(a)

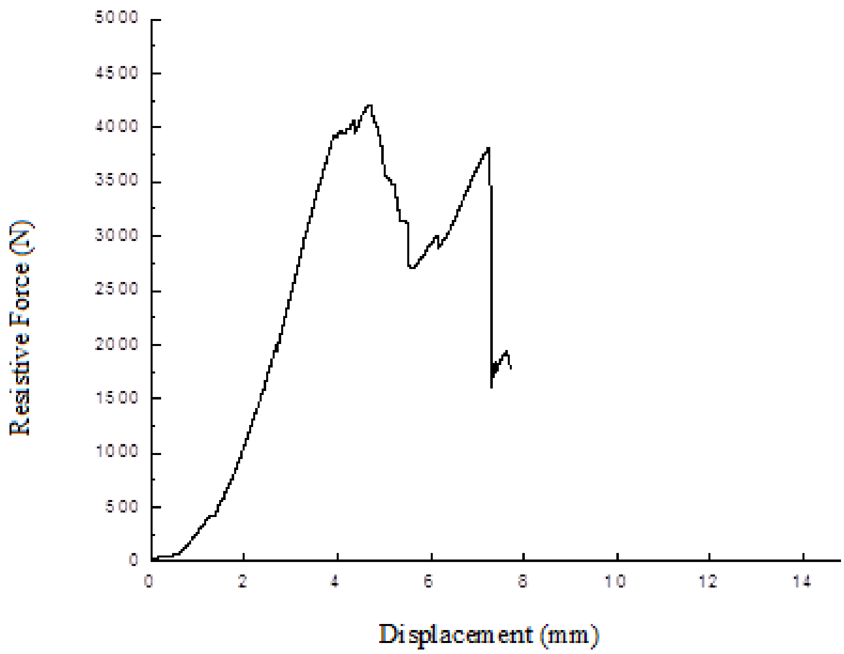

(b)

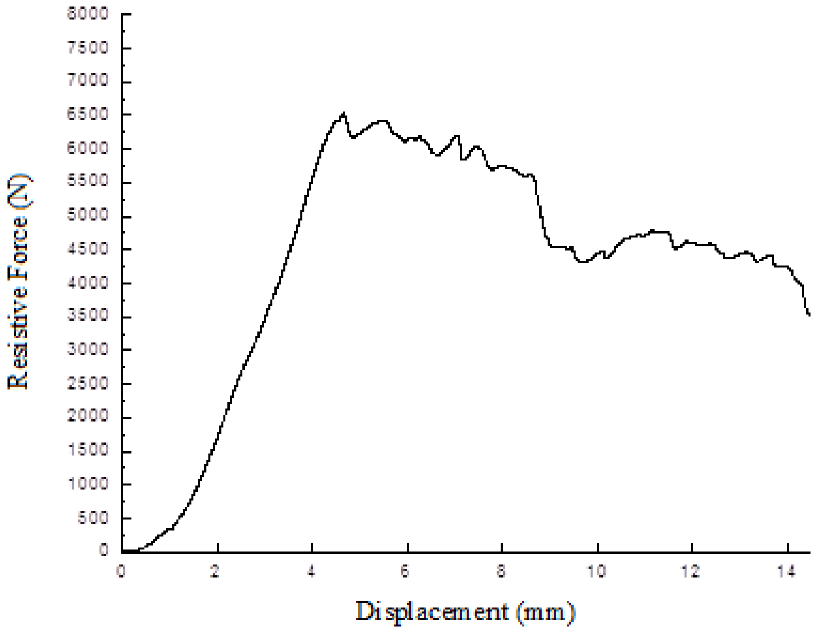

(c)

Fig. 5.4 Force vs. Displacement curves for serial hole configurations with nanoclay (a) Net Tension type of failure for E/D=2, W/D=2, P/D=2 (b) Shear Out type of failure for E/D=2, W/D=4, P/D=4 (c) Bearing type of failure for E/D=4, W/D=5, P/D=3

Figure 5.5 shows the main effect plots for S/N ratio for specimens with 3 wt.% of the nanoclay.

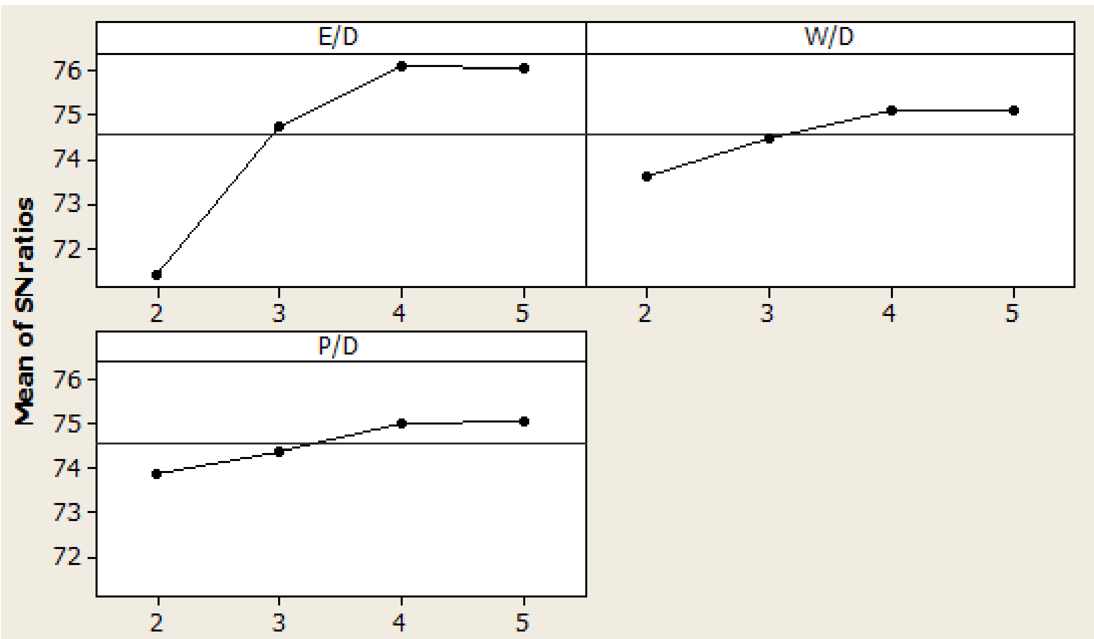

Fig. 5.5 Main effect plots of serial holes configuration for S/N ratio for 3 wt. % of the nanoclay

The 'main effect' is the effect of levels on the response for a particular geometric parameter. This is done by plotting the mean S/N ratio across the levels for that parameter.

As can be seen from Fig. 5.5, the slope gradient of E/D ratio was higher than that of W/D and P/D ratios which means that the contribution of E/D was more significant than W/D and P/D ratios. With the lower value of E/D, the failure was catastrophic which may be net tension or shear out. This further depends upon the width of the specimen, *i.e.* W/D ratio. At the lower value of W/D, the failure mode was net tension. If the W/D value increased, the width of the specimen increased and the failure mode shifted to shear out.

With the higher value of E/D ratio, the failure was net tension or bearing. This again depends upon the W/D ratio. At the lower value of W/D, the failure mode was net tension which converted to bearing as the W/D ratio increased. It was also found from Fig. 5.5 that the combination of E/D, W/D, and P/D ratios for higher bearing strength is 4, 4 and 5, respectively.

Figure 5.6 shows the graphical plots for average resistive force and displacement variations depicting the net tension, shear out, and bearing type of failure mode in parallel holes configurations with the addition of nanoclay. The plots are given only for three different combinations of E/D, K/D, and P/D pertaining to the type of failure modes.

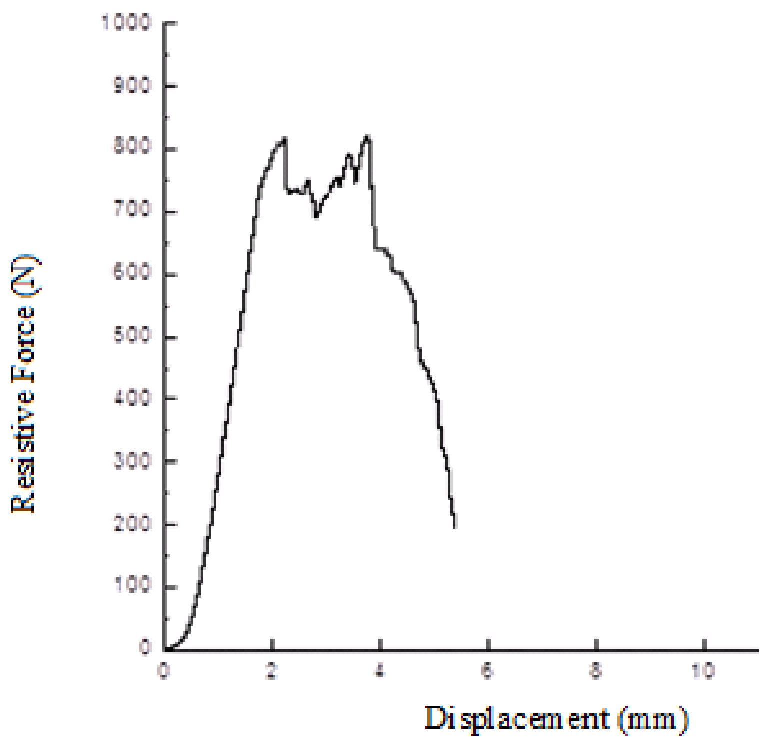

(a)

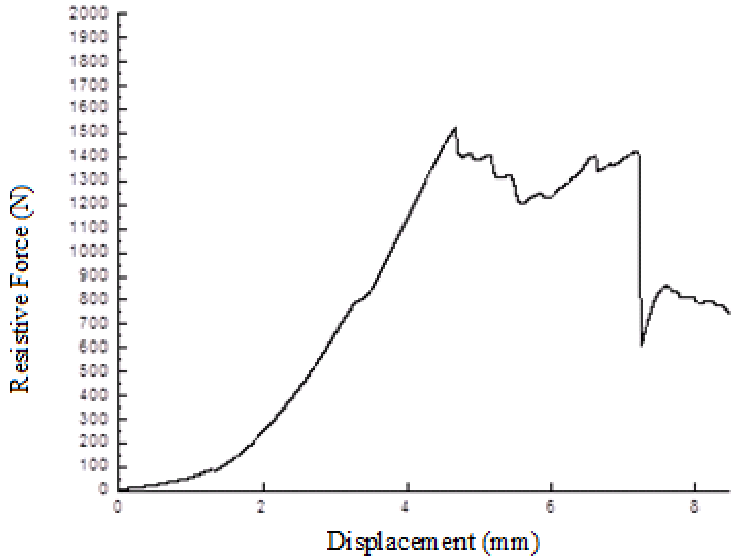

(b)

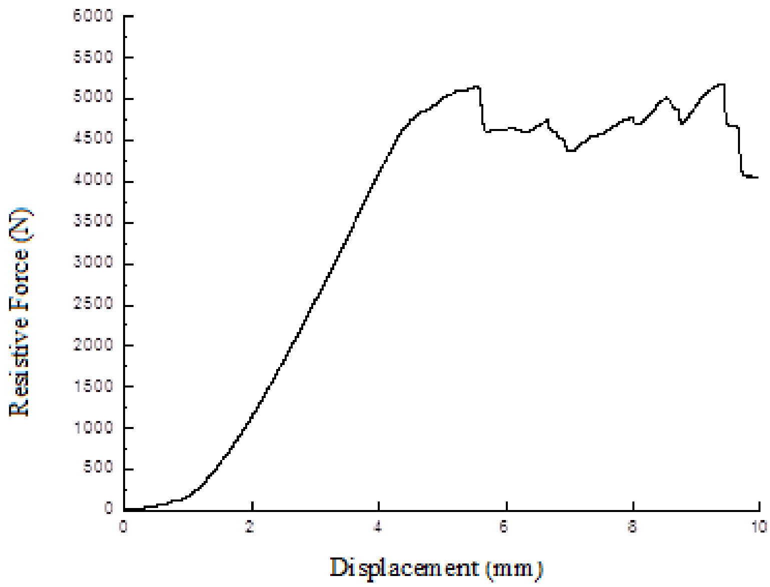

(c)

Fig. 5.6 Force vs. Displacement curves for parallel hole configurations with nanoclay (a) Bearing with Net Tension type of failure for E/D=2, K/D=1, P/D=2 (b) Shear Out type of failure for E/D=2, K/D=2, P/D=3 (c) Bearing type of failure for E/D=4, K/D=4, P/D=3

It can be seen from Fig. 5.6 (a) that the net tension failure mode is in combination with the bearing type of failure mode due to the larger width of the plate in parallel hole configuration as compared to serial hole configuration. Figures 5.6 (b) and 5.6 (c) show the shear out and bearing failure mode as depicted from the force vs. displacement graph.

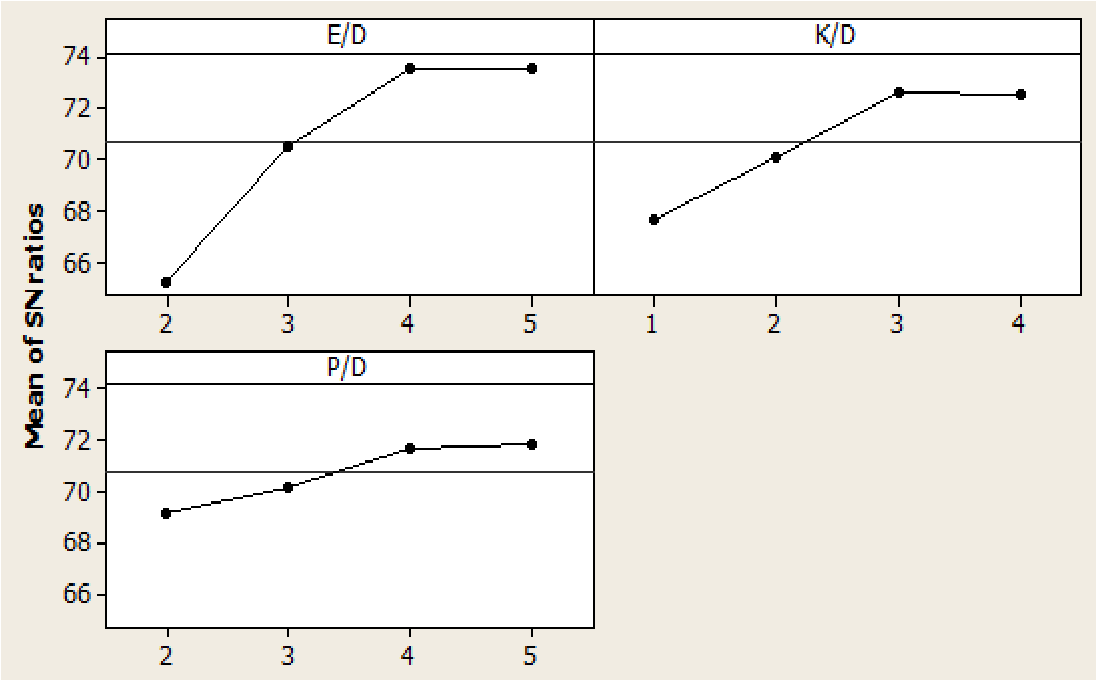

Fig 5.7 Main effect plots for S/N ratio for parallel holes configuration with 3 wt. % of nanoclay

Main effect plot for S/N ratio for parallel hole configuration with 3 wt.% of nanoclay are shown in the Fig. 5.7. It can be seen from Fig. 5.7 that the slope gradient of E/D and K/D ratios was higher than that of P/D ratio which means that the contribution of E/D and K/D ratios was more significant as compared to P/D ratio.

With the lower value of E/D, the failure may be net tension or shear out. This was further depending upon the width of the specimen, *i.e.* K/D and P/D ratios. K/D ratio was more significant than P/D ratio as the distance from the hole to the side edge is responsible for net tension failure mode. At the lower value of K/D, the failure mode was net tension. If the K/D value increased, the failure mode shifted to shear out.

With the higher value of E/D ratio, the failure was net tension or bearing. This again depends upon the K/D ratio. At the lower value of K/D, the failure mode was net-tension which converted to bearing as K/D ratio increased. It was also found from Fig. 5.7 that the combination of E/D, K/D and P/D ratios for higher bearing strength is 4, 3 and 5 respectively.

5.1.3 Analysis of Variance

The purpose of the Analysis of Variance (ANOVA) is to investigate the process parameters that significantly effect the performance characteristics that is analyzed by the multi-response of the S/N ratio by the sum square of the deviation from the total mean of the S/N response ratio with contribution of each process parameter and error. The total sum of the squared deviation, SS_T was calculated from the total mean of the multi-response S/N ratio, N_m by using equation (5.2).

$$SS_T = \sum_{j=1}^{n} \left(N_j - N_m\right)^2 \tag{5.2}$$

Where, n is the number of experiments in the orthogonal array and N_j is the mean of the multi-response S/N ratio of the j^{th} experiment. SS_T is decomposed into two sources, the sum of the squared deviations, SS_d due to each process parameter and the sum of the squared error, SS_e. The percentage contribution by each of the process parameter in the total sum of the squared deviation was then calculated.

To estimate which parameter significantly effect the performance of the process, a tool called the *F*-test is applied. In performing the *F*-test, the mean of the squared deviations, SS_m is calculated by dividing the sum of squared deviation, SS_d with number of degree of freedom of the process parameter. Thereafter the *F* value of each process parameter is a ratio of the mean of the sum square deviations, SS_m to the mean of the squared error, SS_e. Usually, larger the F value, greater the effect of the change in parameter on the performance of the process (Nalbant *et al.*, 2007; Bhutta *et al.*, 2011).

Table 5.5 ANOVA for the serial pin joints with nanoclay

Source	**DF (Degree of freedom)**	**Sum of square**	**Mean square**	**F**	**Contribution (%)**
E/D	3	58.5408	19.5136	118.42	84.50
W/D	3	6.0324	2.0108	12.20	8.7
P/D	3	3.7128	1.2376	7.51	5.359
Residual Error	6	0.9887	0.1648	-	1.43
Total	15	69.2746	-	-	100

Table 5.6 ANOVA for the parallel pin joints with nanoclay

Source	DF (Degree of freedom)	Sum of square	Mean square	F	Contribution (%)
E/D	3	186.84	62.281	19.72	64.228
K/D	3	66.12	22.040	6.98	22.72
P/D	3	18.99	6.330	2.00	6.52
Residual Error	6	18.95	3.158	-	6.52
Total	15	290.90	-	-	100

Table 5.5 and 5.6 shows the results of ANOVA for resistive force with the addition of nanoclay for serial and parallel hole configurations, respectively. The values are calculated at 95% confidence level. It can be analyzed from Table 5.5 that the E/D ratio had the maximum contribution or effect on the resistive force of the joint. It can also be seen from the table that the W/D and P/D ratios had the least and almost similar effect on the resistive force of the serial joints.

Table 5.6 shows that the E/D ratio had the maximum contribution on the resistive force of parallel pin joints. The P/D ratio had the minimum contribution whereas K/D ratio had significant contribution on the resistive force of the parallel pin joints.

5.1.4 Confirmation Tests

Once the optimal level of geometric parameters is selected, the final step is to predict and verify the improvement in the resistive force of the joint at optimal level of geometric parameters. Tests were conducted experimentally for the optimized configuration *i.e.*, $E/D = 4$, $W/D = 4$ and $P/D = 5$ for the serial pin joints and $E/D = 4$, $K/D = 3$ and $P/D = 5$ for the parallel pin joints. Figure 5.8 shows the graphical plots of force displacement variation for optimized parameters along with the specimens for both serial and parallel hole configurations. The graphs are shown for the samples prepared with the addition of nanoclay as filler material. It can be seen from the Fig. 5.8 that there is bearing type of failure mode in the serial and parallel joint configuration for the optimized geometric parameters. The bearing failure mode is the most desirable one as compared to net-tension and shear-out failure modes as it is non-catastrophic and has higher strength. The resistive force values obtained after conducting the confirmation experiments for specimens prepared with nanoclay and without nanoclay are shown in Fig. 5.9. It can also be seen that there is about 12-15 % increase in the resistive force for the specimens with nanoclay material as compared to neat specimens.

The predicted or estimated resistive force at the optimal level of the geometric parameters was calculated using equation (5.3).

$$F_{opt}^2 = \frac{1}{10^{\left(\frac{-S/N_{opt}}{10}\right)}} \tag{5.3}$$

The optimized value of S/N ratio *i.e.*, S/N_{opt} at the optimized process parameters conditions was calculated using equation (5.4).

$$S/N_{opt} = S/N_{mean} + S/N_{E/D4} - S/N_{mean} + S/N_{W/D4} - S/N_{mean} + S/N_{P/D5} - S/N_{mean} \tag{5.4}$$

Where, S/N_{mean} is the mean of the S/N data, $S/N_{E/D4}$ is the mean of the S/N data for the parameter E/D at 4, $S/N_{W/D4}$ is the mean of the S/N data for the parameter W/D at 4 and $S/N_{P/D5}$ is the mean of the S/N data for the parameter P/D at 5.

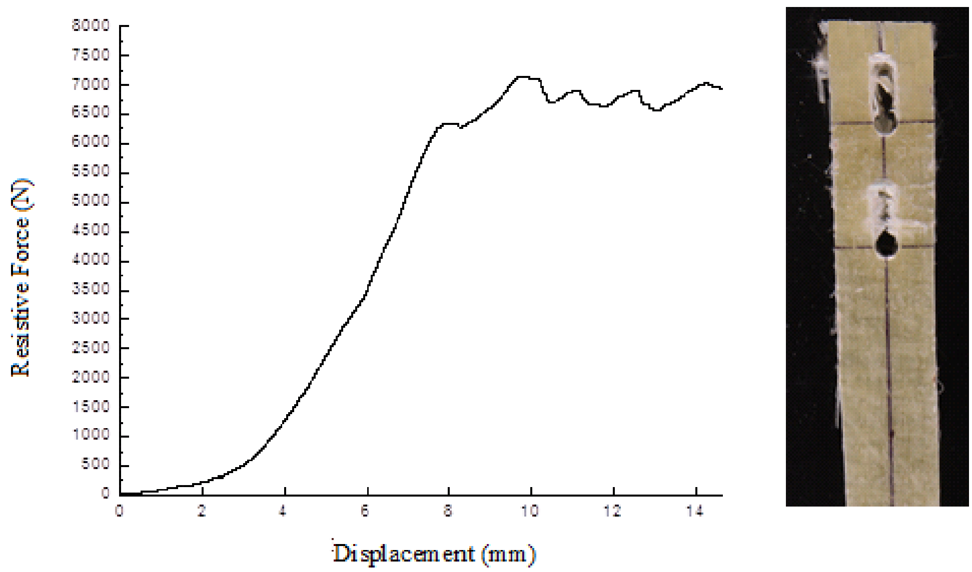

(a)

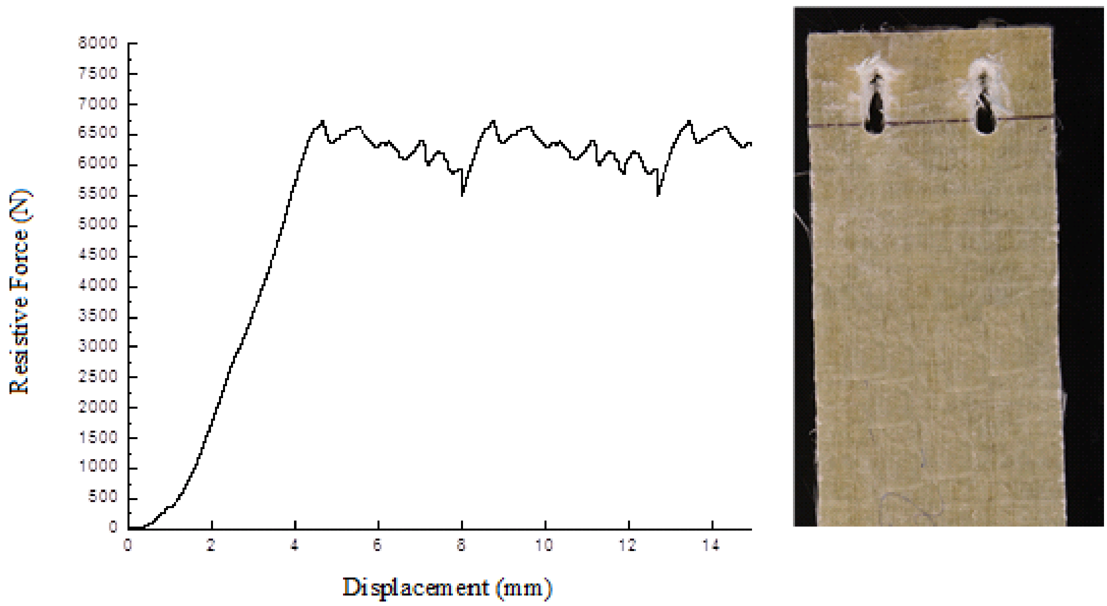

(b)

Fig. 5.8 Force vs. Displacement curves for optimized parameters for specimens prepared from nanoclay for (a) Serial holes configuration for E/D=4, W/D=4, P/D=5 (b) Parallel holes configuration for E/D=4, K/D=3, P/D=5

Similarly, the resistive force for parallel joint configuration was estimated at the optimized parameters of E/D=4, K/D=3 and P/D=5.

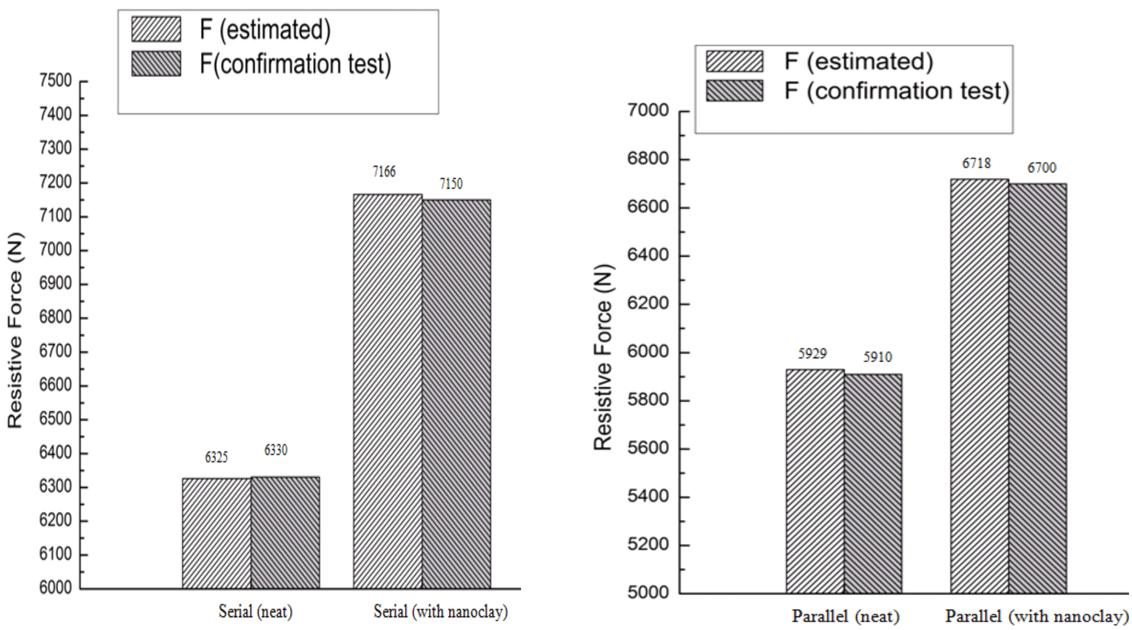

(a) **(b)**

Fig. 5.9 Comparison of the estimated and confirmation test values of the resistive forces for the optimized geometric parameters (a) Serial hole pin joint configuration (b) Parallel hole pin joint configuration

The estimated values for both the serial and parallel joint configurations are also shown in Fig. 5.9. It can be seen from Fig. 5.9 that there is a good agreement between the predicted and the experimental resistive force in both the configurations.

5.2 Finite Element Modeling

As discussed in the previous chapter, finite element analysis was done using the characteristic curve method (Whitney *et al.* 1974; Chang *et al.*, 1982) and Tsai-Wu failure theory (Tsai and Wu, 1971) for the double holes configuration.

Geometric model was prepared in Pro-E modeling software with the different geometric parameters for double-hole configurations. The basic geometries are shown in Fig. 5.1. The model was converted into IGES format and imported into HyperMesh software for analysis. The ply orientation was symmetric with respect to the z = 0 plane. High density four-noded shell quadrilateral elements were used to discretize the model. The inbuilt functions of the package were used for the verification of the quality of the mesh generated.

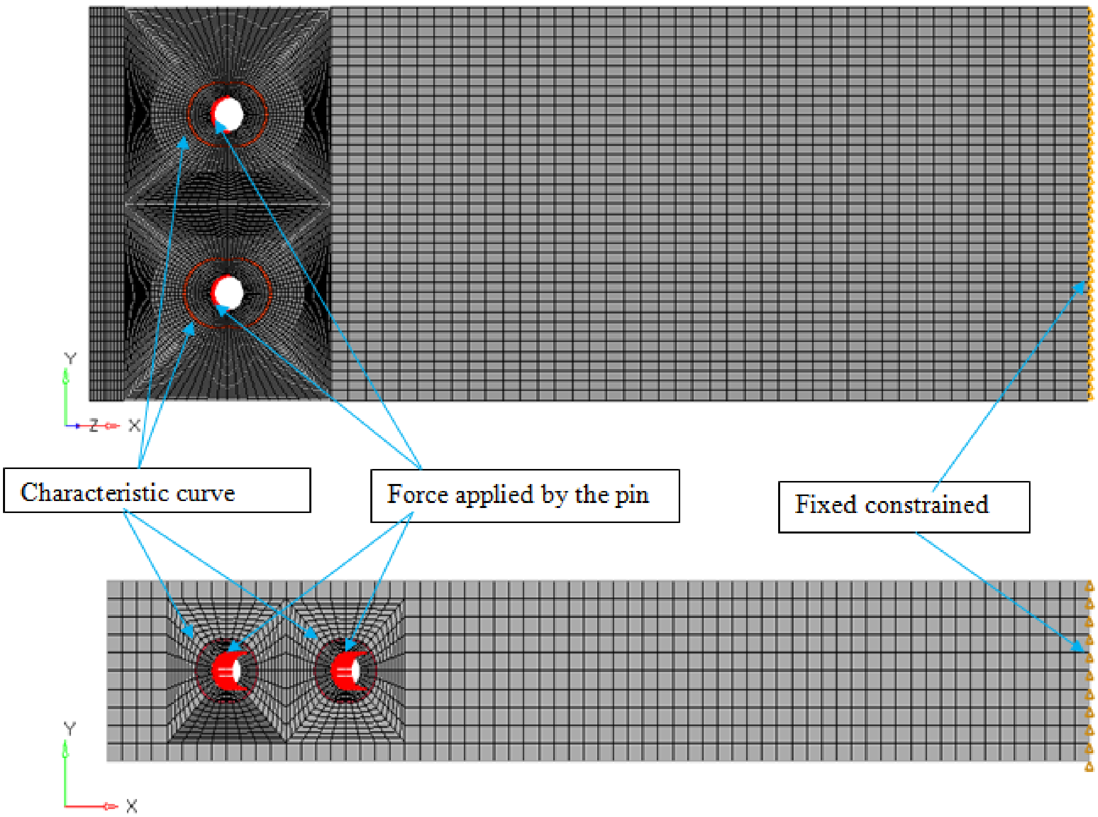

Fig. 5.10 Applied forces and boundry conditions for the serial and parallel pin jonts

The direction of applied forces and boundary conditions for the serial and parallel pin joints are shown in Fig. 5.10. Convergence study was performed for the generated mesh by re-creating the denser elements around the holes and re-analyzing the results.

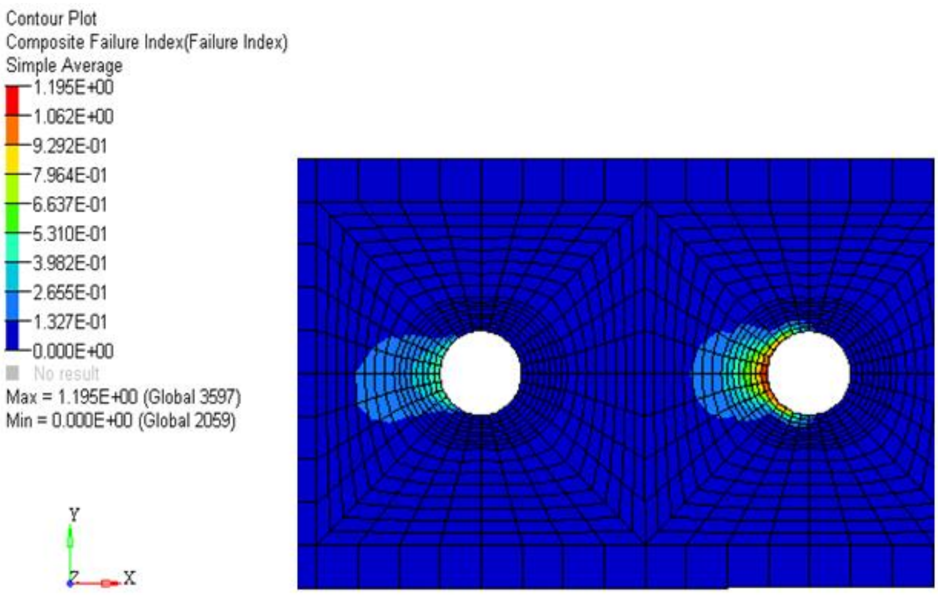

(a)

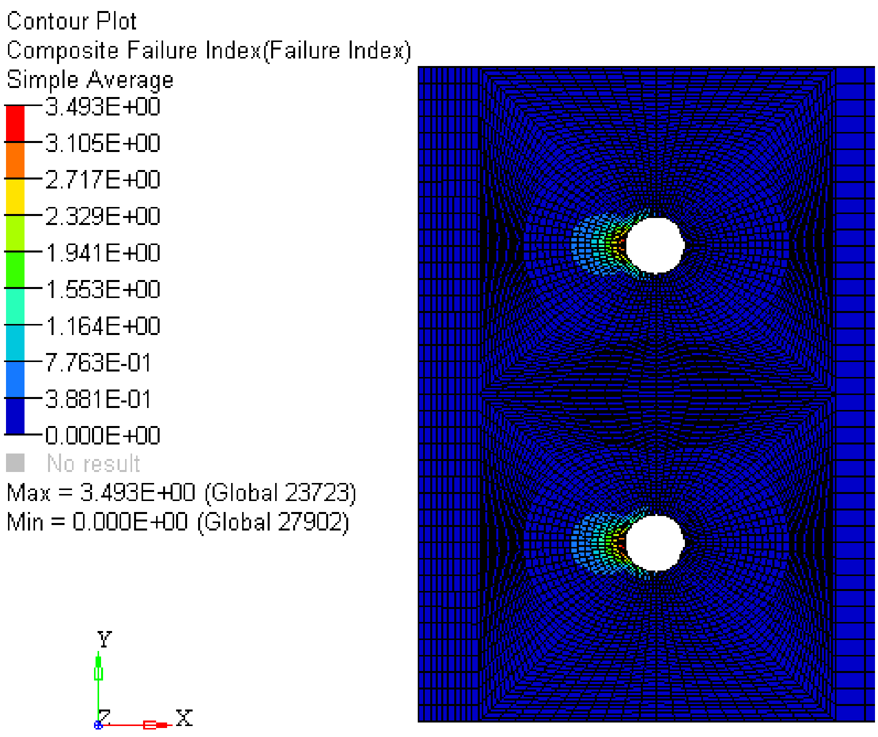

(b)

Fig. 5.11 *FI* for the optimized configuration of (a) Serial pin joints (b) Parallel pin joints

The characteristics curves, as shown in Fig. 5.10, was drawn using the R_{ot} and R_{oc} values for serial and parallel pin joint models. Failure angle was measured using the *FI* value on the characteristic curve as was done in the previous chapter.

Figure 5.11 shows the *FI* values around the holes for optimized combination of geometric parameters *i.e.*, E/D=4, W/D=4, P/D=5 for serial and E/D=4, K/D=3, P/D=5 for parallel pin joint configurations

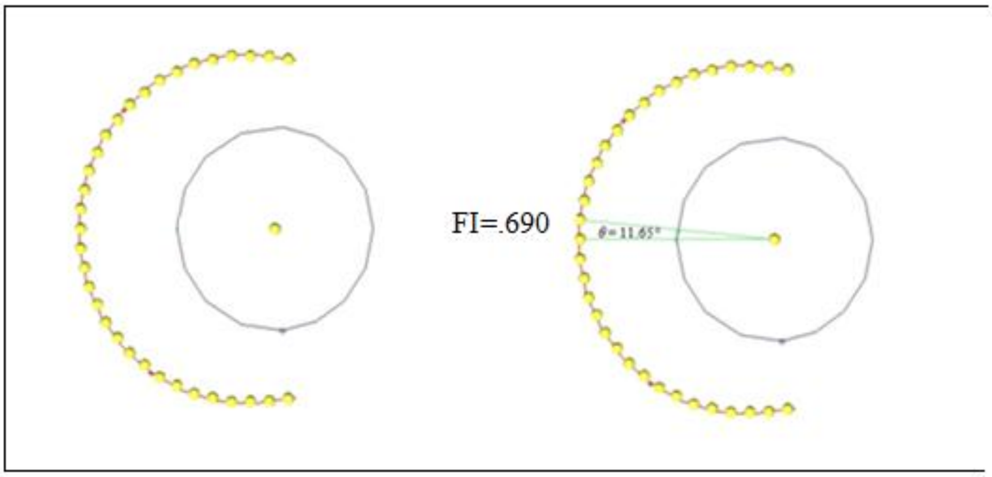

(a)

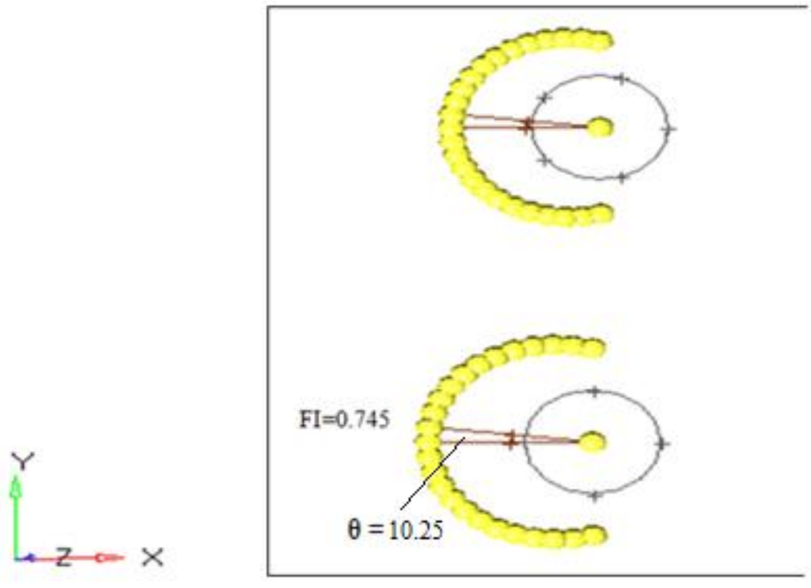

(b)

Fig. 5.12 *FI* on the characteristic curve for the optimized parameters for configuration (a) Serial pin joints (E/D=4, W/D=4, P/D=5) (b) Parallel pin joints (E/D=4, K/D=3, P/D=5)

Figure 5.12 (a) and (b) shows the different points on the characteristic curve for calculating the *FI* value and failure angle for optimized parameters of serial and parallel pin joint configuration, respectively. By determining the value of FI on the characteristic curve, optimized value of force F_{opt} was calculated using equation (5.6).

$$F_{opt} = F / FI_{max} \tag{5.6}$$

Where, F is the applied force and FI_{max} is the maximum value of the Failure Index on the characterstic curve. The value of optimized force calculated numerically using the characteristic curve method is shown in Fig. 5.13.

The comparison between the optimized resistive forces predicted using Taguchi philosophy, from confirmation test and calculated using characteristic curve can be made from Fig. 5.13. The results show that there is fairly good correlation between the resistive force from the three different methods for both the serial and parallel pin joint configurations.

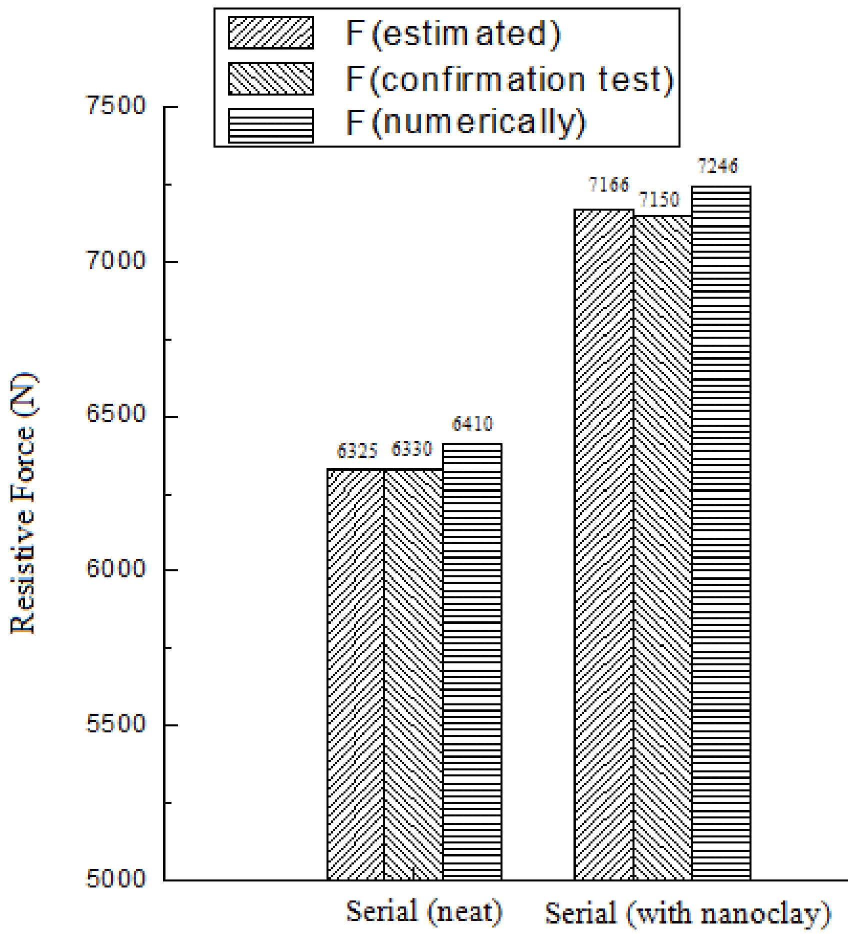

(a)

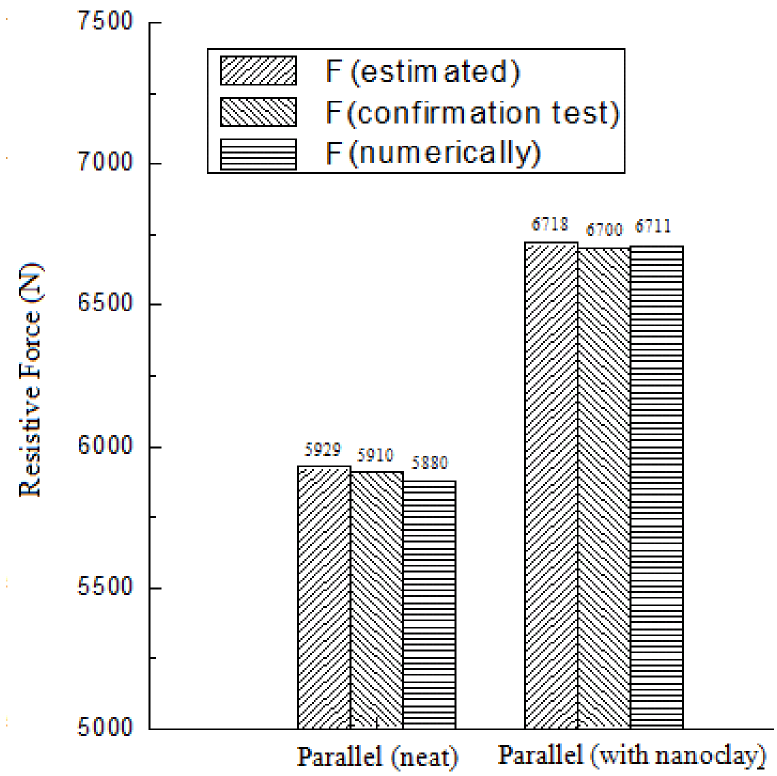

(b)

Fig. 5.13 Comparison of optimized value of force for (a) Serial pin joint configuration (b) Parallel pin joint configuration

5.3 Closure

In the present chapter, the bearing strength of the double pin-loaded glass epoxy nanoclay laminates for serial and parallel configuration was investigated. Taguchi method provides a systematic and efficient methodology for the optimization of the geometric parameters to analyze the resistive force. The E/D ratio is the most significant parameter to increase the bearing strength of the double hole pin joint configurations. The percentage contribution of E/D ratio in serial hole configuration is 84.5% and in parallel hole configuration is 64.23%, of the total contribution of all the parameters combined together. It is seen that K/D ratio also has a notable contribution of 22.72% in parallel configuration. It is also observed in the present chapter that the joints with double holes pin joints must have a minimum value of E/D–W/D–P/D as 4–4–5 in serial configuration and E/D–K/D–P/D as 4–3–5 in parallel configuration for the bearing mode which gives the significant increase in strength. With the addition of the nanoclay, the interfacial bond between fiber and epoxy increases which contributes to enhance the bearing strength of the joint. The bearing strength of the double pin joints increased by 12–15% as compared to the joints prepared without the nanoclay content. The characteristic curve method along with the Tsai–Wu failure criterion was used to analyze the double pin joint configurations. The results were in a good correlation with the experimental ones.

The work was further extended for multi holes pin joints. The failure analysis of multi holes pin joints is given in the next chapter.

Chapter 6 - Failure Analysis of Multi Holes Pin Joint

From the previous chapter it was seen that the resistive force can be increased with increase in number of pins in the laminates as load is distributed among the fasteners. Failure analysis of double holes pin joints was done for [0°/90°/0°] ply orientation with and without the addition of the nanoclay content, for comparing the strength. In the double holes pin joints there were three independent geometric parameters for both serial and parallel holes configurations. The effect of these geometric parameters on the resistive force was studied. The contribution of each geometric parameter was analyzed with the help of Taguchi method and ANOVA.

The strength of the pin joints can be further increased with the increase in number of fasteners. But as the number of the fasteners is increased in the pin joints, the numbers of the geometric parameters required to locate the hole are also increased. So, the present chapter deals with the failure analysis of the multi holes pin joint to study the contribution of different geometric parameters on the resistive force. Multi holes pin joints were prepared with [0°/90°/0°] ply orientation and with 3 wt.% of the nanoclay.

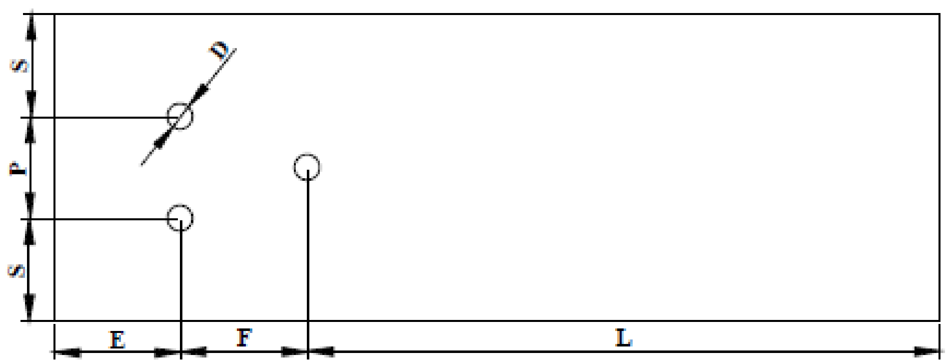

(a)

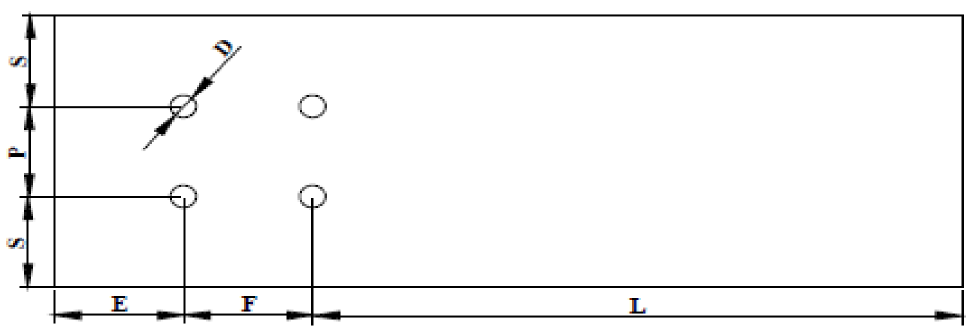

(b)

Fig. 6.1 Multi holes configuration pin joints with different geometric parameters (a) Three holes configuration (b) Four holes configuration

In the present work on multi holes pin joints, the three and four holes pin joints were studied for their failure strength and failure mode. The configurations along with the geometric parameters are shown in Fig. 6.1. The geometric parameters *i.e.*, the distance from the free edge of the specimen to the diameter of the first two holes (E/D) ratio, the distance between two holes along the length of the specimen to the diameter of the hole (F/D) ratio, the distance between the two holes along the width of the specimen to the diameter of the hole (P/D) ratio and side width to diameter (S/D) ratio were studied for their effect on strength and failure modes of the multi holes joint.

As discussed in the previous chapter, Taguchi method and ANOVA were applied to analyze the effect of the geometric parameters in the multi holes pin joints. Failure analysis was also done numerically using the characteristic curve along with the Tsai-wu failure theory.

6.1 Design of Experiments

As discussed in the previous chapter, Taguchi method was applied for defining the layouts of the experiments using the different geometric parameters in three and four holes pin joints. The work is to study the effect of the maximum independent geometric parameters on the bearing strength and failure modes in the multi hole pin joints. Table 6.1 shows the variation of the input geometric parameters used in the present work.

Table 6.1 Input parameters for three and four holes configurations

Levels	**Parameters for three and four holes configurations**			
	E/D	**F/D**	**S/D**	**P/D**
L1	2	2	2	2
L2	3	3	3	3
L3	4	4	4	4
L4	5	5	5	5

6.1.1 Orthogonal Array

Taguchi method was applied for defining the layouts of the experiments using the different geometric parameters in three and four holes pin joints. As discussed in the previous chapter, Taguchi method has a set of pre-designed tables called Orthogonal array.

Table 6.2 Experimental layout using an L_{16} orthogonal array

Experimental Run	E/D	F/D	S/D	P/D
1	2	2	2	2
2	2	3	3	3
3	2	4	4	4
4	2	5	5	5
5	3	2	3	4
6	3	3	2	5
7	3	4	5	2
8	3	5	4	3
9	4	2	4	5
10	4	3	5	4
11	4	4	2	3
12	4	5	3	2
13	5	2	5	3
14	5	3	4	2
15	5	4	3	5
16	5	5	2	4

Orthogonal array reduce the total number of experiments to be conducted to a smaller value, by selecting only a few combinations of parameters and level for conducting the experiments. Orthogonal arrays are selected on the basis of the total number of parameters and levels of each parameter in the problem. The degree of freedom is the main criteria of selection of the orthogonal array. According to the rule, the degrees of freedom of the problem must be less than or equal to the degree of freedom of the orthogonal array selected. In the present work on multi holes pin joints, four number of parameters with four levels are selected. The degree of freedom in the present work becomes 12 *i.e.*, (number of parameters) × (number of levels-1). The orthogonal array should be selected such that its degree of freedom should be greater than the degree of freedom of the problem.

As per the Taguchi method, the pre-defined table of L16 Orthogonal array has 15 degree of freedom which is greater than the present problem. L16 array denotes that a total of 16 trials have to be run with pre-defined sequence of parameters with their levels. These pre-defined sequences for experimental runs are given in Table 6.2.

6.1.2 Analysis of the Signal-to-Noise (S/N) ratio

S/N ratio analysis determines the most robust set of operating conditions from variations within the results. As discussed in the previous chapter, to obtain the optimal strength, the average resistive force is to be maximized, so the higher-the-better performance characteristic is taken in the present work. Equation (5.1) given in the previous chapter is used to calculate the S/N ratio for higher-the-better characteristic.

Tests were carried out in tension mode on a Zwick-Roell Universal Testing Machine – Model Z010, Zwick-Roell, Germany. The lower edge of the specimen was clamped and its opposite edge was loaded through steel pins as discussed in the previous chapter. The fixtures for P/D as 2 and all the other geometric combinations, prepared for testing of the multi pin joints is given in Fig. 6.2. Similar fixtures are prepared for testing of all the combinations of the geometric parameters.

Table 6.3 shows the experimental results for failure load and the corresponding S/N ratio for both three and four hole configuration with 3 wt.% of the nanoclay. It can be seen from Table 6.3 that the four holes pin joints have the higher failure load compared to the three holes pin joints. This is due to the fact that the load is distributed among larger number of fasteners in case of the four holes pin joints as compared to the three holes pin joints.

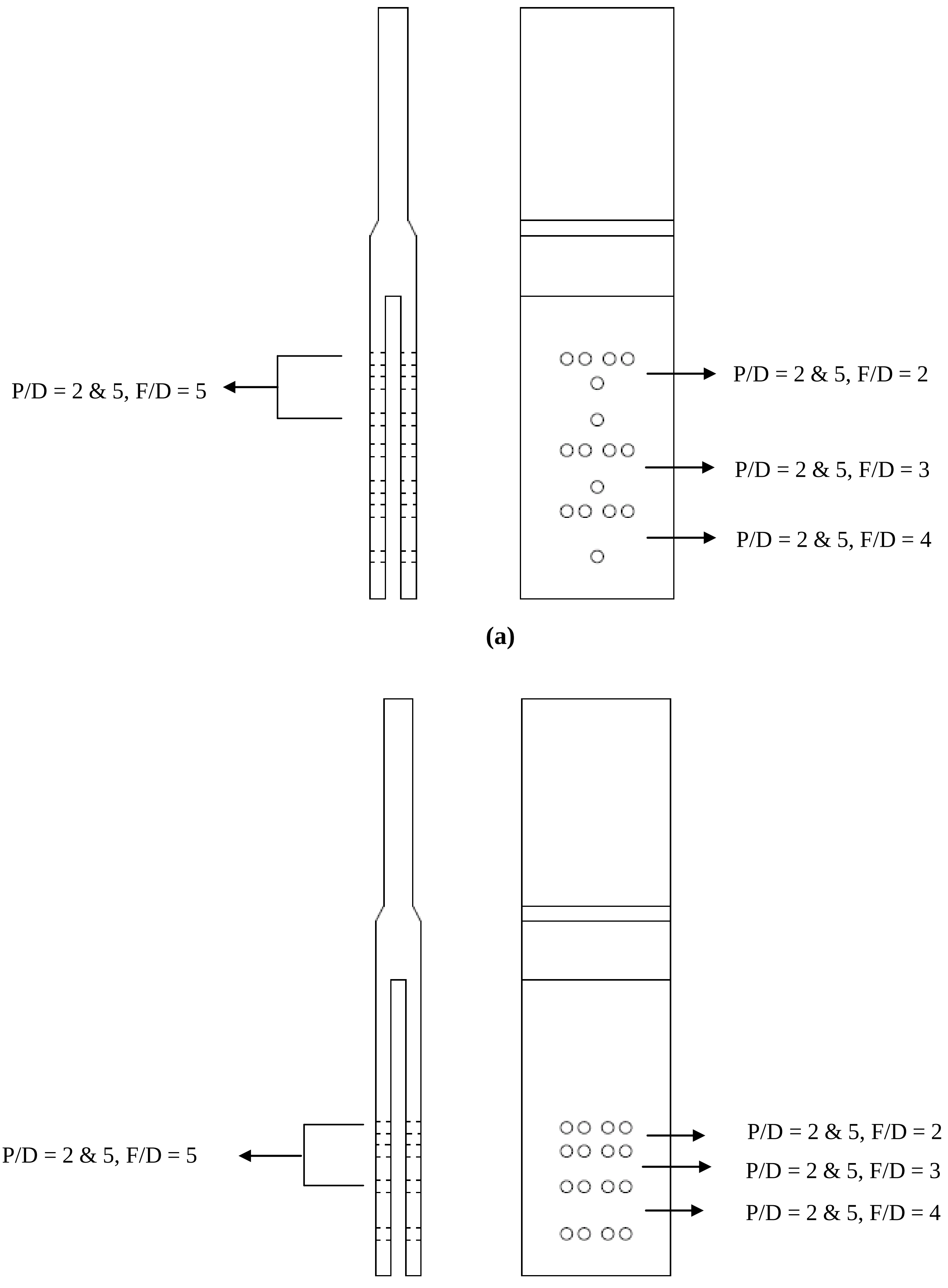

(b)

Fig. 6.2 Basic shape of the fixture used for the testing of (a) Three holes pin joint configurations (b) Four holes pin joint configuration

Table 6.3 Experimental results of the failure load and corresponding S/N response

Experimental run	E/D	F/D	S/D	P/D	Three holes pin joints		Four holes pin joints	
					Average Failure load (N)	S/N ratio (dB)	Average Failure load (N)	S/N ratio (dB)
1	2	2	2	2	5045.6	74.0583	7568.4	77.5801
2	2	3	3	3	6895.2	76.7709	10792.8	80.6627
3	2	4	4	4	8758.4	78.8485	13737.6	82.7582
4	2	5	5	5	9016.8	79.1010	13746.0	82.7635
5	3	2	3	4	7752.0	77.7883	11628.0	81.3101
6	3	3	2	5	8404.8	78.4905	13057.2	82.3170
7	3	4	5	2	9764.8	79.7933	15247.2	83.6638
8	3	5	4	3	10186.4	80.1604	15384.6	83.7417
9	4	2	4	5	10621.6	80.5238	15932.4	84.0456
10	4	3	5	4	11600.8	81.2898	17851.2	85.0333
11	4	4	2	3	11430.8	81.1615	17746.2	84.9821
12	4	5	3	2	11750.4	81.4011	17760.0	84.9889
13	5	2	5	3	10281.6	80.2412	15423.9	83.7639
14	5	3	4	2	10920.8	80.7651	16831.2	84.5223
15	5	4	3	5	12199.2	81.7266	18898.8	85.5287
16	5	5	2	4	12008.8	81.5900	18118.2	85.1623

Figure 6.3 shows the main effect plots for S/N ratio in three and four holes pin joints. It can be seem from Fig. 6.3, that the strength of joint increased with E/D, F/D, S/D and P/D ratios.

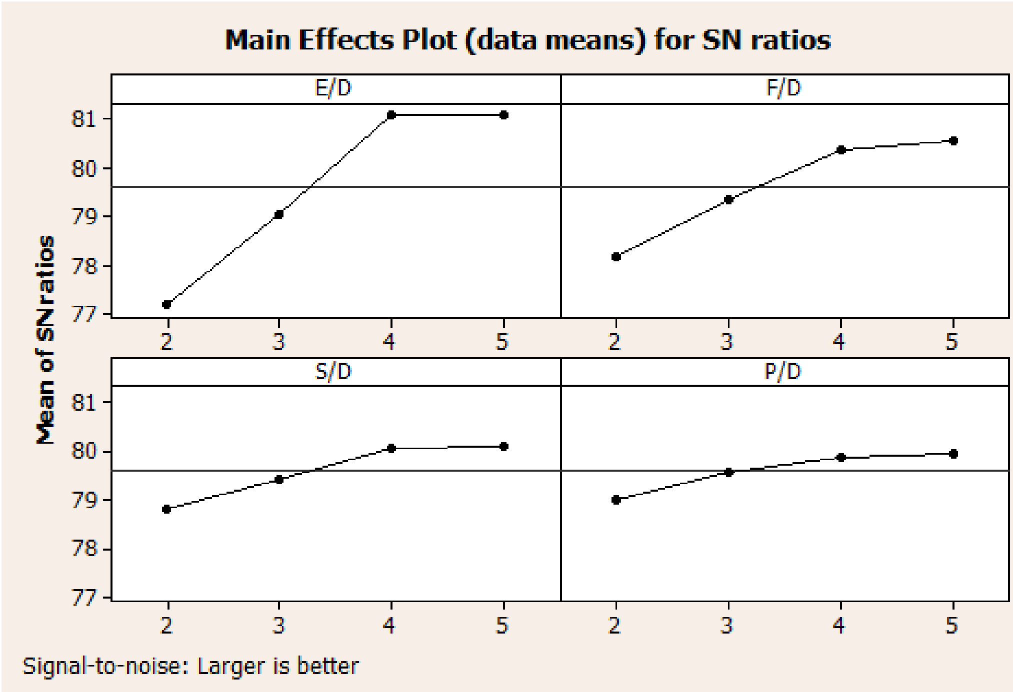

(a)

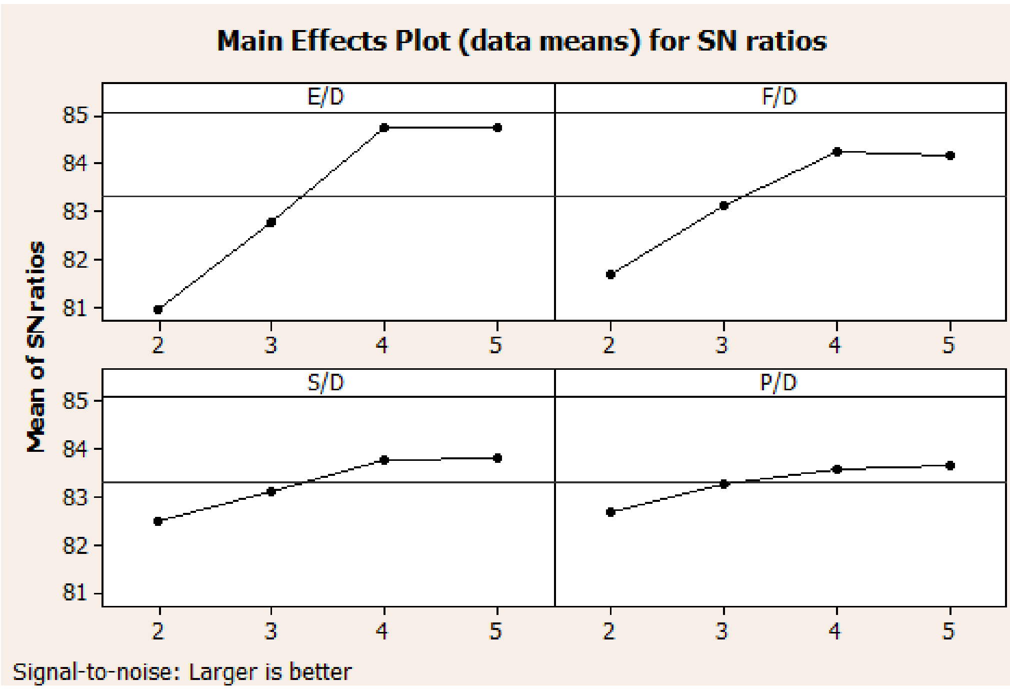

(b)

Fig. 6.3 Main effect plots for S/N ratio (a) Three holes pin joint configurations (b) Four holes pin joint configurations

It can also be seen from the Fig. 6.3, that E/D and F/D ratio have the maximum contribution towards the increase in strength of the joints as the slope of the plots have the maximum variation with the parameter ratio varying from 2 to 4. Thereafter, when the value changes from 4 to 5, the variation is not so significant.

Table 6.4 ANOVA for the triple holes pin joint configuration

Source	DF (Degree of freedom)	Sum of square	Mean square	F	Contribution (%)
E/D	3	42.0147	14.0049	86.53	65.61290685
F/D	3	14.8289	4.942967	30.54	23.15778131
S/D	3	4.4542	1.484733	9.17	6.955970403
P/D	3	2.2507	0.750233	4.64	3.514840507
Residual Error	3	0.4856	0.1619	-	0.75
Total	15	64.0342	-	-	99.99

Table 6.5 ANOVA for the four holes pin joint configuration

Source	DF (Degree of freedom)	Sum of square	Mean square	F	Contribution (%)
E/D	3	40.3308	13.4436	67.75	62.14844755
F/D	3	17.1441	5.7147	28.8	26.41849901
S/D	3	4.5169	1.505633	7.59	6.960395597
P/D	3	2.3072	0.769067	3.88	3.555319959
Residual Error	3	0.5953	0.1984	-	0.917337886
Total	15	64.8943	-	-	99.99

Tables 6.4 and 6.5 show the calculations of ANOVA on three and four holes configuration. The values were calculated at 95% confidence level. It can be analyzed from Table 6.4 and 6.5 that the E/D and F/D ratios had the maximum contribution or effect, on the strength of the joint. It can also be seen from the tables that the S/D and P/D ratios had the minimum contribution towards the strength.

6.2 Failure Analysis

As discussed in the previous chapters, there are three basic failure modes in pin joints *i.e.*, net tension, shear out and bearing. Net tension and shear out modes are catastrophic and should be avoided by varying the geometric parameters of the joint. However, the bearing failure mode is non-catastrophic and is related to compressive stresses developed on the hole surface area. Bearing mode is the preferred mode of failure as it has less serious consequences and can sustain loading for long duration. The joints should be designed such that there is bearing failure mode instead of the net tension and shear out modes of failure.

From the ANOVA calculations, it was seen that S/D and P/D ratios had least contribution towards the strength of the joint. So the ratios of both these geometric parameter were fixed to 5 as per their plots for S/N ratios shown in Fig. 6.3. It can be seen from the ANOVA tables and main effect plots that three and four holes configuration shows similar behavior as they have same number of parameters and levels.

Fixing S/D and P/D ratios to 5, F/D and E/D ratios were varied from 2 to 5, to analyze the type of failure modes in the joint. Figure 6.4 shows the failure load and the displacement curves for the different combinations of F/D and E/D ratios for three holes configurations. Similar trend is obtained for the four holes configuration.

After analyzing the failure load and the displacement curves given in Fig. 6.4, it can be seen that there is only shear out and bearing failure modes. If there is a decrease after couple of peak points then the shear out failure mode has occurred in the joint. If the values decreases after the peak point and thereafter remain nearly constant with zig-zag formation, then it is confirmed that the bearing failure mode occurred in the joint.

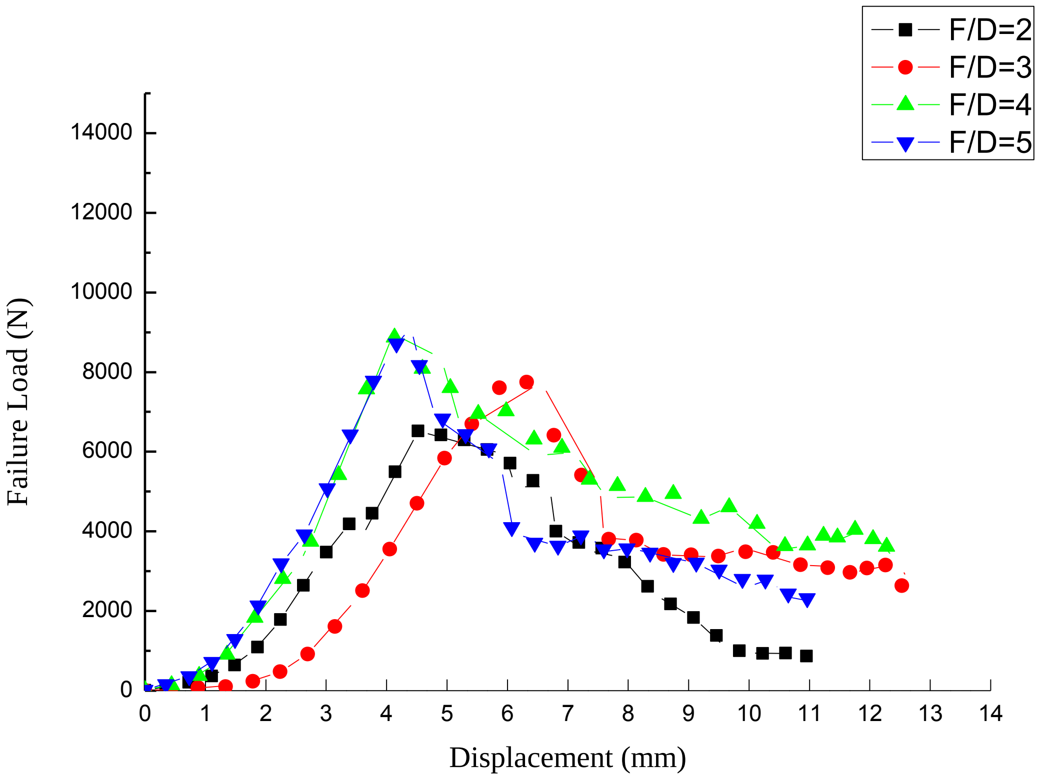
F/D=2
F/D=3
F/D=4
F/D=5
Failure Load (N)
Displacement (mm)

(a)

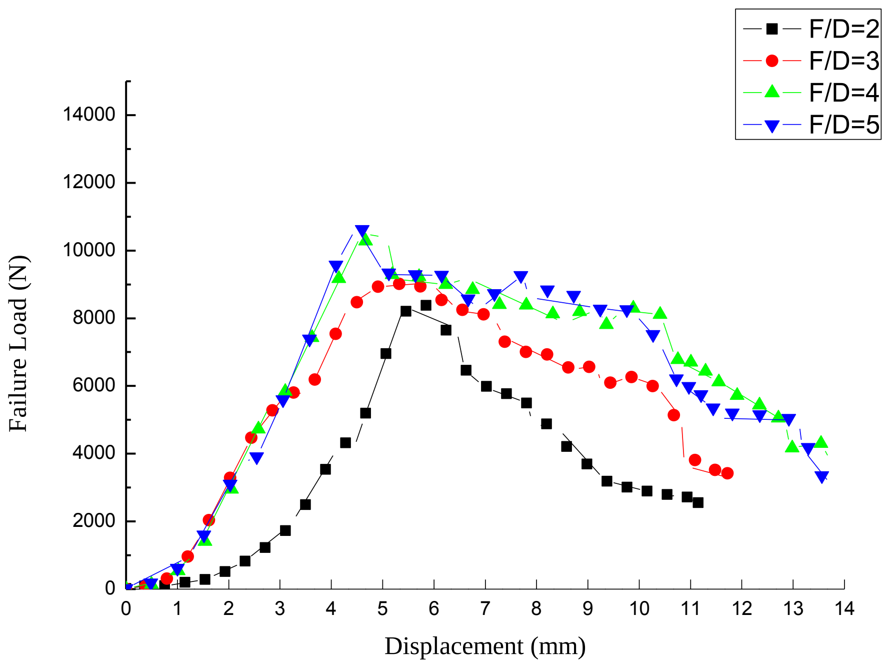
F/D=2
F/D=3
F/D=4
F/D=5
Failure Load (N)
Displacement (mm)

(b)

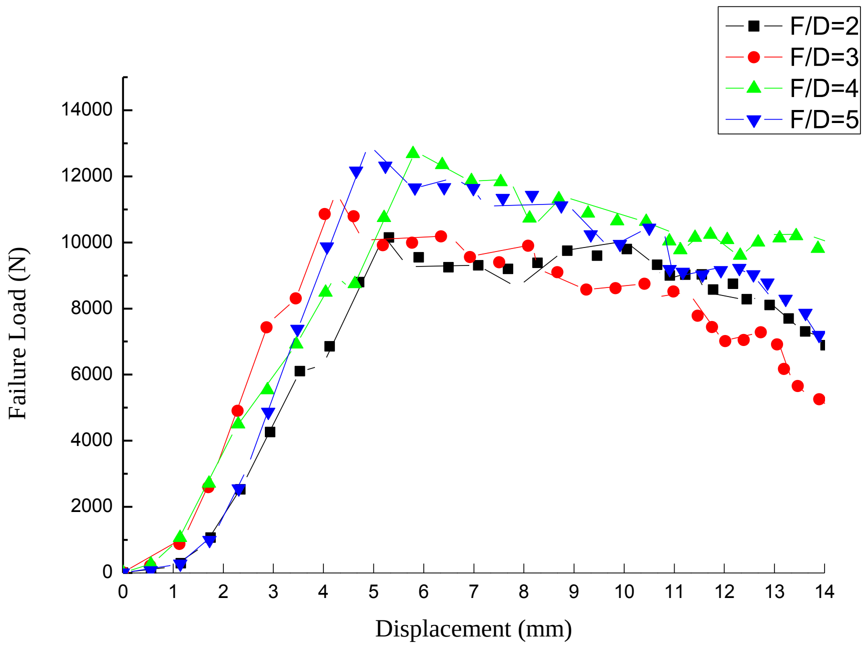

(c)

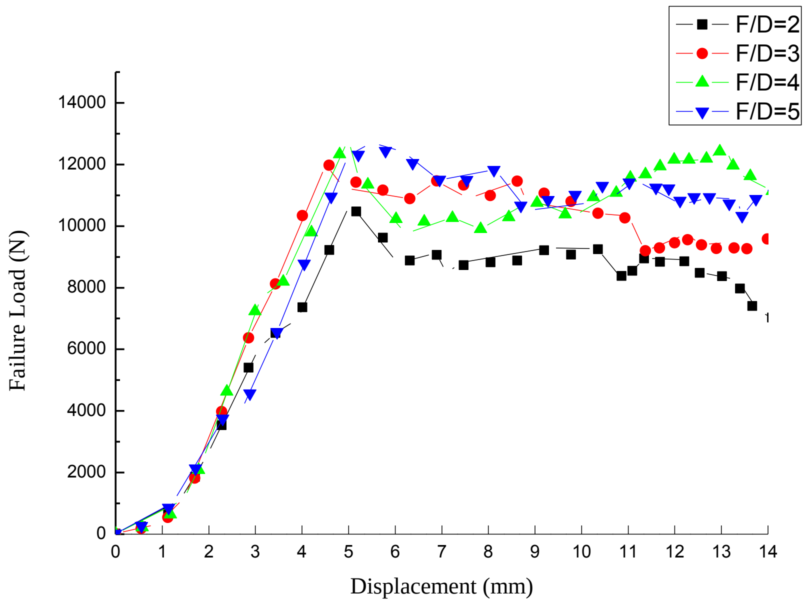

(d)

Fig. 6.4 Failure Load vs. Displacement curves for three holes pin joints (a) E/D=2 (b) E/D=3 (c) E/D=4 (d) E/D=5

It can also be seen from the Fig. 6.4 that there was no net tension type of failure mode in the joint as none of the curve decreased drastically after the first peak. There was no net tension failure in the joint due to the fact that the S/D and P/D ratios were fixed to 5 as per their plots for S/N ratios.

The failure modes for both the three and four holes pin joints are same but failure load of four holes pin joints is higher as compared to three holes pin joints as shown in the Fig. 6.5.

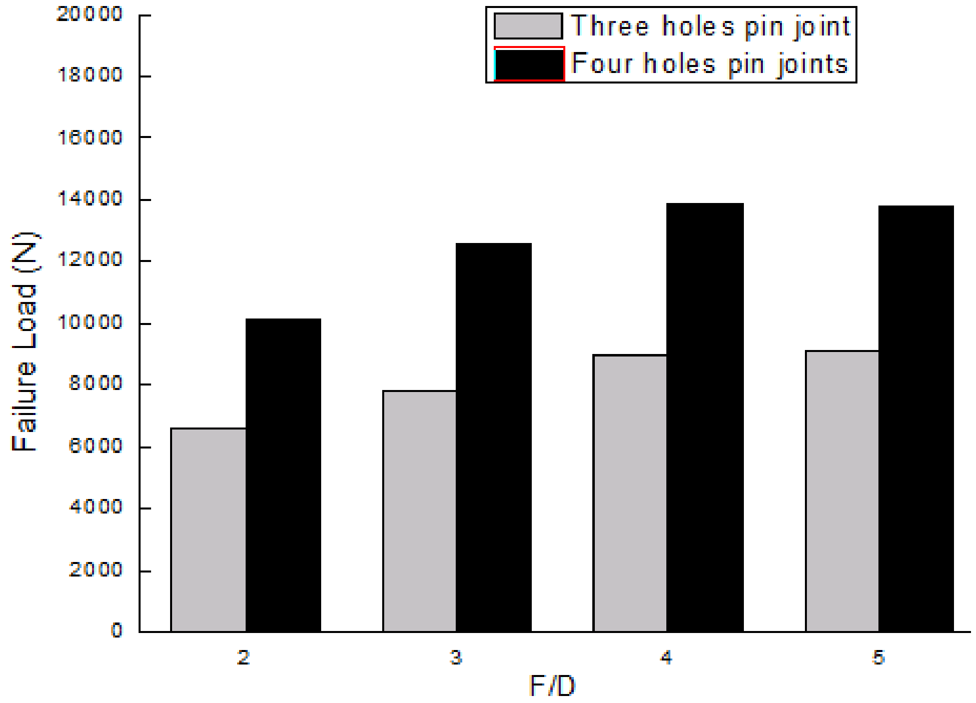

(a)

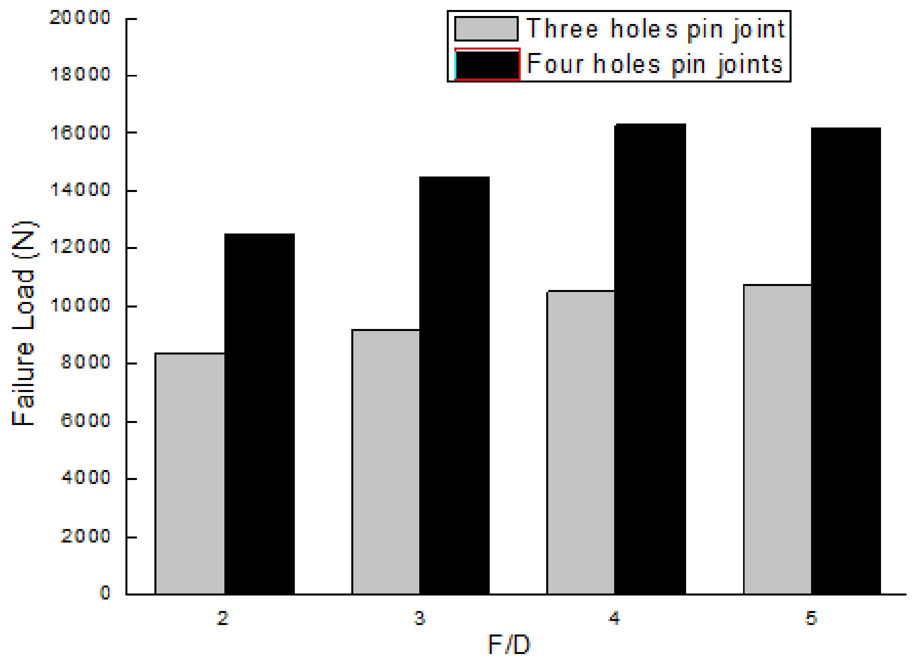

(b)

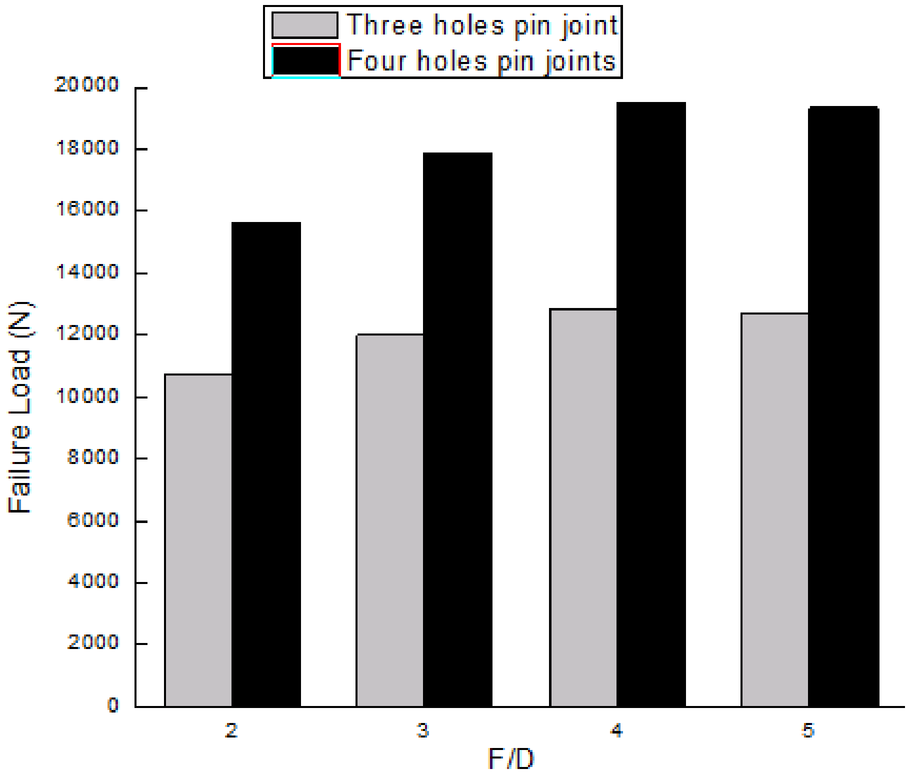

(c)

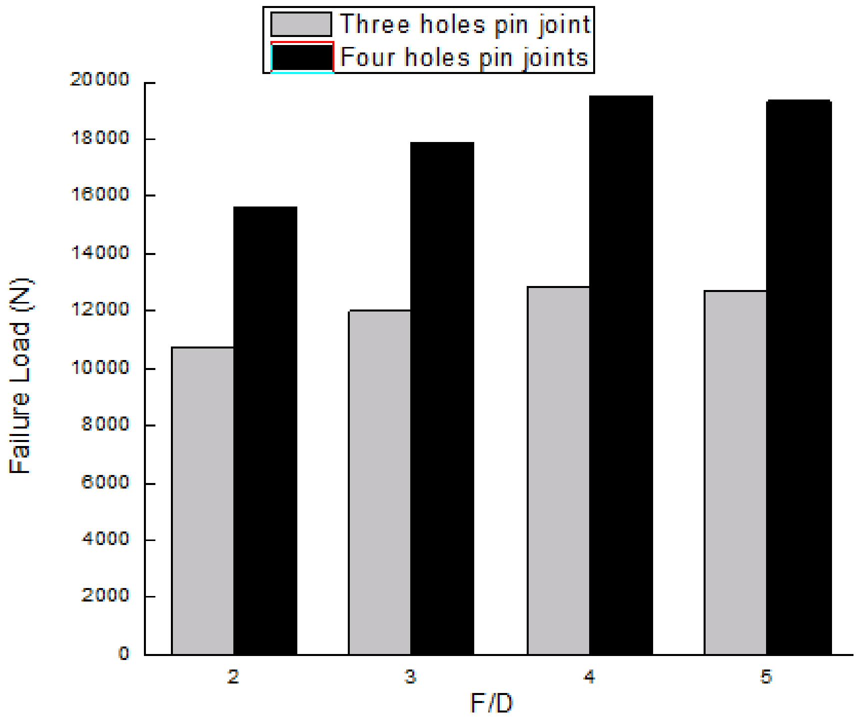

(d)

Fig. 6.5 Failure load of three and four holes pin joints (a) E/D=2 (b) E/D=3 (c) E/D=4 and (d) E/D=5

Failure load and failure modes obtained for the different parameters in three and four holes pin joints are given in Table 6.6. In Table 6.6, the symbol B means bearing and S is shear out type of failure mode for the outer holes. It can be seen from the Fig. 6.4 and Table 6.6 that the failure mode was more dependent on E/D ratio as compared to F/D ratio.

Table 6.6 Failure Mode and Failure load of the three and four holes pin joints

Sr. No.	E/D	F/D	Failure Load (N)		Failure Modes of three and four hole pin joints
			Three hole pin joints	Four hole pin joints	
1	2	2	6600	10150	S
2	2	3	7800	12560	S
3	2	4	8970	13890	B
4	2	5	9130	13800	B
5	3	2	8390	12500	S
6	3	3	9200	14490	S
7	3	4	10500	16300	B
8	3	5	10700	16150	B
9	4	2	10200	15900	S
10	4	3	11500	17770	B + S
11	4	4	12900	19600	B
12	4	5	12990	19760	B
13	5	2	10700	15600	S
14	5	3	12000	17870	B + S
15	5	4	12800	19500	B
16	5	5	12700	19350	B

For the lower value of E/D and F/D ratios there was shear out failure mode. As the value of E/D ratio increases to 4, there is bearing type of failure mode in the joint irrespective of the F/D ratio. The specimen was weakest for E/D ratio to be 2, which indicates that the outer holes was very close to the edge.

Table 6.7 Images showing the failure modes for different E/D and F/D ratios of three holes pin joints

	F/D=2	F/D=3	F/D=4	F/D=5
E/D=2				
Failure modes	Shear out	Shear out	Bearing	Bearing
E/D=3				
Failure modes	Shear out	Shear out	Bearing	Bearing
E/D=4				
Failure modes	Shear out	Bearing + Shear out	Bearing	Bearing
E/D=5				
Failure modes	Shear out	Bearing + Shear out	Bearing	Bearing

The actual images of the specimens showing the failure modes for the different values of E/D and F/D ratios are given in Table 6.7. It is also confirmed from these images that there is only shear-out and bearing failure mode in three holes pin joints. Similar trend was observed for four holes pin joints.

6.3 Numerical Analysis

Geometric model of multi holes pin joint was made in Hypermesh software by varying different geometric parameters for both three holes and four holes pin joints. The ply orientation was symmetric with respect to the z = 0 plane. Pcomp shell elements were used to discretize the laminates with three and four holes. The direction of applied forces and boundary conditions for the three and four holes pin joints are shown in Fig. 6.6.

As discussed in the previous chapters, Failure Index (*FI*) values were found at different points on the characteristic curve. Thereafter, the mode of failure (for $FI \geq 1$) was judged using the failure angle (θ) on the characteristic curve.

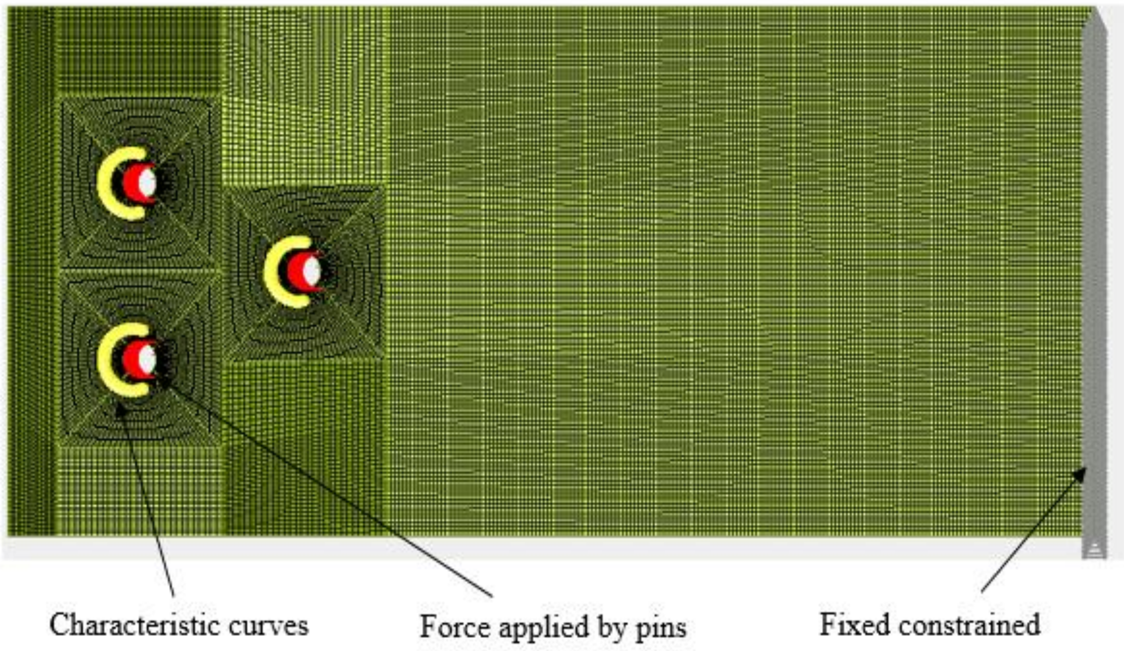

(a)

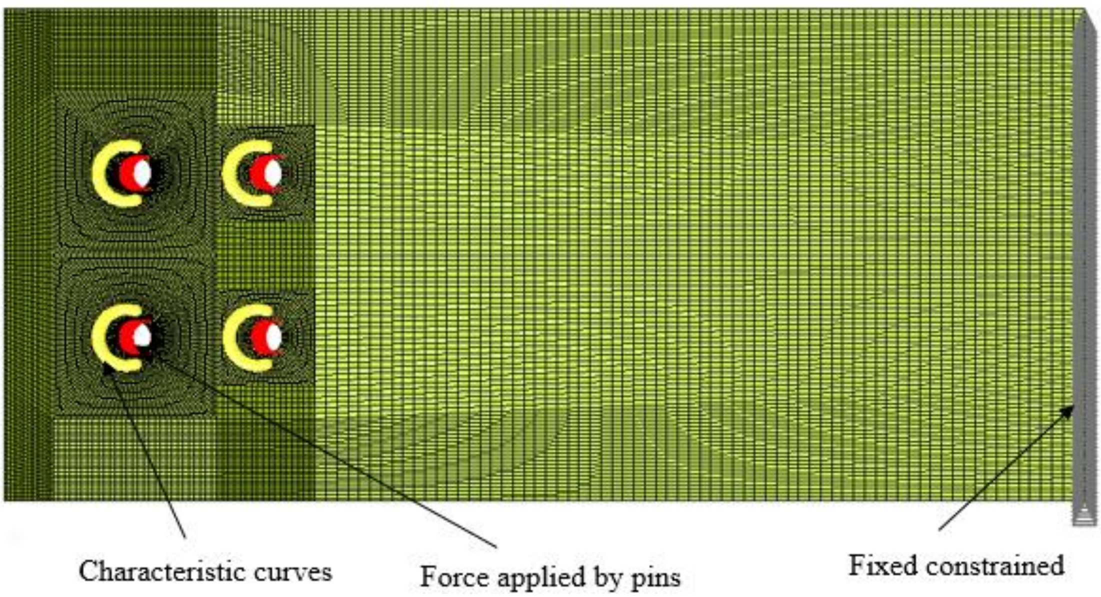

(b)

Fig. 6.6 Applied forces and boundry conditions for (a) Three holes pin joints (b) Four holes pin joints

Figure 6.7 shows the *FI* values around the holes for optimized combination of geometric parameters *i.e.*, E/D=4, F/D=4, P/D=5 S/D= 5 for three and four holes configurations.

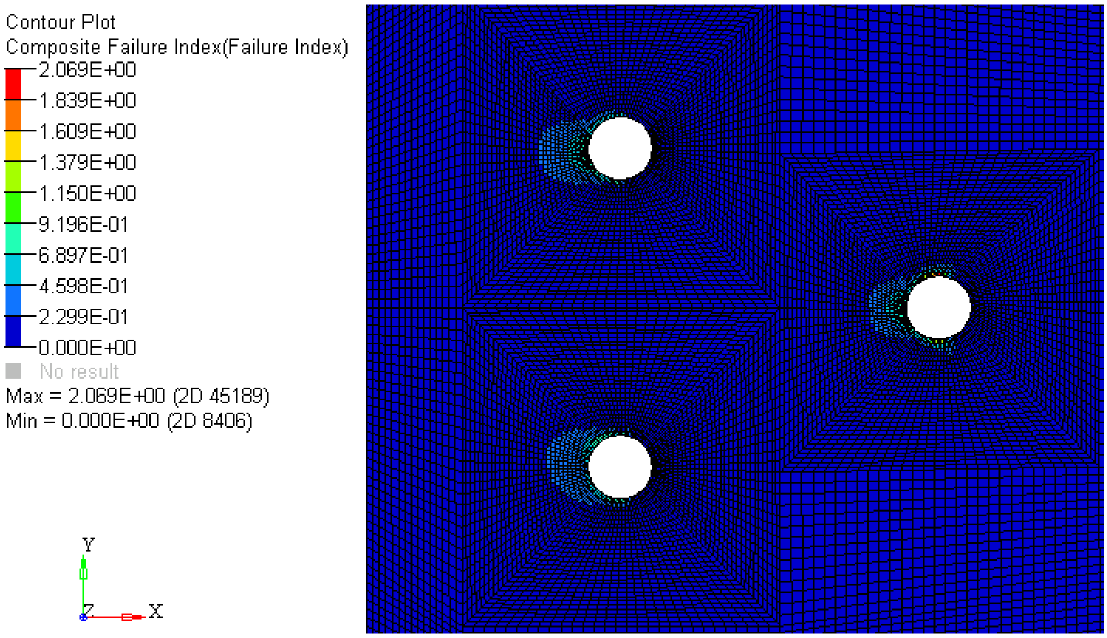

(a)

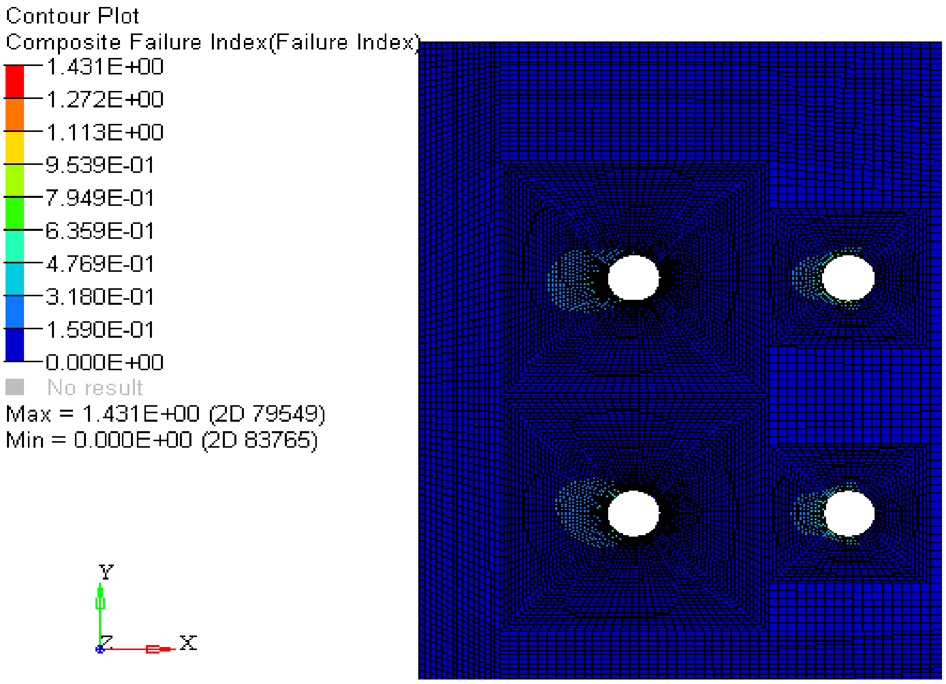

(b)

Fig. 6.7 *FI* for the optimized configuration of (a) Three holes pin joints (b) Four holes Pin Joints

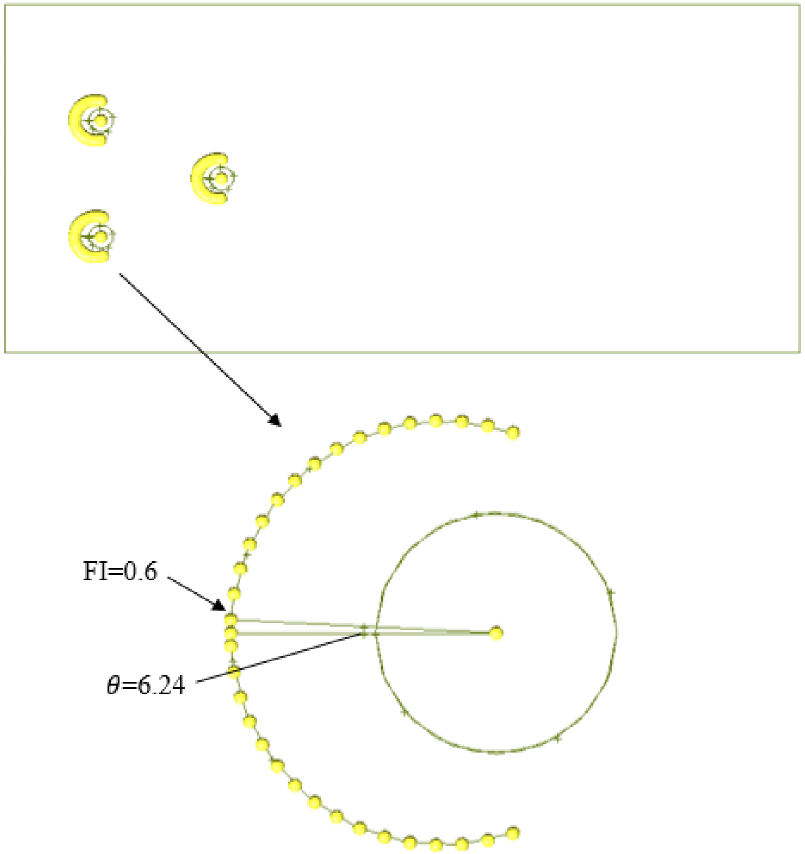

(a)

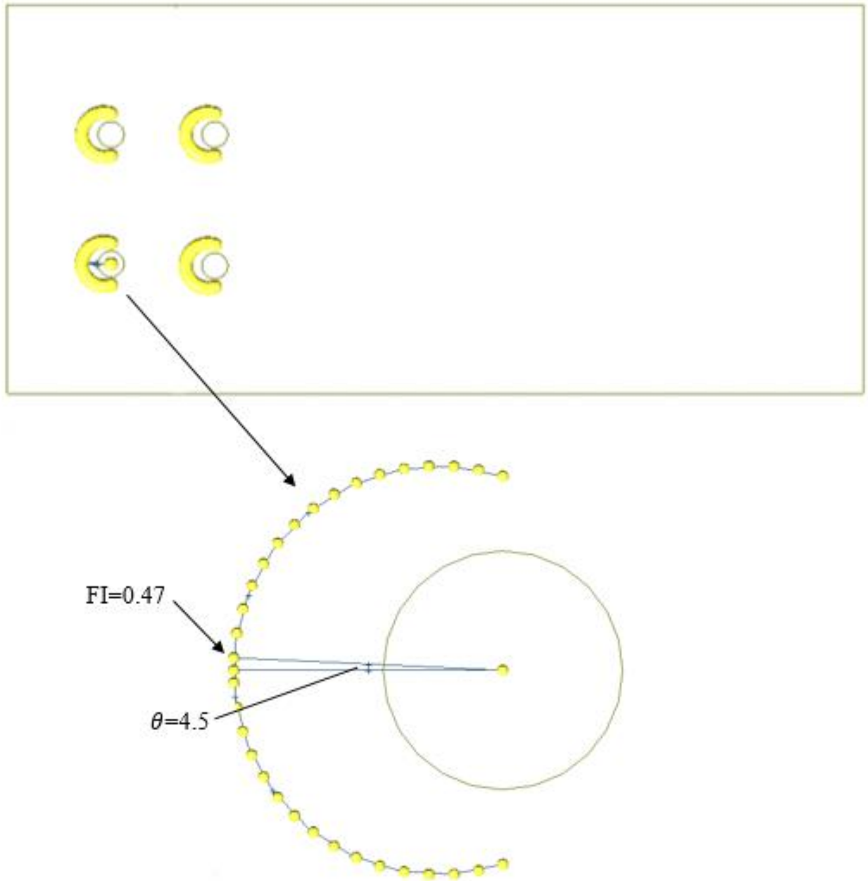

(b)

Fig. 6.8 *FI* on the characteristic curve for the optimized parameters for configuration (a) Three holes pin joints (b) Four holes pin joints

Figure 6.8 (a) and (b) shows the different points on the characteristic curve for calculating the *FI* value and failure angle for optimized parameters of three and four hole pin joint configurations, respectively. The figures show that the failure angle is less than 15^0, confirming the bearing failure mode in the selected parameters for both the configurations

The finite element analysis was carried out for different combinations of E/D and F/D ratios using the characteristic curve method. The failure modes and failure load predicted using finite element analysis are given in Tables 6.8 and 6.9. Table 6.8 and 6.9 also reports the comparison between the experimental findings and the numerical predictions for three and four pin joints, respectively. It is evident that the results are in good correlation with each other.

Table 6.8 Failure Mode and Failure load of the three holes pin joints using experimental and numerical method

Sr. No.	E/D	F/D	Experimental		Numerical	
			Failure Load (N)	Failure Mode	Failure Load (N)	Failure Mode
1	2	2	6600	S	6420	S
2	2	3	7800	S	7180	S
3	2	4	8970	B	8450	B
4	2	5	9130	B	8990	B
5	3	2	8390	S	7800	S
6	3	3	9200	S	9450	B + S
7	3	4	10500	B	11200	B
8	3	5	10700	B	11900	B
9	4	2	10200	S	12010	S
10	4	3	11500	B+S	12800	B + S
11	4	4	12900	B	13780	B
12	4	5	12990	B	14200	B
13	5	2	10700	S	11200	B + S
14	5	3	12000	B+S	13500	B + S
15	5	4	12800	B	14020	B
16	5	5	12700	B	14300	B

Table 6.9 Failure Mode and Failure load of the four holes pin joints using experimental and numerical method

Sr. No.	E/D	F/D	Experimental		Numerical	
			Failure Load (N)	Failure Mode	Failure Load (N)	Failure Mode
1	2	2	10150	S	9960	S
2	2	3	12560	S	13700	S
3	2	4	13890	B	14020	B
4	2	5	13800	B	14400	B
5	3	2	12500	S	13010	S
6	3	3	14490	S	15000	B
7	3	4	16300	B	17120	B
8	3	5	16150	B	17200	B
9	4	2	15900	S	16500	S
10	4	3	17770	B + S	18820	B
11	4	4	19600	B	20100	B
12	4	5	19760	B	20500	B
13	5	2	15600	S	14780	B + S
14	5	3	17870	B + S	18000	B
15	5	4	19500	B	20280	B
16	5	5	19350	B	20110	B

6.4 Closure

In the present chapter, the strength of multi holes pin joints were investigated both experimentally and numerically, for the effect of different geometric parameters. Taguchi methodology gave a systematic approach to reduce the number of the experimentations as compared to the full factorial design. ANOVA was used to predict the contribution of all the geometric parameters. The results revealed that the E/D and F/D ratios have the maximum contribution to increase the strength of the multi hole pin joints. Their contribution was 62% to 65% and 23% to 26 %, respectively for three and four holes pin joints. It was also found that S/D and P/D ratios had very less contribution towards the strength of the joint. Failure modes in multi holes pin joints were most dependent on the E/D ratio. The joint had the bearing failure mode for $E/D \geq 4$ and $F/D \geq 3$.

The next chapter gives the conclusions and recommendations for further work of the present thesis.

Chapter 7 - Conclusions and Recommendations for Future Work

7.1 Conclusions

In the present work, pin joints prepared from glass fiber reinforced epoxy laminates were studied. First of all, laminates were investigated for higher strength or mechanical properties, which was the function of ply orientation and nanoclay filler. Then single hole pin joints were prepared from these laminates with and without the addition of nanoclay to analyze the strength and failure modes of the joints by varying the E/D and W/D ratios. Thereafter, this study was extended for double and multi holes pin joints to analyze the contribution of the different geometric parameters.

There is a definite dependence of joint strength on ply orientations and the nanoclay composition. The tensile strength and tensile modulus of glass/epoxy nanoclay laminate specimens increased with the increasing amount of nanoclay upto 3 wt.% of nanoclay. Thereafter, it decreased with further increase in the wt.% of nanoclay. The same pattern is followed for the different selected ply orientations *i.e*, [0°/45°/90°], [0°/90°/0°] and [0°/45°/0°]. The strength was around 15-20 % higher than neat glass/epoxy composite for the studied ply orientations.

The ply orientation of [0°/45°/0°] has higher mechanical properties in longitudinal direction whereas ply orientation of [0°/90°/0°] have high mechanical properties in transverse direction. Bearing strength of the pin joints depend on both longitudinal and transverse mechanical properties. Results show that the bearing strength of [0°/90°/0°] ply orientation was about 10-12% higher than [0°/45°/0°] ply orientation.

Type of failure in single pin joint is totally dependent on the geometric parameter *i.e.*, W/D and E/D ratios. Net-tension and shear-out failure modes occur with small W/D and E/D values, respectively. These failures are immediate and without warning. But the bearing mode of failure is progressive, which is the desirable mode. The bearing mode of failure occurs for W/D and E/D ratios to be greater than 4 for single hole pin joint.

Taguchi method provides a systematic and efficient methodology for the optimization of the geometric parameters to analyze the failure load in double hole pin joints. The results demonstrate that the E/D ratio was the most significant parameter to increase the bearing strength in serial and parallel pin joint configuration. Its contribution was 84.5% of the total contribution of all the parameters combined together. In parallel pin joint configuration, the percentage contribution of E/D ratio was 64.23% of the total contribution of all the parameters combined together. It was also seen that K/D ratio also had a notable contribution of 22.72% in parallel configuration.

ANOVA was used to predict the contribution of all the geometric parameters in the multi hole pin joints. The results revealed that the E/D and F/D ratios have the maximum contribution to increase the strength of the multi hole joints. Their contribution was 62% to 65% and 23% to 26%, respectively for three and four holes pin joints. It was also found that S/D and P/D ratios had very less contribution towards the strength of the joint. The joint had the bearing failure mode for E/D≥4 and F/D≥3.

Finite element method was used to analyze the pin joints numerically. Characteristic curve was drawn around the hole. Thereafter, Tsai-Wu failure theory was used to calculate the Failure Index on the curve. Failure load and failure modes were calculated based upon the value and position of the Failure Index on the characteristic curve. The results were in good correlation with the experimental ones.

7.2 Recommendations for Future Work

The present work can be extended in the following directions:

(i) The present study deals with glass fiber reinforced laminates with the addition of the nanoclay which was used for the preparation and failure analysis of the pin joints. However, this study can be extended to analyze the effect of hygrothermal conditions on the failure analysis of the pin joints.

(ii) The present work can be extended for different materials *i.e.*, fibers and nanofillers, as the strength of the laminates and joints also depend upon the selected materials.

(iii) Different method can be used for the preparation of the laminates.

(iv) The analysis can be extended for different types of mechanical joints.

References

Agnihotri PK, Kar KK, Basu S. Cohesive zone model of carbon nanotube-coated carbon fiber/polyester composites. *Modelling and Simulation in Materials Science and Engineering* 2012; 20: 35014-35027.

Aktas A. Failure analysis of serial pinned joints in composites materials. *Indian Journal of Engineering & Materials Sciences* 2011; 18: 102-110.

Aktas A, Imrek H, Cunedioglu Y. Experimental and numerical failure analysis of pinned-joints in composite materials. *Composite Structures* 2009; 89: 459-466.

Anawa EM, Olabi AG, Hashmi MSJ. Application of Taguchi method to optimise dissimilar laser welded components. *International journal of Manufacturing Technology and Management* 2008; 15: 219-227.

Arun KV, Kumar DS, Murugesh MC. Influence of bolt configuration and TiO_2/ZnS fillers content on the strength of composites fasteners. *Materials and Design* 2014; 53: 51-57.

Atas A, C. Soutis C. Strength prediction of bolted joints in CFRP composite laminates using cohesive zone elements. *Composites Part B* 2014; 58: 25-34.

Atas C. Bearing strength of pinned joints in woven fabric composites with small weaving angles. *Composite Structures* 2009; 88: 40-45.

Asi O. Effect of different woven linear densities on the bearing strength behaviour of glass fiber reinforced epoxy composites pinned joints. *Composite Structures* 2009; 90: 43-52.

Asi O. An experimental study on the bearing strength behavior of Al_2O_3 particle filled glass fiber reinforced epoxy composites pinned joints. *Composite Structures* 2010; 92: 354-363.

Azeez AA, Rhee KY, Park SJ, Hui D. Epoxy clay nanocomposites – processing, properties and applications: A review. *Composites: Part B* 2012; 45: 308-320.

Baba O. Behavior of Pin-loaded Laminated Composites. *Experimental Mechanics* 2006; 46: 589-600.

Bhutta M, Ohama Y, Tsuruta K. Strength properties of polymer mortar panels using methyl methacrylate solution of waste expanded polystyrene as binder. *Construction Building Material* 2011; 25: 779-784.

Bittmann B, Haupert F, Schlarb AK. Preparation of TiO_2/epoxy nanocomposites by ultrasonic dispersion and their structure property relationship. *Ultrasonics Sonochemistry* 2011; 18: 120-126.

Brunner AJ, Necola A, Rees M, Gasser PH, Kornmann X, Thomann R, Barbezat M. The influence of silicate-based nano-filler on the fracture toughness of epoxy resin. *Engineering Fracture Mechanics* 2006; 73: 2336-2345.

Callister WD. Material Science and Engineering: An Introduction. 7th ed. US: *John Wiley & Sons*, 2007.

Chang, FK, Scott RA, Springer GS. Strength of mechanically fastened composite joints. *Journal of Composite. Materials* 1982; 6: 470-494.

Chang L, Zhang Z, Breidt C, Friedrich K. Tribological properties of epoxy nanocomposites Enhancement of the wear resistance by nano-TiO_2 particles. *Wear* 2005; 258: 141-148.

Chang L, Zhang Z. Tribological properties of epoxy nanocomposites Part II. A combinative effect of short carbon fibre with nano-TiO_2. *Wear* 2006; 260: 869-878.

Chawla KK. Composite Materials Science and Engineering 2nd ed. USA: *Springer*, 1998.

Chowdhury FH, Hosur MV, Jeelani S. Investigations on the thermal and flexural properties of plain weave carbon/epoxy-nanoclay composites by hand-layup technique, *Journal of Material Science* 2007; 42: 2690-2700.

Davim JP, Reisa P, Antonio CC. Experimental study of drilling glass fiber reinforced plastics (GFRP) manufactured by hand layup. *Composites Science and Technology* 2004; 64: 289-297.

Fakirov S. Nano–Size Polymers Preparation, Properties, applications Switzerland: *Springer* 2016.

Friedrich K, Fakirov S, Zhang Z. Polymer composites, from nano- to macro scale. UK: *Springer*, 2005.

Ghani JA, Choughury IA, Hassan HH. Application of Taguchi method in the optimization of the end milling parameters. *Journal of Material Processing Technology* 2004; 145: 84-92.

Hameed N, Sreekumar PA, Valsaraj VS, Thomas S. High-Performance Composite From Epoxy and Glass Fibers: Morphology, Mechanical, Dynamic Mechanical, and Thermal Analysis. *Polymer Composites* 2009; 982-992.

Hua Y, Gu L, Watanabe H. Micromechanical analysis of nanoparticle-reinforced dental composites. *International Journal of Engineering Science* 2013; 69: 69-76.

Icten BM, Karakuzu R, Toygar ME. Failure analysis of woven kevlar fiber reinforced epoxy composites pinned joints. *Composite Structures* 2006; 73: 443-450.

Irisarri FX, Laurin F, Carrere N, Maire JF. Progressive damage and failure of mechanically fastened joints in CFRP laminates – Part I: Refined Finite Element modelling of single-fastener joints. *Composite Structures* 2012; 94: 2269-2277.

Jawahar P, Gnanamoorthy R, Balasubramanian M. Tribological behaviour of clay – thermoset polyester nanocomposites. *Wear* 2006; 261: 835-840.

Jones RM. Mechanics of composite materials. 2nd ed. USA: *Taylor and Francis*, 1999.

Jumahat A, Soutis C, Abdullah SA, Kasolang S. Tensile properties of nanosilica/epoxy nanocomposites. *Procedia Engineering* 2012; 41: 1634-1640.

Jumahat A, Soutis C, Mahmud J, Ahmad N. Compressive properties of nanoclay/epoxy nanocomposites, *Procedia Engineering* 2012;. 41: 1607-1613.

Karakuzu R, Caliskan CR, Aktas M, Icten, BM . Failure behavior of laminated composite plates with two serial pin-loaded holes. *Composite Structures* 2008 a; 82: 225-234.

Karakuzu R, Demirgoren O, Icten BM, Deniz ME. Failure behavior of quasi-isotropic laminates with three-pin loaded holes. *Materials and Design* 2010; 31:2029-3032.

Karakuzu R, Gulem T, Icten BM. Failure analysis of woven laminated glass–vinylester composites with pin-loaded hole. *Composite Structures* 2006; 72: 27-32.

Karakuzu R, Taylak N, Icten, BM, Aktas M. Effects of geometric parameters on failure behavior in laminated composite plates with two parallel pin- loaded holes. *Composite Structures* 2008 b; 85: 1-9.

Khashaba UA, Sebaey TA, Alnefaie KA. Failure and reliability analysis of pinned-joints composite laminates: Effects of stacking sequences. *Composites: Part B* 2013; 45: 1694-1703.

Kim BC, Park SW, Lee DG. Fracture toughness of the nano-particle reinforced epoxy composite. *Composite Structures* 2008; 86: 69-77.

Kishore N, Malhotra SK, Prasad NS. Failure analysis of multi-pin joints in glass fibre/epoxy composite laminates. *Composite Structures* 2009; 91: 266-277.

Kweon JH, Ahn HS, Choi JH. A new method to determine the characteristic lengths of composite joints without testing. *Composite Structures* 2004; 66:305-315.

Lama CK, Cheunga HY, Laua KT, Zhoua LM, Hob MW, Hui D. Cluster size effect in hardness of nanoclay/epoxy composites. *Composites: Part B* 2005; 36: 263-269.

Li H, Zhang Z, Ma X, Hu M, Wang X, Fan P. Synthesis and characterization of epoxy resin modified with nano-SiO_2 and γ-glycidoxypropyltrimethoxy silane. *Surface & Coatings Technology* 2007; 201: 5269-5272.

Limam O, Foret G, Zenzri H. Ultimate strength of pin-loaded composite laminates: A limit analysis approach. *Composite Structures* 2011; 93: 1217-1224.

Li HS, Xia S, Luo DM. A probabilistic analysis for pin joint bearing strength in composite laminates using Subset Simulation. *Composites: Part B* 2014; 56: 780-789.

Li X, Zhan Z, Peng G, Wang W. A new method for preparing completely exfoliated epoxy/clay nanocomposites: nano-disassembling method. *Polymer Bulletin* 2011; 67: 719-727.

McCarthy MA, McCarthy CT, Lawlor VP, Stanley WF. Three-dimensional finite element analysis of single-bolt, single-lap composite bolted joints: part I—model development and validation. *Composite Structures* 2005; 71: 140-158.

Mehrabadi FA. Experimental and Numerical Failure Analysis of Adhesive Composite Joints. *International Journal of Aerospace Engineering* 2012; 2012: Article ID 925340, 10 pages.

Mohan TP, Kanny K, Velmurugan R. Epoxy – clay nanocomposites – effect of curing temperature in mechanical properties. *International journal of Plastics Technology* 2009; 13: 123-132.

Myskova MZ, Zelenka J, Spacek V, Socha F. Properties of Epoxy systems with Clay Nanocomposites. *Mechanics of Composite Materials* 2003; 39: 119-122.

Nalbant M, Gokkaya H, Sur G. Application of Taguchi method in the optimization of cutting parameters for the surface roughness in turning. *Material & Design* 2007; 28: 1379-1385.

Nerillia F, Marinob M, Vairoc G. A numerical failure analysis of multi-bolted joints in FRP laminates based on basalt fibers. *Procedia Engineering* 2015; 109: 492-506.

Nian CY, Yang WH, Tarng YS. Optimization of the turning operations with multiple performance characteristics. *Journal of Material Processing Technology* 1999; 95: 90-96.

Okutan B, Karakuzu R. The strength of pinned joints in laminated composites. *Composites Science and Technology* 2003; 63: 893-905.

Okutan B, Aslan Z, Karakuzu R. A study of the effects of various geometric parameters on the failure strength of pin-loaded woven-glass-fiber reinforced epoxy laminate. *Composite Science and Technology* 2001; 61: 1491-1497.

Okutan, B. The effects of geometric parameters on the failure strength for pin -loaded multi-directional fiber-glass reinforced epoxy laminate. *Composites* 2002; 33: 567-578.

Olmedo A, Santiuste C, Barbero E. An analytical model for predicting the stiffness and strength of pinned-joint composite laminates. *Composites Science and Technology* 2014; 90: 67-73.

Ondurucu A, Esendemir U, Tunay RF. Progressive failure analysis of glass-epoxy laminated composite pinned-joints. *Materials and Design* 2012; 36: 617-625.

Peters ST, Handbook of Composites. *Chapman & Hall*, London, 1998.

Petrovic Z, Maksimovic M, Ilic SSI, Stamenkovic D. Computation Method in Failure Analysis of Mechanically Fastened Joints at Layered Composites. *Journal of Mechanical Engineering* 2012; 58: 553-559.

Pisano AA, Fuschi P, Domenico DD. A layered limit analysis of pinned-joints composite laminates: Numerical versus experimental findings. *Composites: Part B* 2012; 43: 940-952.

Pisano AA, Fuschi P, Domenico DD. Failure modes prediction of multi-pin joints FRP laminates by limit analysis, *Composites: Part B* 2013; 46: 197-206.

Qin T, Zhao L, Zhang J. Fastener effects on mechanical behaviors of double-lap composite joints. *Composite Structures* 2013; 100: 413-423.

Roy KR. A primer on the Taguchi Method. Birmingham, UK: *Society of Manufacturing Engineers*, 2010.

Sen F, Pakdil M, Sayman O, Benli S. Experimental failure analysis of mechanically fastened joints with clearance in composite laminates under preload. *Materials and Design* 2008; 29: 1159-1169.

Sen F, Sayman O. Failure Response of Two Serial Bolted Joints in Composite Laminates. *Journal of Mechanics* 2011; 27: 293-307.

Singh IV, Shedbale AS, Mishra BK. Material property evaluation of particle reinforced composites using finite element approach. *Journal of Composite Materials* 2016; 50: 2757-2771.

Sundaram S, Nagalingam R, Raja RS. Experimental analysis on tensile properties of FRP with nano clay. *International Journal of Advanced Manufacturing Technology* 2008; 170: 1868-1876.

Tsai SW, Wu EM. A General Theory of Strength for Anisotropic Materials. *Journal of Composite Materials* 1971; 5: 58-80.

Uddin MF, Sun CT. Strength of unidirectional glass/epoxy composite with silica nano particle-enhanced matrix. *Composites Science and Technology* 2008; 68: 1637-1643.

Whitney JM, Nuismer RJ. Stress fracture criteria for laminated composites containing stress concentration. *Journal of Composite Materials* 1974; 8: 253-265.

Yao XF, Zhou D, Yeh HY. Macro/microscopic fracture characterizations of SiO_2/epoxy nanocomposites. *Aerospace Science and Technology* 2008; 12: 223-230.

Zhou Y, Hosur M, Jeelani S, Mallick PK, Fabrication and characterization of carbon fiber reinforced clay/epoxy composite. *Journal of Material Science* 2012; 47: 5002-5012.

Zhu Y, Sun DX, Zheng H, Wei M, Zhang LM. Improvement in properties of epoxy-based electrophoretic coating by silica/polyurethane nanocomposites. *Journal of Material Science* 2007; 42: 545-550.